ABSTRACT

Title of Document:	THE ROLE OF EXCITATION-CONTRACTION COUPLING FAILURE IN MUSCLE FATIGUE AND WEAKNESS OF DYSTROPHIC SKELETAL MUSCLE
	Davi Augusto Garcia Mázala, Master's Thesis Defense, 2011
Directed By:	Dr. Eva Chin, PhD, Department of Kinesiology, University of Maryland

Abstract

Alterations in intracellular calcium (Ca^{2+}) are thought to play an important role in skeletal muscle weakness associated with muscular dystrophy due to the activation of Ca^{2+}-regulated proteases (calpains). It was hypothesized that impairments in Ca^{2+} regulation are exacerbated in dystrophic muscle and that calpain inhibition could attenuate the muscle weakness induced by fatiguing contractions. Single muscle fibres from control and dystrophic mice lacking dystrophin (*mdx)* and utrophin plus dystrophin ($Utr^{-/-}$/*mdx*) were used. Fibres from $Utr^{-/-}$/*mdx* mice had similar peak tetanic Ca^{2+} compared to control and *mdx* mice, however $Utr^{-/-}$/*mdx* mice took longer to clear the released Ca^{2+}. All fibres showed similar time to fatigue but fewer *mdx* and $Utr^{-/-}$/*mdx* fibres remained excitable 1hr after fatiguing contractions. Exposure to a calpain inhibitor improved Ca^{2+} levels in dystrophic fibres (*mdx*; trend only in $Utr^{-/-}$/*mdx*) after fatigue. Together, these data indicate that calpains play a role in prolonged muscle weakness after fatiguing contractions.

THE ROLE OF EXCITATION-CONTRACTION COUPLING FAILURE IN MUSCLE FATIGUE AND WEAKNESS OF DYSTROPHIC SKELETAL MUSCLE

By

Davi Augusto Garcia Mázala

Thesis submitted to the Faculty of the Graduate School of the
University of Maryland, College Park, in partial fulfillment
of the requirements for the degree of
Master of Art
2011

Advisory Committee:
Dr. Eva Chin, Chair
Dr. Stephen Roth
Dr. Espen Spangenburg

Dedication

Dedico este projeto aos meus pais, Carlos Roberto Mázala e Elisabete Victor Garcia Mázala. Muito obrigado pelos anos de suporte, amor e confiança, e pelo exemplo de vida, persistência e simplicidade.

Ao meu tio Joao Victor, pelos anos de suporte, confiança e por ter me ajudado a estar aqui hoje. Muito obrigado pelos seus ensinamentos.

I also dedicate this work to Dr. Marcio Oliveira for all the support during these past years. You have been a great role model as a person and scientist. Thank you for everything.

Acknowledgements

I would like to thank all graduate students who have helped throughout this past two years. In special, I would like to thank Andy Ludlow, Dapeng Chen, and Sam English.

Special thanks to Dr. Espen Spangenburg and Dr. Steve Roth for being part of my committee and giving me advice on this project. Thank you for your time and patience. Also, thanks to Dr. Espen Spangenburg for your help in the laboratory and for the times we discussed science in your office.

I would like to thank Dr. Eva Chin for being a wonderful advisor and friend during these past years. Thank you for taking time to teach me all the techniques required to perform this project, and helping me throughout the entire process. Also, your passion for research has greatly motivated me to perform this project.

Table of Contents:

Abbreviations

°C - Degrees Celsius
$[Ca^{2+}]_i$ - Intracellular calcium concentration
ADP - Adenosine diphosphate
AIDS - Acquired immune deficiency syndrome
ALLN - N-Acetyl-Leu-Leu-Norleu-al
AM - Acetoxymethyl
Anova - Analysis of Variance
AP - Action potential
ATP - Adenosine triphosphate
Ca^{2+} - Calcium
$CaCl_2$ - Calcium chloride
CARF - Central animal research facility
Cav - caveolin
Cr - Creatine
CrP - Creatine phosphate
CS Tg/*mdx* - *mdx* mice overexpressing calpastatin
CK - Creatine kinase
CO_2 - Carbon dioxide
CON - control
DAC - Dystrophin associated complex
DHPR - Dihydropyridine receptors
DMD - Duchenne muscular dystrophy
EC - Excitation contraction
EDL - Extensor digitotum longus
FBS - Fetal bovine serum
FDB - Flexor digitorum brevis
H^+ - Hydrogen ions
Hz - Hertz
IACUC - Institutional Animal Care and Use Committee
KCl - Potassium chloride
kDa - Kilodalton
Ki - Kinetic inhibitor
mdx/mTR – mdx telomerase knockout
µM - Micromolar
µm - Micrometer
MEM - Minimal essential media
$MgCl_2$ - Magnesium chloride
mRNA – Messenger RNA
NaCl - Sodium chloride
NaH_2PO_4 - Sodium Phosphate
$NaHCO_3$ - Sodium bicarbonate
nM - Nanomolar
nNOS - neural nitric oxide synthase
O_2 - Oxygen
P_i - Inorganic phosphate

PV - Parvalbumin
ROS - Reactive oxygen species
RyR - Ryanodine receptor
SERCA - Sarcoplasmic/Endoplasmic reticulum calcium pump
SMF(s) - Single muscle fibre(s)
SR - Sarcoplasmic reticulum
TRPC - Transient receptor potential canonical
TRPV2 - Transient receptor potential vanilloid 2
$Utr^{-/-}$/*mdx* - utrophin/dystrophin null mice

List of Tables

List of Figures

Chapter 1: Introduction

Duchenne muscular dystrophy (DMD) is one of the most frequent and devastating types of muscular dystrophy affecting humans (6; 26). One in 3500 boys are born with the disease and few cases have been reported in girls (111). Although DMD has received considerable attention due to its rapid progression and the early death of patients (12), there still is no cure for the disease. Despite appearing normal at birth, affected individuals are often diagnosed as early as 3 years of age, become wheelchair bound between 8 and 12 years of age, and do not extend their life beyond the age of 30 (6). It is known that skeletal muscle of patients with DMD lacks dystrophin (79), an essential protein maintaining stability in the muscle membrane (48; 104). Dystrophin is a member of the dystrophin-associated complex (DAC) which connects the cytoskeleton of muscle fibres to proteins in its membrane (see Figure 1) (6). The absence of dystrophin from the DAC contributes to the inability of the complex to function properly (6). The absence of dystrophin also affects intrinsic mechanisms responsible for muscle force production and function (149), and increases the muscle's susceptibility to stretch-induced damage (169).

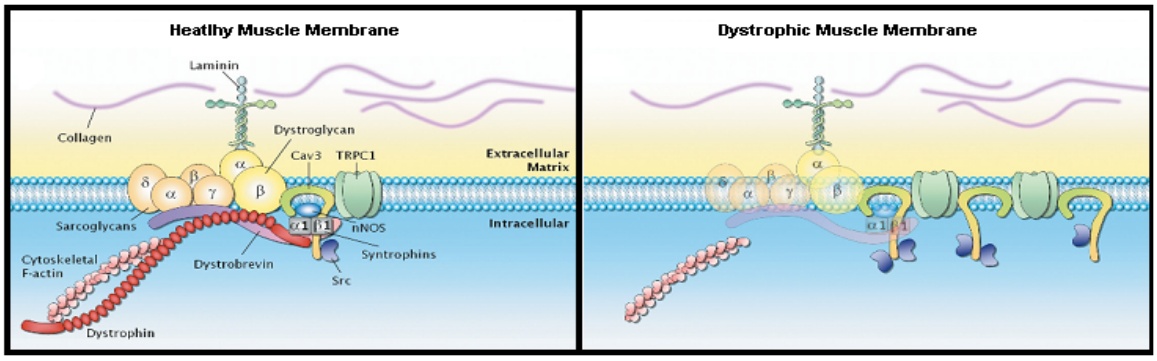

Figure 1. Schematic illustration demonstrating the role of dystrophin in the muscle fibre membrane. Healthy muscle membrane with dystrophin in place maintaining the dystrophin-associated complex (DAC) together (left) and dystrophic muscle where the absence of dystrophin leads to instability of the DAC (right). The DAC is composed of syntrophins (α-1 and β-1), neuronal nitric oxide synthase (nNOS), α- and β-dystroglycans, laminin, sarcoglycans (α, β, δ, and γ), caveolin-3 (Cav-3), and dystrobrevin. Also shown are filamentous (F)-actin which binds dystrophin to the cytoskeleton, collagen and the transient receptor potential canonical 1 (TRPC1) channel responsible for Ca^{2+} entry. Adapted from (6).

One of the proposed mechanisms by which dystrophin deficiency affects force production is the impairment in excitation-contraction (E-C) coupling (6; 149). The process of E-C coupling involves all cellular events that link muscle excitation to force production (see Figure 2) (31). This process is initiated by activation from the motoneuron, resulting in depolarization of the muscle membrane and activation of calcium (Ca^{2+}) release (12). The released Ca^{2+} binds to troponin C which allows force to be produced (12). Several studies have demonstrated that muscle fatigue occurs in response to a failure in some process of E-C coupling (8; 32; 156). This impairment in E-C coupling, leading to a decrease in free intracellular Ca^{2+} concentration ($[Ca^{2+}]_i$) and force during repeated tetanic contractions (i.e. prolonged muscle activity), is due to both metabolite accumulation and to the elevation in resting $[Ca^{2+}]_i$ (35). Possible underlying causes for the impairments in E-C coupling and force production include defects in depolarization, slower rate of membrane repolarization, failure to activate dihydropyridine receptors (DHPR), impaired communication between the voltage sensors (DHPRs) and the Ca^{2+} release channels, and reduced rate of Ca^{2+} uptake by the sarcoplasmic reticulum (SR) leading to higher resting $[Ca^{2+}]_i$ between contractions (7). The prolonged effects of muscle fatigue (i.e. muscle weakness) which persist after metabolic recovery (> 1 hr after a fatigue bout) are thought to be due primarily to the increases in $[Ca^{2+}]_i$ during the tetanic contractions (32). The accumulation of $[Ca^{2+}]_i$ during repeated muscle contractions, which contributes to acute muscle weakness (33; 98; 151), may also be responsible for decreased force producing capacity observed in certain muscle diseases.

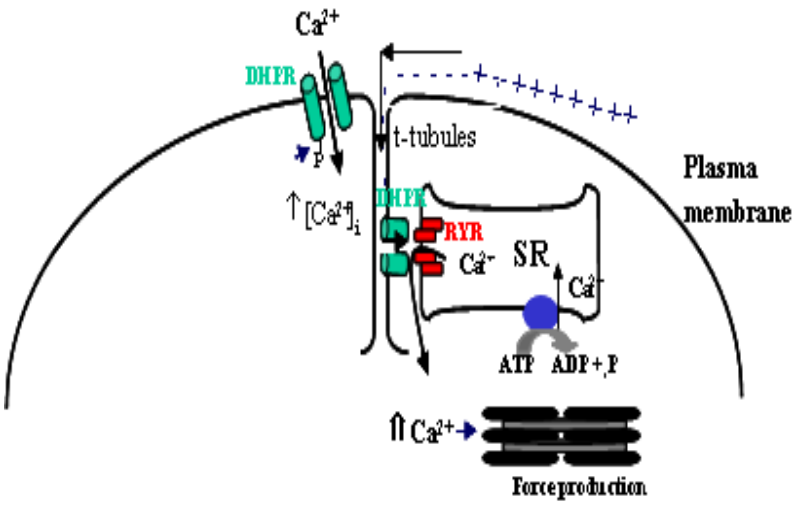

Figure 2 - Skeletal muscle excitation-contraction coupling. Muscle activation results in depolarization of the plasma membrane and the transverse tubules (t-tubules), which carry the signal to the interior of the fibre. The voltage sensing dihydropyridine receptor (DHPR) detects the change in membrane potential and transmits the signal to the calcium release channel or ryanodine receptor (RYR). The process of E-C-coupling is known to be impaired in DMD (adapted from 31).

Ca^{2+} homeostasis is impaired in dystrophic muscle (14; 82). Resting $[Ca^{2+}]_i$ has been shown to be higher in single muscle fibres (SMF) from the *mdx* mice (dystrophic mouse model for DMD) compared to control mice, as well as in humans (148; 24; 39; 75). Yet, others have reported no differences (61; 102; 126). It was previously reported that depolarization-induced SR Ca^{2+} release is reduced in SMF from *mdx* mice (169). However, more recent data suggest that stimulation-induced Ca^{2+} release is reduced only in a subset of branched fibres and not in non-branched SMFs (76). The chronic change in Ca^{2+} homeostasis may affect SR function (87; 145). The increased resting Ca^{2+} levels can lead to saturation of the SR Ca^{2+} pump responsible for Ca^{2+} uptake (48). The increase in free $[Ca^{2+}]_i$ is augmented by repeated muscle contractions, with the accumulation of Ca^{2+} being greater in branched muscle fibres (76). The decline in force output with repeated muscle contractions (i.e. fatigue) is associated with a decrease in peak tetanic $[Ca^{2+}]_i$ secondary to impaired E-C coupling (8). This fatigue-induced impairment in E-C coupling has been shown to be similar

in control and non-branched single fibres from *mdx* mice but is greater in branched single fibres, leading to further decreases in peak $[Ca^{2+}]_i$ and an accelerated rate of fatigue (76).

It has been proposed that Ca^{2+}-activated proteases (calpains) play a role in this prolonged disruption of E-C coupling (98; 152). This is a feasible hypothesis supported by studies demonstrating the activation of calpains (calpain-3 and μ-calpain) by $[Ca^{2+}]_i$ in the physiological range of muscle contractions (0.5 – 3.0μM) (26; 117; 118). Calpains are non-lysosomal Ca^{2+}-activated proteases that, when activated, participate in the breakdown of muscle constituents. Although the role of calpains is still unclear, it has been suggested that they participate in the process of remodeling the cytoskeletal structure and have close interaction with the plasma membrane (62). Calpains are necessary during the development of muscle fibres, due to the extensive remodeling required, but only calpain-3 is essential for adult muscle, since its absence is related to the development of limb-girdle muscular dystrophy type 2A (62, 116).

The two calpains most commonly found in muscle are calpain-3 (also referred to p94), which is bound near the triad junction at the N2A line in titin, and μ-calpain (also called calpain-1), localized in the I-band region (91; 120, 170). Calpain-3 is autolyzed in the presence of Ca^{2+} by removal of a propeptide that covers its catalytic site, thus producing three different protein products with molecular weights of 60-, 58-, and 55kDa (63). The process by which μ-calpain is autolyzed, in a Ca^{2+} dependent manner, involves the cleavage of the NH_2-terminal domain which reduces its size from 80kDa to 78kDa and 76kDa (67). Due to the increased muscle breakdown and protein turnover in the *mdx* mice, several groups have investigated the level of calpain activation in this mouse model (62; 156; 141). It has been reported that the *mdx* mice have an average 1.5-fold increase in calpain activation compared to controls (62), and this increase has been suggested to occur by post-translational

modification (139). This enhanced activation has been reported in muscles undergoing damage, with the calpain levels returning to normal when the muscle is regenerating (139).

Studies investigating underlying mechanisms (62; 76; 169) and potential treatments (48; 134) for DMD have largely been done in *mdx* mice. However, the only muscle in the *mdx* mice demonstrating similar disease progression to DMD patients, with progressive degeneration and detectable muscle weakness, is the diaphragm (143). This is because utrophin, a protein with a similar role to dystrophin in muscle, is upregulated in these animals therefore compensating for the lack of dystrophin in most muscles (70; 149). Also, it has been shown that satellite cell function in the *mdx* mouse is higher, thus enhancing muscle regenerative capacity and contributing to the milder disease severity (131). Consequently, a double mutant model (animals lacking both dystrophin and utrophin) is thought to be a more suitable model for DMD (37; 70). In a study by Capote and colleagues (29), $[Ca^{2+}]_i$ was assessed in SMFs from control, *mdx* and the utrophin knockout ($Utr^{-/-}$)/*mdx* double mutant mice ($Utr^{-/-}$/*mdx*). The study demonstrated that peak Ca^{2+} release was not different between *mdx* and $Utr^{-/-}$/*mdx* mice, although Ca^{2+} release was suppressed by 28-32% in fibres from both these models compared to control mice (29). These authors proposed that the *mdx* phenotype is not significantly ameliorated by utrophin overexpression (29). In response to repeated tetanic contractions, muscle fibres from the $Utr^{-/-}$/*mdx* mice had a greater decay in Ca^{2+} transients (i.e. greater fatigue) compared to the *mdx* and control mice (29). However, it is not fully known whether the prolonged reduction in muscle force akin to muscle weakness is exacerbated in the muscle fibres from the $Utr^{-/-}$/*mdx* mice.

Muscle fibre recovery after fatigue has been described to be dependent upon the frequency at which the muscle is stimulated and the levels of $[Ca^{2+}]_i$. As first presented by Edwards et al. in 1977 (55), muscles are not able to recover force production when stimulated at low frequency after fatigue (a mechanism that lasts for over a day), while force is fully

recovered when the muscle is stimulated at high frequency after fatigue (approximately 20 minutes for full recovery). Thus, this slow component of recovery from fatigue is not caused by depletion of high energy phosphate (55) or damage to myofibrillar proteins. It was further shown that the slow recovery from fatigue was not caused by decreased levels of metabolites, but rather due to a reduction in free $[Ca^{2+}]_i$ (159). Chin and Allen (33) showed that prolonged reductions in force following fatigue were not related to decreases in Ca^{2+} sensitivity or decreases in force-generating capacity, but instead occurred due to a reduction in Ca^{2+} release. This impairment in Ca^{2+} release, which adds to the long-lasting recovery from fatigue, occurs due to increases in $[Ca^{2+}]_i$ during fatiguing stimuli affecting E-C coupling (33; 98). This failure in E-C coupling can be caused by either exposing muscle fibres to high Ca^{2+} concentrations (1mM for 10 seconds) or by prolonged exposure (60 seconds) to lower concentrations (2.5µM) (98).

It is hypothesized that E-C coupling disruption is greater in muscles that lack both dystrophin and utrophin leading to prolonged decrease in force production following bouts of contractions. Therefore, the purpose of the present study was to investigate the effects of repeated contractions leading to muscle fatigue on $[Ca^{2+}]_i$ and E-C coupling failure. The prolonged muscle weakness after fatigue in $Utr^{-/-}$/*mdx* compared to *mdx* and control mice, as well as the role of calpains in this prolonged decrease in E-C-coupling was evaluated.

Specific Aim 1: to determine if E-C coupling failure during fatigue was more pronounced in SMFs from $Utr^{-/-}$/*mdx* compared to *mdx* and control mice.

Hypothesis 1: E-C coupling disruption will be greater in SMFs from $Utr^{-/-}$/*mdx* compared to *mdx* and control mice.

Specific Aim 2: to determine if prolonged muscle weakness due to E-C coupling disruption was exaggerated in SMFs from Utr$^{-/-}$/*mdx* compared to *mdx* and control mice.

Hypothesis 2: prolonged muscle weakness will be greater in SMFs from Utr$^{-/-}$/*mdx* compared to *mdx* and control mice.

Specific Aim 3: to determine whether prolonged muscle weakness was due to calpain activation in *mdx* and Utr$^{-/-}$/*mdx* mice.

Hypothesis 3: calpain inhibition will attenuate the prolonged muscle weakness after fatigue and would result in similar intracellular Ca^{2+} levels in SMFs from *mdx* and Utr$^{-/-}$/*mdx* mice.

Chapter 2: Methods

2.1 - Animals

All protocols for animal handling have been approved by the Institutional Animal Care and Use Committee (IACUC). An IACUC approved protocol for breeding these mice was obtained by Dr. Eva Chin. All groups were kept in the same room (regular ambient conditions – 20.9% of oxygen and 22±1^{o}C) and had the same access to food and water, bedding, and light cycle (12h light/12h dark).

Three controls (C57BL/10ScSn) were obtained from Jackson laboratories. Three Utr$^{+/-}$/*mdx* breeders (two females and one male) were obtained in collaboration with Dr. Diego Fraidenraich from University of Medicine and Dentistry, New Jersey, and in collaboration with Dr. Robert Grange from Virginia Tech University. Colonies of Utr$^{+/-}$/*mdx* mice were bred at the University of Maryland Central Animal Research Facility (CARF) according to previously published breeding schemes (50). Once females appeared pregnant, they were removed from the male and housed separately until after pups were born and weaned. Offspring were weaned at day 21 and sorted by gender and then used for assessment of SMF contractile function at approximately two months of age. It was expected that 25% of the pups born would be Utr$^{+/+}$/*mdx* (or *mdx*) and 25% would be Utr$^{-/-}$/*mdx*, while the other 50% would be Utr$^{+/-}$/*mdx*. However, out of 3 generations and a total of 30 animals only 2 animals were characterized as Utr$^{-/-}$/*mdx*. This is consistent with the findings of others (R. Grange, personal communication) and indicates some *in utero* loss of the Utr$^{-/-}$/*mdx* mice. The criteria for distinguishing *mdx* and Utr$^{-/-}$/*mdx* included body weight and spine curvature of animals (see Figure 3). It is known that the Utr$^{-/-}$/*mdx* mice demonstrate kyphotic posture and have lower body weight (approximately 10 grams less) compared to *mdx* and controls (50).

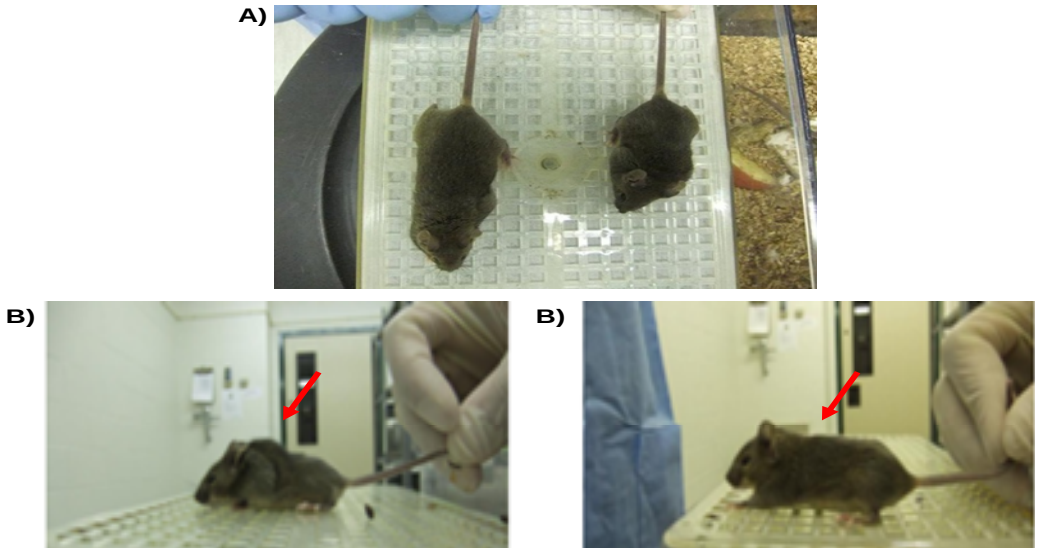

Figure 3. Utr$^{-/-}$/*mdx* were distinguished from *mdx* based on body weight and spine curvature. Picture on the top (A) demonstrates differences in size between *mdx* and Utr$^{-/-}$/*mdx*, while bottom picture (B) shows the kyphosis present in the Utr$^{-/-}$/*mdx* compared to *mdx* mouse (red arrows).

2.2 Study Design

The present study had 3 groups: a control (CON) group (n=3), a Utr$^{+/-}$/*mdx* or Utr$^{+/+}$/*mdx* (these animals will be referred as *mdx* throughout the document since we cannot currently distinguish between these genotypes) (n=9), and a Utr$^{-/-}$/*mdx* group (n=2). Muscle fibres from dystrophic animals demonstrate differences in fibre shape (some normal while some are called "branched") as they age (29; 104; 76). However, the present study only investigated fibres that had normal shape.

2.3 Data collection procedures

Animals were euthanized by cervical dislocation after exposure to carbon dioxide (CO_2) in a closed chamber. The feet were removed for dissection of SMFs from the flexor digitorum brevis (FDB) muscle. Furthermore, the protocol for isolating SMF from the FDB muscle has been previously tested (108). Muscle fibres were acquired after 4h digestion in a collagenase/minimal essential medium (MEM) solution. Fibres were incubated during digestion at 37^{o}C in order to maintain their normal physiological characteristics. Subsequently, fibres were incubated and preserved in MEM solution with 10% fetal bovine serum (FBS) at 37^{o}C. The protocol has been tested in a previous study (108).

2.3.1 Intracellular Ca^{2+} measurements. One day after dissection (day 1) fibres were loaded with Fura-2AM for 15 minutes in order to measure $[Ca^{2+}]_i$. Fifteen minutes of incubation with Fura-2AM allows enough time for fusion of the fluorescent indicator into the muscle fibre myoplasm. The presence of the AM portion in the Fura-2 compound gives the advantage of loading without injecting the dye into the fibre. The addition of the AM portion allows the indicator to enter the myoplasm, where esterases remove the AM group, which then traps the indicator in the cytoplasm (153). Loaded fibres were then placed in a stimulation chamber containing parallel electrodes on top of a Nikon TiU microscope. Intracellular Ca^{2+} levels were assessed using Fura-fluorescence with an IonOptix Hyperswitch system for dual excitation, single emission dyes with filters sets for Fura-2. The Ca^{2+} indicator Fura-2 has peak fluorescence at 510 nm when excited at 380nm in the unbound state but shifts to peak fluorescence at 510nm when excited at 340nm when bound to Ca^{2+}. The ratio of emission at 510nm when excited at 340 and 380nm (i.e. Ratio = 340nm/380nm) represents the intracellular free $[Ca^{2+}]_i$. The IonOptix hardware includes the MyoCam-S which allows for control over the spatial field of video acquisition and fluorescence detection. The input into the detector is controlled on the MyoCam-S itself and

shown on the video window of the computer screen, effectively allowing one to obtain fluorescence signals from one fibre at a time. Fluorescence from other nearby muscle fibres do not influence the Fura-2 ratio of the fibre in the image acquisition field.

2.3.2 Single muscle fibre stimulation protocol. The muscle fibres used in the present study were selected based on having a normal shape (non-branched) and responding to 15Hz stimuli. This criteria was used to avoid bias when selecting fibres for data collection. Single fibre $[Ca^{2+}]_i$ was assessed in muscle fibres using 350msec tetani at 10, 30, 50, 70, 100, 120, and 150Hz stimulation frequencies. One minute of rest was allowed between frequencies, and then fibres rested for 10 minutes before assessing the 7 frequencies again. Right after the first set of stimuli, fibres were either perfused with drug or vehicle for testing the acute effects of either exposure. Then, fibres rested for 10 more minutes before inducing fatigue. Fibres were then assessed again 1 hour after fatigue at the same 7 stimulation frequencies to evaluate the prolonged decrease in muscle function. Muscle fibres were continuously perfused with a stimulating tyrode solution throughout data collection (units in mM - NaCl, 121.0; KCl, 5.0; $CaCl_2$, 1.8; $MgCl_2$, 0.5; NaH_2PO_4, 0.4; $NaHCO_3$, 24.0; and glucose, 5.5) (34). This solution was bubbled with 95% O_2/5% CO_2 to give a pH of 7.3 (34). To assist in the survival of SMFs during perfusion, 0.2 % FBS was added to each solution (34). After the first set of stimuli, fibres were continually perfused with stimulating tyrode with the addition of either drug or vehicle throughout the entire protocol.

2.3.3 Assessment of muscle fatigue and prolonged muscle weakness. Fatigue was induced by intermittent 100Hz tetani (350msec duration) starting at 1 contraction every 4 seconds for 2 minutes, then 1 contraction every 3 seconds for 2 minutes, then 1 contraction

every 2 seconds for 2 minutes, and then 1 contraction every second for 2 minutes (32). Time to 50% of initial Fura-2 ratio was used as index of fatigue. One hour following fatigue, single fibre $[Ca^{2+}]_i$ were re-assessed in the same fibre using the same stimulation protocol (10, 30, 50, 70, 100, 120, and 150Hz) to determine the prolonged decrease in E-C coupling as an index of muscle weakness (35).

2.4 Determining the role of Calpains in Muscle Weakness

In order to evaluate the role of calpains in the prolonged decrease in E-C coupling, muscle fibres were continuously perfused with a calpain inhibitor after the first set of stimulation frequencies and throughout the entire protocol. The 60 min recovery from fatigue was compared between fibres exposed to the calpain inhibitor and those exposed to a vehicle solution (stimulating tyrode with 100% ethanol). In this study calpain was inhibited by a pan-protease inhibitor (ALLN, EMD Biosciences) which is most potent for the Ca^{2+} activated proteases μ-calpain (inhibitor constant (Ki) 190nM) and calpain-2 (Ki 220nM), compared to other proteases (Cysteine Proteases and Proteasome Ki 6uM), although it also potently inhibits Cathepsin B (Ki 150nM) and Cathepsin L (Ki 500pM). The limited choice of commercially available calpain inhibitors in addition to their lack of specificity was the main reason for selecting the pan-protease inhibitor ALLN.

2.5 Statistical Analysis

SPSS software (version 18.0; IBM Somers, NY) was used to calculate differences between and within groups in Fura-2 ratio (resting, peak, and 75% of Fura-2 peak clearance), time to fatigue, increase in resting Fura-2 ratio during fatigue, and pre- vs. post fatigue Fura-2 ratios at each frequency. One way Analysis of Variance (ANOVA) was used for group

comparisons with the Tukey test for post-hoc analyses. For changes in fluorescence pre- vs. post fatigue, a paired t-test was performed. The statistical significance was defined at $p<0.05$. Appendix A has the outputs from SPSS for all comparisons.

Chapter 3: Results

Animals and single muscle fibres

The experiments were carried out in 2 month old mice. The body weight of Utr$^{-/-}$/*mdx* was lower than *mdx* ($p<0.05$) and CON ($p<0.05$) mice. A total of 13 SMF from CON were analyzed while 46 and 14 fibres from *mdx* and Utr$^{-/-}$/*mdx* were analyzed, respectively. All 13 fibres analyzed from CON were used for the entire protocol. In the *mdx* group, 24 out of 46 fibres were exposed to the full protocol, while 7 out of 14 fibres were assessed in the Utr$^{-/-}$/*mdx* group. The number of total fibres included those that responded to the 15Hz stimulus and were used for the entire protocol or only part of it. The number of fibres treated with either ALLN or Vehicle represents all fibres that completed the entire protocol and which did not fail to respond to a stimulus prior to the last set of stimulation frequencies. Table 1 shows the characteristics of animals and the number of fibres used per group.

Table 1 – Number of animals and single muscle fibres assessed per group

	n (animals)	Body weight	Total fibres	Fibres treated with vehicle	Fibres treated with ALLN
CON	3	26.15 ± 0.47g	13	7	6
mdx	9	27.85 ± 2.73g	46	9	15
Utr$^{-/-}$/*mdx*	2	14.75* ± 3.04g	14	4	3

The number of fibres completing the full protocol was lower than the starting number of fibres. Fibres where the Ca^{2+} plateau did not maintain a peak or that would not respond to stimuli were not assessed for the rest of the protocol. Therefore, any fibre failing to maintain peak at any frequency prior to fatigue was not exposed to the entire protocol. Table 2 shows the number of fibres either failing or not responding to stimulus during the protocol in each group. The denominator in the first and third columns corresponds to the total number of

fibres in each group, while the denominator in the second and fourth columns corresponds to the total number of fibres exposed to the full protocol.

Table 2 - Number of fibres failing or not responding to stimulus before or after fatigue.

	Fibres failing to maintain peak		Fibres not responding to stimulus	
	Before fatigue	**After fatigue**	**Before fatigue**	**After fatigue**
CON	0/13	1/13	0/13	2/13
mdx	18/46	6/24	4/46	4/24
Utr$^{-/-}$/*mdx*	7/14	4/7	0/14	2/7

The diameter and length of SMFs are shown in Figures 4 and 5. Fibre diameter from the Utr$^{-/-}$/*mdx* mice was smaller compared to the fibres in the two other groups ($p<0.05$). There were no differences in fibre length between groups (CON vs. *mdx*, $p=0.69$; CON vs. Utr$^{-/-}$/*mdx*, $p=0.92$; *mdx* vs. Utr$^{-/-}$/*mdx*, $p=0.38$).

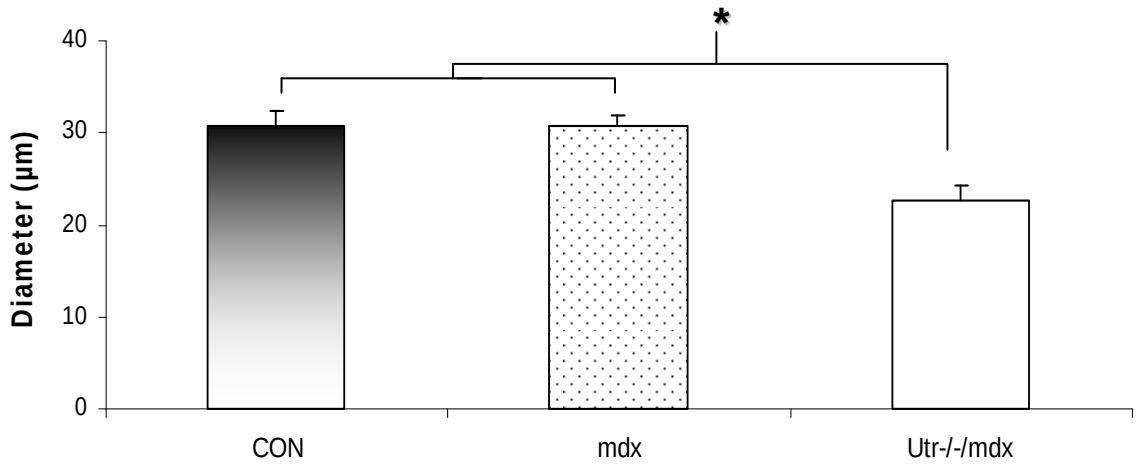

Figure 4. Single muscle fibres from Utr$^{-/-}$/*mdx* mice had a reduced diameter compared to CON and *mdx* mice. Average fibre diameter was calculated for all fibres from each group (n= CON: 13; *mdx*: 46; Utr$^{-/-}$/*mdx*: 14). Data shown are mean ± SE. * $p<0.05$.

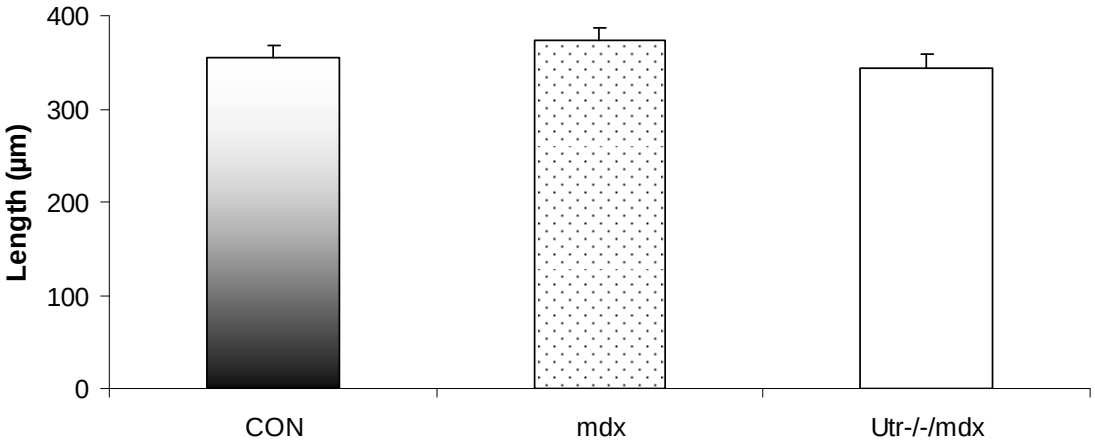

Figure 5. Fibre length was similar between groups. Average fibre length was calculated based on all fibres from each group (n= CON: 13; *mdx*: 46; Utr$^{-/-}$/*mdx*: 14). Data shown are mean ± SE.

<u>Ca^{2+} handling</u>

Resting Fura-2 ratio, representing resting intracellular Ca^{2+}, was higher in *mdx* fibres compared to CON ($p<0.05$), but not in comparison to Utr$^{-/-}$/*mdx* mice ($p=0.44$) (Figure 6). There were no differences in resting Fura-2 ratio between CON and Utr$^{-/-}$/*mdx* ($p=0.32$) (Figure 6). Peak Fura-2 ratio was not different between groups for all stimulation frequencies, which demonstrate that fibres from all groups had similar starting levels of tetanic intracellular Ca^{2+} (p values are listed in appendix). In order to assess Ca^{2+} clearance by parvalbumin (PV) binding and the SR Ca^{2+} ATPase, the time required to reduce the Fura-2 level back to 25% of the peak level (i.e. 75% peak Fura-2 clearance) was determined (see Figure 7). There were no differences in 75% peak Fura-2 clearance between 50Hz and 120Hz within groups (CON, $p=0.38$; *mdx*, $p=0.32$; Utr$^{-/-}$/*mdx*, $p=0.19$) (Figure 8). These two frequencies were selected because they represent examples of low and high stimulation frequencies. Figure 8 also shows that the time for 75% of Fura-2 peak clearance at 50Hz was longer in Utr$^{-/-}$/*mdx* compared to controls ($p<0.05$), but not compared to *mdx* mice ($p<0.10$).

Similar results were reported at 120Hz, in which Utr$^{-/-}$/*mdx* fibres required a longer time to clear 75% of total released Fura-2 peak compared to controls (Figure 8).

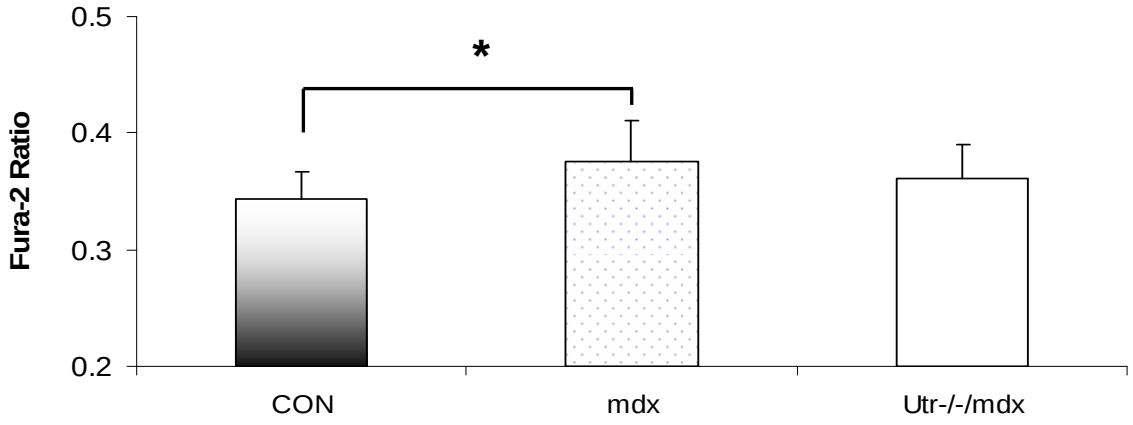

Figure 6. Resting Fura-2 ratio was higher in *mdx* compared to CON. Resting Fura-2 ratio was calculated from all fibres in each group (n= CON: 13; mdx: 46; Utr$^{-/-}$/*mdx*: 14). Data shown are mean ± SE. * $p<0.05$.

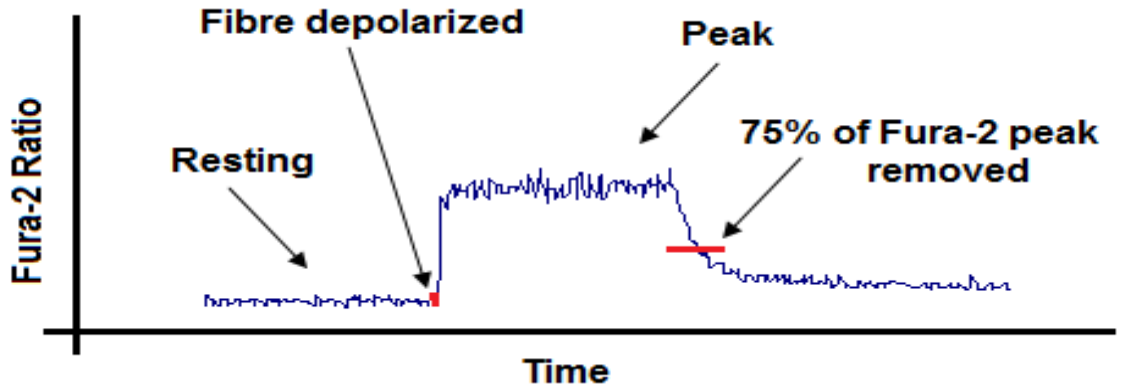

Figure 7. Raw data figure demonstrating the Fura-2 ratio response to a stimulation frequency. Different parts of the Fura-2 tracing shown: resting Fura-2 ratio, time point when single muscle fibre is depolarized, peak Fura-2 ratio, and the time point at which 75% of Fura-2 peak is removed. The first step in determining 75% of Fura-2 peak clearance involves the calculation of the difference between Fura-2 peak (i.e. 1.2) and resting Fura-2 ratio (i.e. 0.3). Then, 25% of the difference is calculated (i.e. (1.2-0.3)*.25=.225). This number is added to the resting Fura-2 ratio (i.e. 0.3+.225=0.525). Then, the time point corresponding to this value when peak Fura-2 is decreasing is recorded (i.e. 1.238 sec). Lastly, the difference between time of 25% of Fura-2 peak and time of last part of the Fura-2 peak is calculated (i.e. 1.238-1.158 = .80sec). This last number represents the time taken for 75% of Fura-2 peak removal.

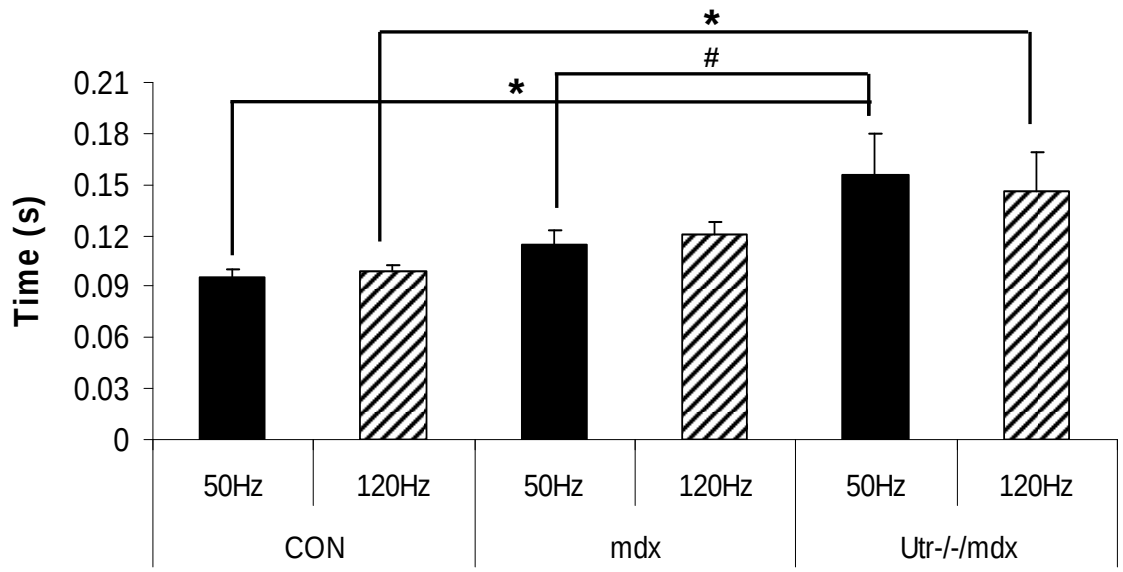

Figure 8. Time taken for 75% of Fura-2 peak clearance at 50 and 120Hz. Time taken for 75% of Fura-2 peak clearance was longer in Utr$^{-/-}$/*mdx* compared to CON at 50Hz and 120Hz (trend seen between *mdx* and Utr$^{-/-}$/*mdx* at 50Hz - $p<0.10$). Time taken for 75% of Fura-2 peak clearance was calculated for all fibres demonstrating normal responses to tetani at the first set of stimulation frequencies (n: CON=13; *mdx*=32; Utr$^{-/-}$/*mdx*=8). Data shown are mean ± SE. * $p<0.05$; # $p<0.10$.

Resistance to fatigue

In the present study, fatigue was determined as 50% decrease in peak Fura-2 ratio during repeated muscle contractions (raw data figure demonstrating fatiguing contractions is shown in Figure 9). As shown in Figure 10, there were no differences between groups in time to fatigue (CON vs. *mdx*, p=0.73; CON vs. Utr$^{-/-}$/*mdx*, p=0.61; *mdx* vs. Utr$^{-/-}$/*mdx*, p=0.23). Also, there were no differences in the magnitude of the increase in resting Fura-2 ratio during fatigue (see Figure 11; CON vs. *mdx*, p=0.98; CON vs. Utr$^{-/-}$/*mdx*, p=0.75; *mdx* vs. Utr$^{-/-}$/*mdx*, p=0.79). However, an interesting finding in the present study was that 6 out of the 7 (~86%) fibres in the Utr$^{-/-}$/*mdx* stimulated to fatigue were either unable to respond to stimuli after fatigue or demonstrated failing peaks. Moreover, the other two groups also had fibres either failing to maintain a Ca^{2+} peak or not responding to stimuli after fatigue, but the

percentage of fibres failing (due to either condition noted above) was lower compared to Utr$^{-/-}$/*mdx* fibres (CON=3/10 (~30%); *mdx*=10/24 (~42%)).

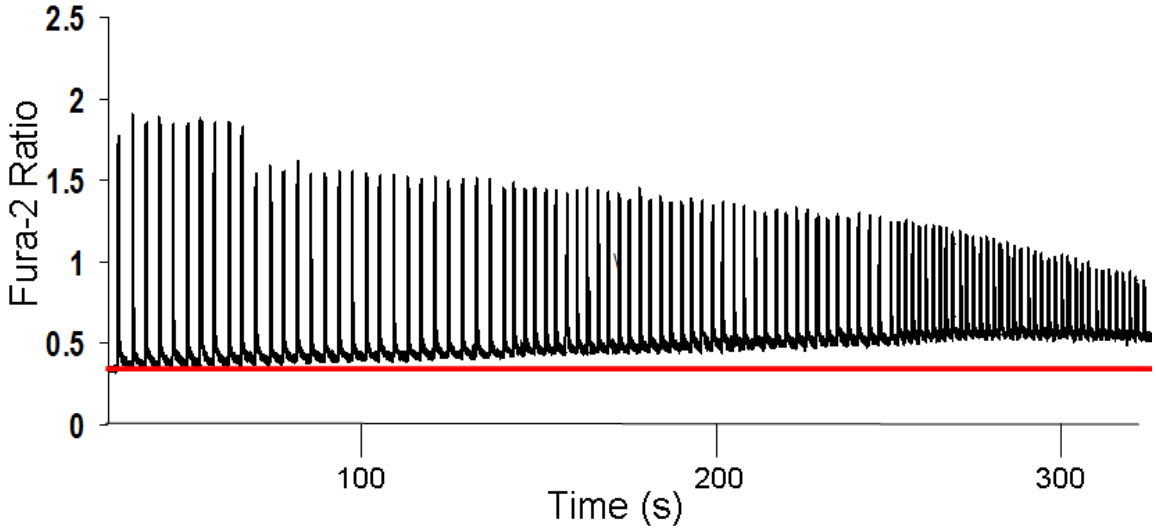

Figure 9. Raw data figure showing an example of fatiguing contractions. Time to fatigue was determined as 50% decrease in peak Fura-2 ratio from first Fura-2 peak (each individual line upwards is a single Fura-2 peak). Note the increase in resting Fura-2 ratio during contractions leading to fatigue (read line shows baseline Fura-2 ratio from the initial Fura-2 resting value).

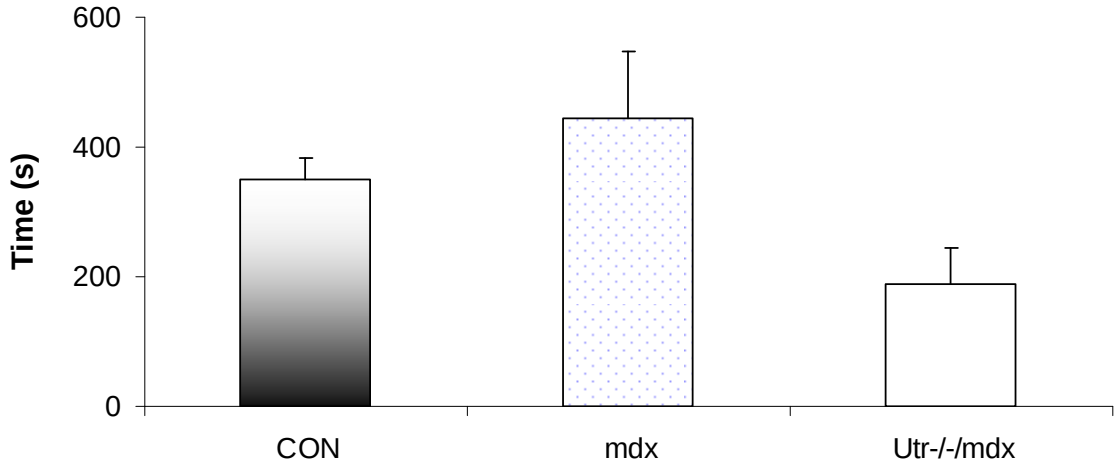

Figure 10. There were no differences in time to fatigue between groups. Time to fatigue was defined as time taken to reach 50% of initial peak during fatigue (n= CON: 13; *mdx*: 24; Utr$^{-/-}$/*mdx*: 7). Data shown are mean ± SE.

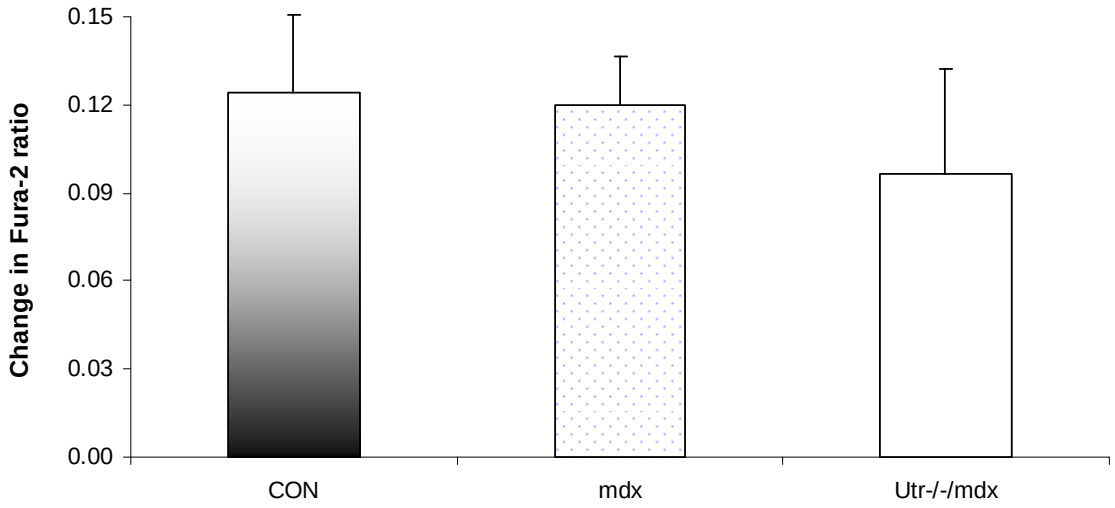

Figure 11. Increase in resting Fura-2 ratio during fatigue was not different between groups. Increase in resting was calculated as the difference between resting Fura-2 ratio for the tetanus demonstrating 50% of initial peak and the starting resting Fura-2 ratio (n= CON: 13; *mdx*: 24; Utr$^{-/-}$/*mdx*: 7). Data shown are mean ± SE.

Effect of drug treatment on fatigue resistance

When comparing time to fatigue for each treatment condition (Vehicle and ALLN), there were no between-group differences (CON vs. *mdx* vs. Utr-/-/*mdx*) in time to fatigue in the sub-set of SMFs (Figure 12). Also, there were no differences in the increase in resting Fura-2 ratio during fatigue in vehicle- or ALLN-treated fibres (Figure 13). No within-group differences between Vehicle vs. ALLN treatment were reported for time to fatigue or increase in resting Fura-2 ratio (Figures 12 and 13).

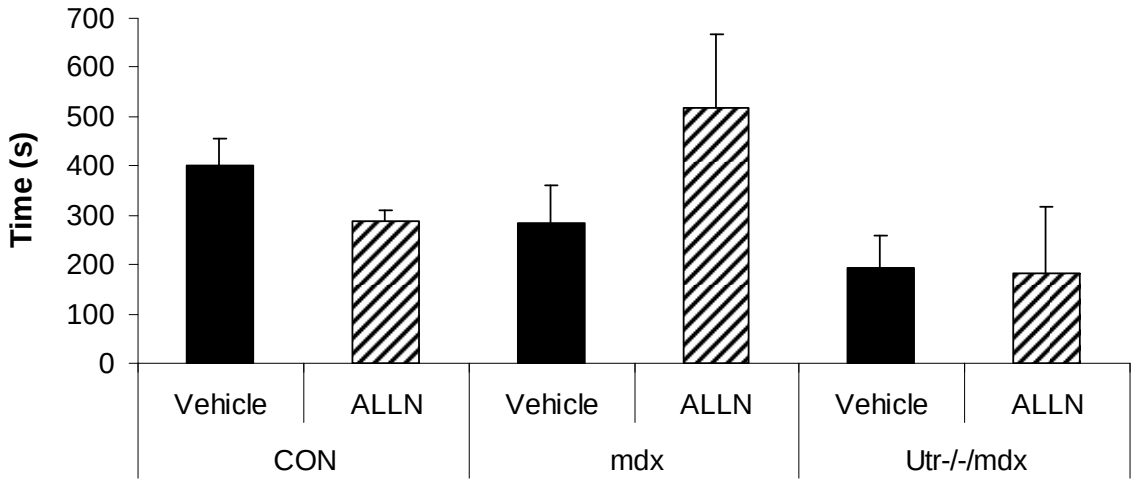

Figure 12. There were no differences within or between groups in time to fatigue between fibres exposed to Vehicle compared to ALLN. Time to fatigue was defined as time taken to reach 50% of initial peak during fatigue (n= CON: 7 Vehicle – 6 ALLN; *mdx*: 9 Vehicle - 15 ALLN; $Utr^{-/-}$/*mdx*: 4 Vehicle - 3 ALLN). Data shown are mean ± SE.

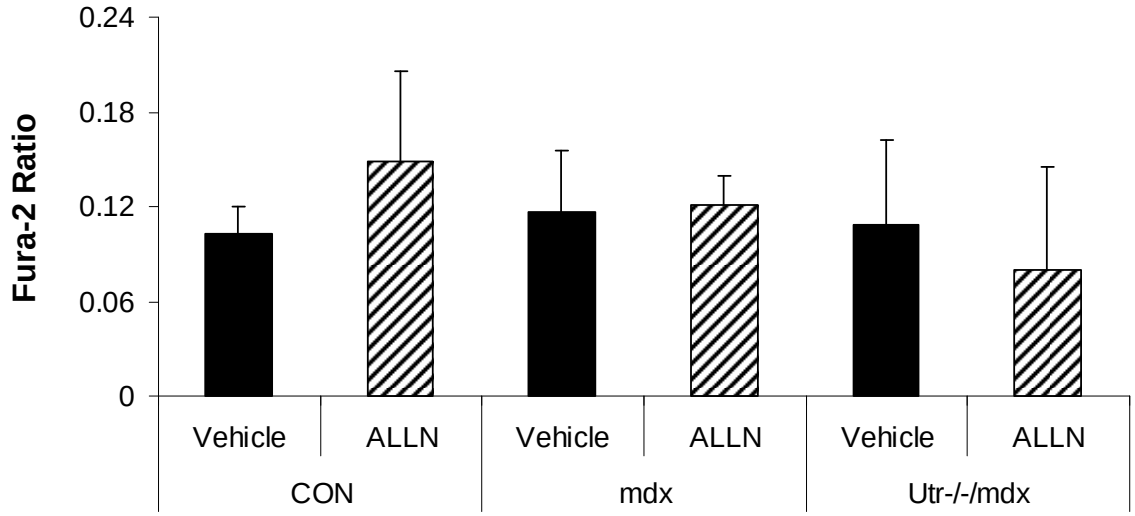

Figure 13. There were no within or between group differences in increase in resting Fura-2 ratio during fatigue for fibres exposed to Vehicle or ALLN. Increase in resting was calculated as the difference between resting Fura-2 ratio from peak demonstrating 50% of initial peak and starting resting Fura-2 ratio (n= CON: 7 Vehicle – 6 ALLN; *mdx*: 9 Vehicle - 15 ALLN; $Utr^{-/-}$/*mdx*: 4 Vehicle - 3 ALLN). Data shown are mean ± SE.

Effects of calpain inhibitor in single muscle fibre function

As shown in Figures 13 (CON) and 14 (Utr$^{-/-}$/*mdx*), SMFs treated with vehicle had similar peak Fura-2 ratio for all stimulation frequencies from pre- to post-fatigue (refer to appendix for p values). This suggests that there was no prolonged impairment in E-C coupling in these fibres (Figures 13 and 14). There were also no peak Fura-2 ratio differences after fatigue with ALLN in these two groups (Figures 16 and 17). However, SMFs from *mdx* mice treated with vehicle had lower peak at 10 ($p<0.05$), 120 ($p<0.05$), and 150Hz ($p<0.05$) after fatigue, while there was a trend for other frequencies (30Hz: $p=0.055$; 50Hz: $p=0.068$; 70Hz: $p=0.063$; 100Hz: $p=0.056$) (Figure 15), a marker of prolonged impairment in E-C coupling induced by the fatiguing tetani. In this group, SMFs treated with ALLN demonstrated no reduction in peak Fura-2 ratio from pre- to post-fatigue measurements indicating that ALLN suppressed the prolonged impairment in E-C coupling and implicating calpain activation in this impairment (Figure 18).

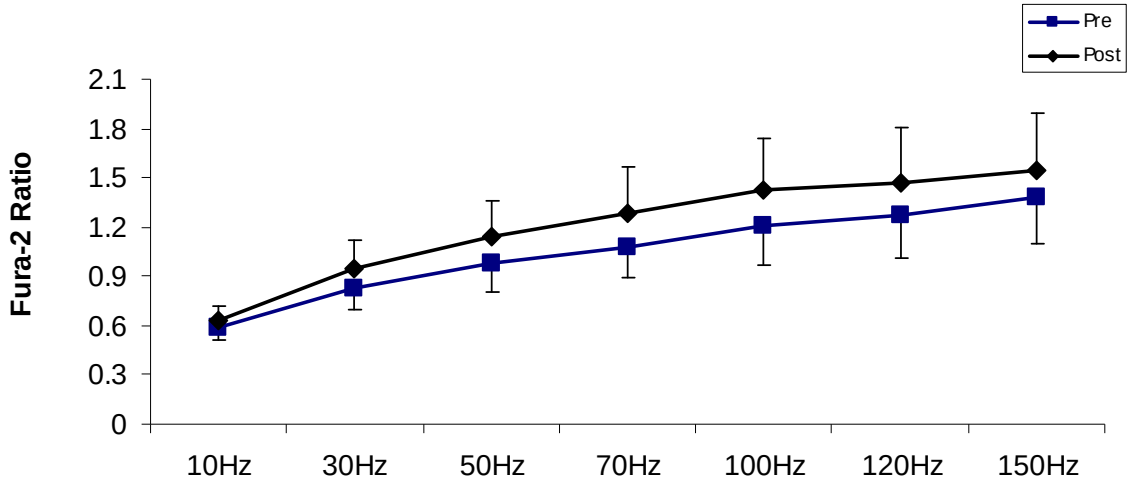

Figure 14. Pre- vs. post-fatigue peak Fura-2 ratio in Vehicle treated single muscle fibres from CON mice. Peak Fura-2 ratios are shown across the range of stimulation frequencies assessed pre- and post-fatigue (n=5). Data shown are mean ± SE.

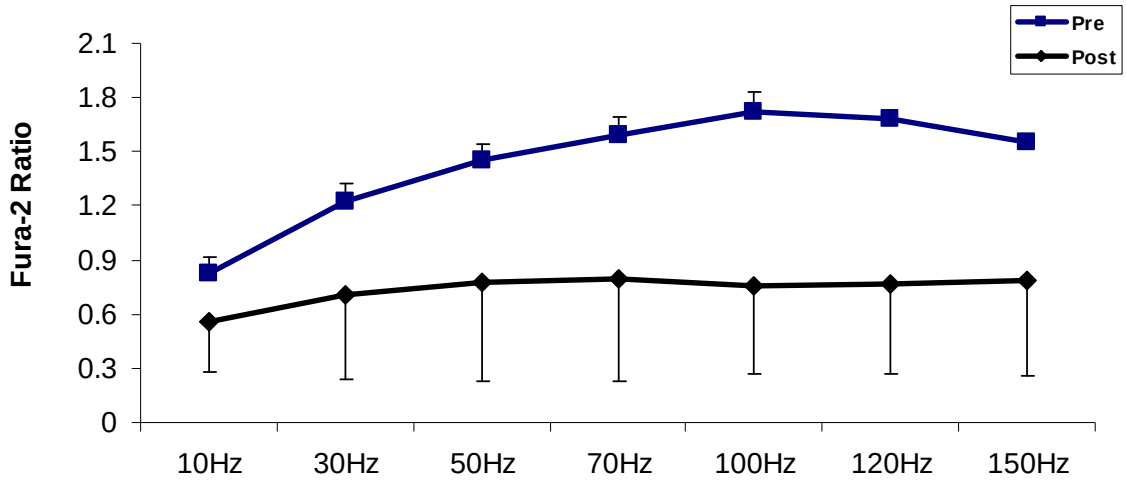

Figure 15. Pre- vs. post-fatigue peak Fura-2 ratio in Vehicle treated single muscle fibres from Utr$^{-/-}$/*mdx* mice. Peak Fura-2 ratios are shown across the range of stimulation frequencies assessed pre- and post-fatigue (n=2). Data shown are mean ± SE.

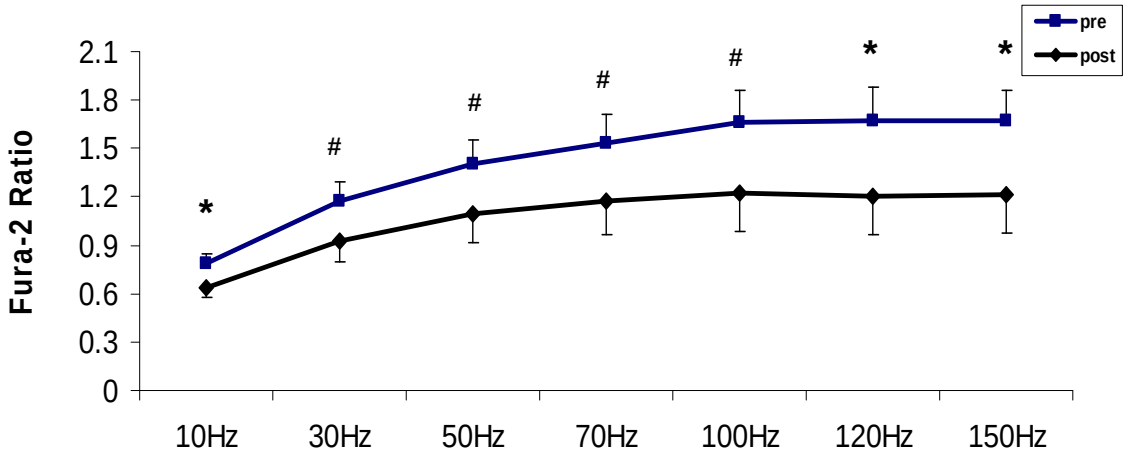

Figure 16. Pre- vs. post-fatigue peak Fura-2 ratio in Vehicle treated single muscle fibres from *mdx* mice. Peak Fura-2 ratios are shown across the range of stimulation frequencies assessed pre- and post-fatigue (n=9). Data shown are mean ± SE. * $p<0.05$; # $p<0.10$.

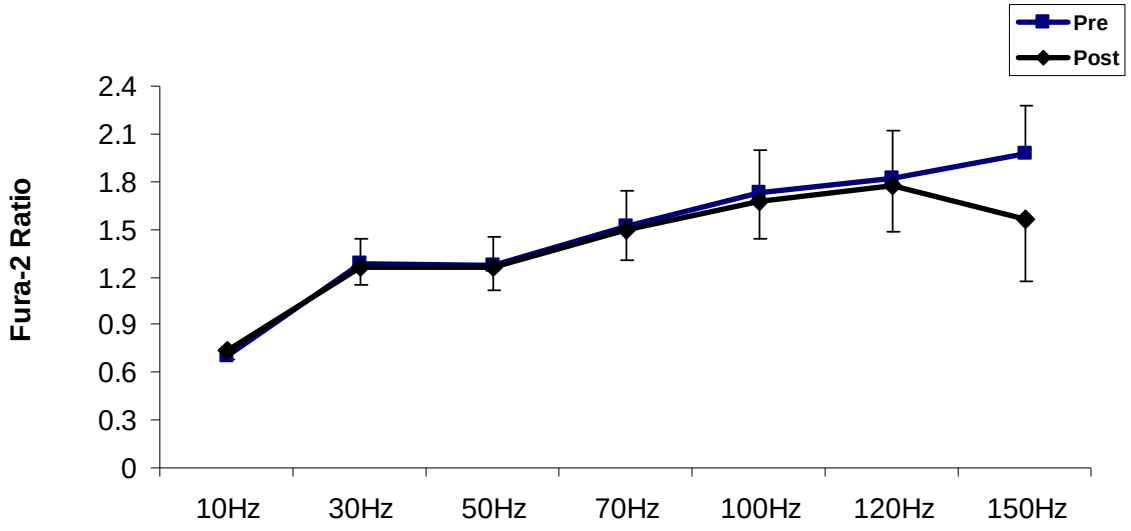

Figure 17. Pre- vs. post-fatigue peak Fura-2 ratio in ALLN treated single muscle fibres from CON mice. Peak Fura-2 ratios are shown across the range of stimulation frequencies assessed pre- and post-fatigue (n=5). Data shown are mean ± SE.

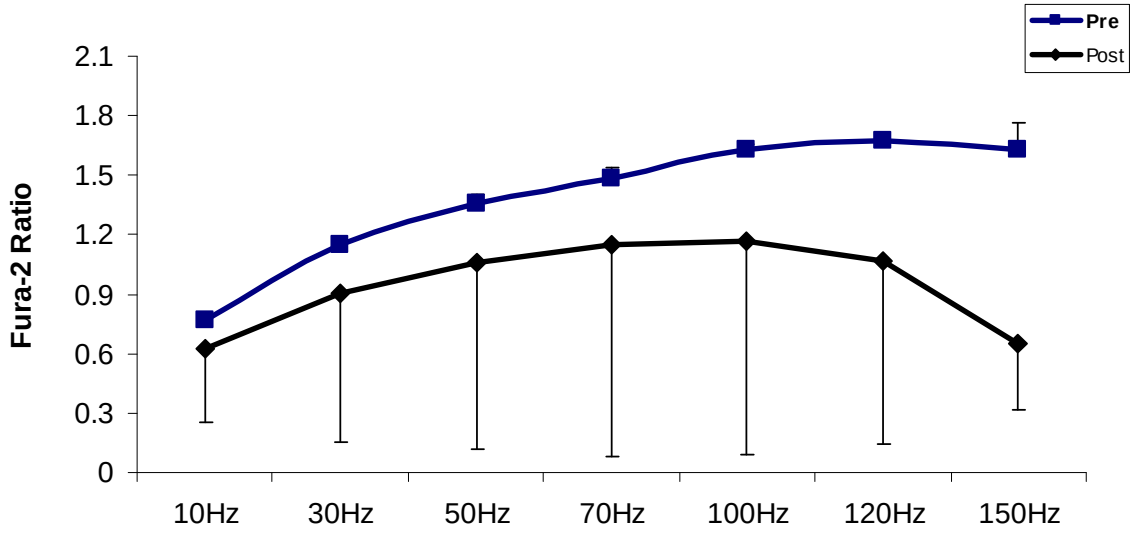

Figure 18. Pre- vs. post-fatigue peak Fura-2 ratio in ALLN treated single muscle fibres from Utr$^{-/-}$/*mdx* mice. Peak Fura-2 ratios are shown across the range of stimulation frequencies assessed pre- and post-fatigue (n=2). Data shown are mean ± SE.

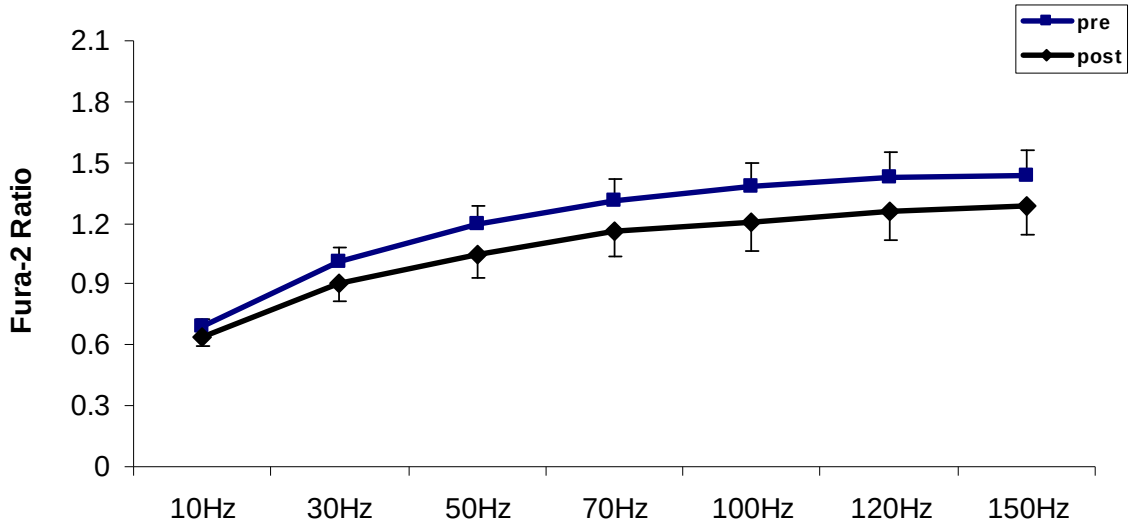

Figure 19. Pre- vs. post-fatigue peak Fura-2 ratio in ALLN treated single muscle fibres from *mdx* mice. Peak Fura-2 ratios are shown across the range of stimulation frequencies assessed pre- and post-fatigue (n=15). Data shown are mean ± SE.

Chapter 4: Discussion

Although the primary cause of DMD has been related to the lack of the protein dystrophin (79), many of the underlying mechanisms contributing to the disease severity have not been identified. The weakening of the muscle membrane is considered to be one of the mechanisms contributing to the disease severity (18). It is known that dystrophic muscle has greater susceptibility to damage during eccentric contractions compared to normal muscle (169). A second mechanism that is thought to contribute to the disease severity is related to signaling modifications within dystrophic muscle. Studies have shown that muscles lacking dystrophin have increased oxidative stress, decreased antioxidant capacity, and poor intracellular Ca^{2+} handling (66; 128; 80).

The present study was designed to compare intracellular Ca^{2+} regulation, fatigue resistance, and the prolonged muscle weakness in two animal models for DMD. Also, we evaluated the role of calpain inhibition in prolonged muscle weakness in dystrophic muscle. Our results agree with previous findings by demonstrating impairments in intracellular Ca^{2+} handling in dystrophic muscle (104; 166; 75). It was observed that dystrophic SMFs have higher resting $[Ca^{2+}]_i$ and slower rate of Ca^{2+} clearance. Yet, we did not observe differences in peak tetanic Ca^{2+} between dystrophic mouse models and controls as previously reported (80; 165; 166). Present findings suggest that SMFs from dystrophic animals have similar resistance to fatigue as controls, but are less likely to respond to electrical activation after being challenged with fatiguing contractions. A novel finding from this investigation is related to the role of calpains in the prolonged muscle weakness in dystrophic muscle. Dystrophin deficient SMFs treated with calpain inhibitor were able to maintain Ca^{2+} peaks after fatiguing contractions, whereas fibres treated with vehicle showed prolonged reductions in peak Ca^{2+} after fatigue. An overall summary of the present findings is shown in table 3.

Table 3 – Summary of differences between the two dystrophic mouse models compared to controls.

	mdx	**Utr$^{-/-}$/*mdx***
Fibre length	Similar to CON	Similar to CON
Fibre diameter	Similar to CON	↓↓
Resistance to fatigue	Similar to CON	Similar to CON
Increase in resting Ca^{2+} during fatigue	Similar to CON	Similar to CON
Resting Ca^{2+}	↑↑	↑
Ca^{2+} clearance	Similar to CON	↓↓↓
Ability to respond to stimulus after fatigue	↓	↓↓↓
Ability to maintain Ca^{2+} peaks after fatigue	↓↓	↓↓↓

Morphology of muscle fibres

Capote and colleagues (29) assessed the morphological characteristics of SMFs from Utr$^{-/-}$/*mdx* mice compared to CON and *mdx*, and found that Utr$^{-/-}$/*mdx* SMFs are thinner and shorter compared to the fibres from other mice. Results from the present study also reported that the diameter of SMFs from Utr$^{-/-}$/*mdx* is smaller compared to CON and *mdx*. However, we did not observe differences in fibre length between groups. Differences in the number of analyzed fibres could be one of the factors contributing to the discrepancies in findings. Therefore, a more thorough evaluation with an increased number of fibres is needed to confirm if Utr$^{-/-}$/*mdx* SMFs have reduced diameter and shorter in length.

Resistance to fatigue in dystrophic muscle

The present results show that resistance to fatigue is similar between dystrophic and normal SMFs. It has been previously reported that the EDL muscle from the *mdx* mice have reduced ability to sustain fatiguing contractions at 35°C (162). However, no differences in

fatigue resistance at 20°C were reported in the same study between *mdx* and age-matched controls during the first 2 minutes of fatiguing contractions, but at the end of the fatigue protocol (5 min.) the EDL from *mdx* mice demonstrated a greater fatigue (162). Contrary to these findings, Hayes and Williams reported that the EDL from *mdx* mice shows greater fatigue than controls during the first 2 minutes of repeated contractions at 20°C, while no differences were present at the end of 5 minutes (74). Other studies have demonstrated that the EDL muscle of *mdx* mice is less fatigable compared to controls at more physiological temperatures (35°C), while no differences are seen under lower temperatures (20°C) (1; 9; 54). Our results agree with the studies demonstrating no changes in fatigue resistance between the EDL muscle from *mdx* and control mice at ambient (20-22^{o}C) temperature.

Differences in findings can be attributed to several factors. First, most studies have evaluated whole muscle resistance to fatigue, while we evaluated individual SMFs. Whole muscle is a mixed population of fibres. The EDL is a mixed fast-twitch muscle with higher percentage of type IIb fibres (88%), whereas the FDB is 75% type IIX/D and 25% of a mix of type I and IIa fibres (13; 5). It is not known if the fibres in the present study were either type I, type IIa, type IIx, or type IIb. Secondly, different results could be related to the type of muscle preparation used. In most studies evaluating fatigue resistance, muscles are set at length for optimal force production, and then exposed to fatiguing contractions. This produces a stretch component to some sarcomeres undergoing fatigue. In the protocol used in the present study, SMFs were not stretched and during stimulation undergo unloaded shortening. Although the protocol used in whole muscle studies does not involve significant lengthening contractions, the stretching of some sarcomeres could have influenced the findings. Dystrophic muscle is known to demonstrate a much greater drop in force during isometric contractions (168), and this could have yielded a faster fatigue rate. In the

unloaded SMFs used in the present study, there would be no sarcomeres being lengthened and therefore they are less susceptible to a stretch-induced damage.

One of the limitations in using SMF for assessing fatigue is the variability between fibres. As shown by Lannergren and Westerblad (101), the time to reach fatigue in SMFs from a normal FDB ranges greatly (between 2 to 24 minutes). This contributes to variability within groups, and could limit our findings regarding differences in fatigue resistance between mouse strains. Resistance to fatigue is related to fibre diameter and length (101), and we attempted to use fibres of similar size in the present study to account for such variability. Yet, as shown in Figure 5, we reported large variability in the time to fatigue within groups (note standard error bars). Another potential limitation in the assessment of muscle fatigue in the present study is related to the criteria used to determine fatigue. Chin and Allen (33) reported that time taken to reach 30% of initial force (their criteria for muscle fatigue) corresponds to a 50% decrease in tetanic Ca^{2+}. Thus, 50% decrease in Fura-2 peak (which would correspond to a 50% decrease in tetanic Ca^{2+}) was the rationale used to determine fatigue in the present study. However, it is not known if the same criteria can be used in dystrophic muscle, since force decrease occurs faster in dystrophic muscle models while the rate of change in Ca^{2+} might not follow the same pattern.

<u>Ca^{2+} handling in dystrophic vs. normal muscle - Resting Ca^{2+}</u>

It has previously been reported that muscle samples from dystrophic patients have higher Ca^{2+} content compared to controls (39; 24) and patients with other myopathies (24). This was further supported by studies demonstrating higher resting $[Ca^{2+}]_i$ in cultured cells from DMD patients and SMFs from dystrophic mouse models (113; 14; 82). Results from the present study agree with previous findings by showing an increased resting $[Ca^{2+}]_i$ in SMFs from *mdx* compared to control mice (14; 82). Yet, other groups found no changes in

resting $[Ca^{2+}]_i$ between *mdx* and controls (36; 75; 104; 61; 102; 126). One of the reasons for such discrepancies is related to the dye used for $[Ca^{2+}]_i$ measurements. Fura-2AM is known to generate variability in $[Ca^{2+}]_i$ measurements, if time of loading and time interval between loading and data collection are not consistent (163). Other reasons for discrepancies in findings are related to the age of mice (36) and the muscles assessed (80).

Potential mechanisms that could explain the higher resting Ca^{2+} in dystrophic muscle are related to leakage of Ca^{2+} from the SR (145; 48; 22) and greater influx of Ca^{2+} through the plasma membrane during muscle contractions (3; 168; 169). Takagi and colleagues (145) evaluated Ca^{2+} control by the SR in dystrophic muscles, and results showed an increased leakiness of the SR to Ca^{2+}. Further, it was shown that dystrophic muscles have hypernitrosylated RyR, which consequently depletes one of the channel binding stabilizing proteins (calstabin). Therefore, this mechanism also contributes to Ca^{2+} leak through RyR. Moreover, this process worsens as dystrophic muscles age (22). The movement of large proteins, such as albumin and CK, through the plasma membrane of muscles lacking dystrophin suggested the potential role of membrane tears in allowing the transit of many different molecules through the plasma membrane (109). Therefore, scientists believe that Ca^{2+} influx was increased in dystrophic muscle due to the presence of such membrane tears (109). However, Yeung and colleagues (169) demonstrated that Ca^{2+} influx happens through Ca^{2+} channels and not membrane tears. Furthermore, it was shown that these channels belong to the TRPC family, and that inhibition of their activity almost completely suppressed the entry of Ca^{2+} in dystrophic fibres (150).

To our knowledge there are no studies investigating resting Ca^{2+} levels in SMFs from $Utr^{-/-}$/*mdx* mice compared to *mdx* and controls. Based on the more pronounced disease severity noticed in double mutant mice, it could be plausible that $Utr^{-/-}$/*mdx* fibres

demonstrate either similar resting $[Ca^{2+}]_i$ than *mdx* fibres, or higher values. However, resting Fura-2 ratio was similar between Utr$^{-/-}$/*mdx* and the other two groups (*mdx* and CON).

Ca^{2+} handling in dystrophic vs. normal muscle - Peak Ca^{2+}

Studies evaluating differences in Ca^{2+} peak between *mdx* and control fibres have shown inconsistent results (36; 80; 104; 165; 166). While some studies have reported no differences between *mdx* and control mice (147; 148; 75), others have shown lower Ca^{2+} release in dystrophic muscle (80; 104; 165; 166). The present study reported no differences in Ca^{2+} peak at several different stimulation frequencies between *mdx*, Utr$^{-/-}$/*mdx*, and con mice. Disagreements in findings could be related to type of fluorescent dye used (high affinity vs. low affinity). Studies using high affinity fluorescent dyes did not report any differences in peak Ca^{2+} (75; 36; 147; 148), whereas studies using low affinity Ca^{2+} dyes showed lower Ca^{2+} release in *mdx* fibres (80; 165; 166). According to Hollingworth (80), high affinity slowly responding Ca^{2+} dyes, such as Fura-2 and Indo-1, do not allow one to accurately distinguish changes in Ca^{2+} amplitude and time course (80), Another reason for disagreements in findings can be related to the method for loading the dye (microinjection vs. AM-loading). Fluorescent dyes that are loaded into fibres by the presence of the AM portion might yield less reliable Ca^{2+} measurements than dyes loaded by microinjection (80). Lastly, as suggested by Hollingworth et al. (80), the method for SMF isolation might influence in the assessment of Ca^{2+} levels (enzyme-dissociated vs. manually dissected).

The dystrophic groups in the present study had more fibres failing to maintain peak Ca^{2+} compared to controls (Utr$^{-/-}$/*mdx*: 50%; *mdx*: 40%; CON: none). As shown by Capote et al. (29) SMFs from *mdx* and Utr$^{-/-}$/*mdx* can be separated in two groups: those with similar action potential (AP) duration and amplitude as controls, and those with longer AP duration

and amplitude as controls. Fibres with similar AP as controls released at least 30% less Ca^{2+} when stimulated compared to controls, whereas fibres with longer AP showed less than 60% of peak Ca^{2+} from controls (29). The authors also observed that SMFs with longer AP had abrupt limitation in Ca^{2+} release at 100Hz, whereas this was almost unnoticed at 50Hz (29). This suggests that some dystrophic muscle fibres have impaired Ca^{2+} release at higher frequencies due to longer AP.

Ca^{2+} handling in dystrophic vs. normal muscle

The rate of muscle relaxation is influenced by factors such as parvalbumin (PV) levels and Ca^{2+} uptake by the SR. Studies evaluating levels of PV in dystrophic muscle have shown dissimilar results. When measuring developmental changes in PV levels in dystrophic muscle, Sano et al. (133) reported a reduced amount of protein levels of PV in *mdx* mice compared to controls. However, others have shown that PV turnover is increased in dystrophic muscle due to increased mRNA levels, but no data on PV protein levels were reported (61). The increased levels of PV mRNA might be a compensatory mechanism due to higher resting Ca^{2+}. Dystrophic muscle is known to have impaired Ca^{2+} uptake due to reduced SERCA activity (87; 51; 94; 41). Kometani and colleagues demonstrated that the rate of relaxation of the EDL of *mdx* mice is slower compared to controls and this due to reduced SR Ca^{2+} uptake (94). In 1988, Tuner et al. (148) demonstrated that the mean half decay time for Ca^{2+} transients is much longer in dystrophic muscle compared to controls. It has been shown that treatment of dystrophic SMF with taurine or CK, increases SERCA activity which consequently speeds SR Ca^{2+} uptake (48; 127). Moreover, the overexpression of SERCA improved the dystrophic phenotype in the *mdx* mice (69; 114). This impaired Ca^{2+} uptake in dystrophic muscle is thought to be one of mechanisms contributing to the

worsening of the disease. Therefore, improving SERCA activity and Ca^{2+} uptake could be a potential target in improving DMD.

Results from the present study demonstrate that Fura-2 peak clearance is not different between *mdx* and controls, but that SMFs from Utr$^{-/-}$/*mdx* mice take longer to clear Fura-2 peak compared to controls. Moreover, a trend for differences between *mdx* and Utr$^{-/-}$/*mdx* was found for 50Hz. Nevertheless, findings should be carefully evaluated. The present study did not measure SR Ca^{2+} uptake or SERCA activity; thus, Ca^{2+} uptake was estimated based on 75% clearance of the total Fura-2 peak at 50 and 120Hz. It is known that most of the Ca^{2+} binds initially to PV after muscle contraction and after that it is taken up by the SR Ca^{2+} ATPase to allow muscle relaxation (133). In the current study we could not differentiate between PV binding and SR Ca^{2+} uptake, although this difference is most likely due to SR function since the SR pumping capacity controls the slower steady state removal of Ca^{2+} in the latter part of the Ca^{2+} transient (156). As proposed by Andrade and colleagues (10), the slow final phase of Ca^{2+} decline after tetanus (Ca^{2+} "tail") can be used to estimate SR Ca^{2+} pump function. Therefore, the evaluation of Ca^{2+}-tails can give a more reliable measure of Ca^{2+} uptake.

No previous study has evaluated Ca^{2+} uptake in SMFs from Utr$^{-/-}$/*mdx* mice. Although it could be hypothesize that Utr$^{-/-}$/*mdx* fibres might have greater impairment in SR Ca^{2+} function, the lack of studies evaluating key components related to muscle relaxation (PV levels and SERCA activity) in these animals, limit a conclusions about their SR Ca^{2+} control.

Increase in resting Ca^{2+} during fatigue

Although we expected a greater increase in resting Ca^{2+} during fatigue in both dystrophic mouse models compared to controls, no differences were observed. This was surprising since dystrophic SR Ca^{2+} uptake is slower compared to controls in response to

single tetanus. Therefore, it would be expected that impaired Ca^{2+} uptake would contribute to a much greater increase in resting Ca^{2+} during fatigue in dystrophic SMFs. Yet, increases in resting Ca^{2+} during fatigue were similar between all mouse strains. We suggest that lack of differences could be due to the time between muscle contractions during fatigue. The shortest time between fatiguing contractions was one minute, which seams to be enough time to allow clearance of most Ca^{2+} in all mouse strains. Thus, the slower rate of Ca^{2+} clearance in the $Utr^{-/-}$/*mdx* was in the millisecond range (see Figure 12). Therefore, we can hypothesize that if the time between contractions decreased (i.e. 1 every 0.5 sec), then differences would be observed.

Effects of calpain inhibition in dystrophic muscle

Calpains are non-lysosomal Ca^{2+}-activated proteases that, when activated, participate in the breakdown of muscle constituents. Due to improper Ca^{2+} handling in dystrophic muscle, with higher resting Ca^{2+} and increased Ca^{2+} influx during muscle contractions, it has been suggested that calpains could be one of the causes for the severe muscle pathology experienced by DMD patients. Therefore, studies have evaluated the treatment of *mdx* mice with calpain inhibitors but results have been inconclusive (135; 14; 140; 27). Differences in the type of calpain inhibitor used (leupeptin or calpastatin), mode of administration, and length of treatment (30 days vs. 6 months), explain differences in these results. Badalamente and Stracher (14) gave direct leupeptin muscle injections in the *mdx* mice for 30 days, while Spencer and Mellgren (140), Briguet et al. (27) and, Selsby et al. (135) crossed the *mdx* with the calpastatin overexpressing mouse. Also, in the study by Briguet and colleagues, mice were studies at 3 and 7 weeks of age (27). Contrarily, in the studies by Selsby et al. (135) and Spencer and Mellgren (140) mice were studies at 6 months and 4 weeks of age, respectively.

No studies have investigated the role of calpains during muscle contractions leading to muscle weakness in dystrophic muscle. Therefore, we hypothesized that inefficient Ca^{2+} control experienced in dystrophic muscle would be exacerbated during fatigue. This would activate calpains and contribute to greater E-C coupling disruption in SMFs lacking dystrophin. Based on our findings, the reduction in Ca^{2+} post-fatigue was eliminated with ALLN, suggesting the role of calpains in prolonged muscle weakness after fatiguing contractions in dystrophic muscle. However, present findings need to be interpreted with caution. In first place, stimulated muscle has not been examined to test if calpains were actually activated during the fatigue protocol. Secondly, if calpains were to be activated, we did not test if the calpain inhibitor was able to suppress calpain activation. In order to address these issues, separate FBD muscles or strips from dystrophic mice have been exposed to different protocols and frozen for future analysis to address these limitations. We will perform an enzyme assay to measure total caseinolysis (indicative of calpain activity) according to previously established protocols.

Conclusion

The present results show that E-C coupling disruption during fatigue is similar between SMFs from $Utr^{-/-}$/*mdx* mice compared to SMFs from both *mdx* and CON mice; therefore the first hypothesis of the present project is rejected. Moreover, observed findings demonstrate that the prolonged muscle weakness due to E-C coupling disruption is exaggerated in SMFs from $Utr^{-/-}$/*mdx* compared to *mdx* and control mice; thus, our second hypothesis is accepted. Lastly, inhibition of calpain activity attenuated the disruption of E-C coupling in *mdx* SMFs while a tendency was seen in $Utr^{-/-}$/*mdx* SMFs. Therefore, our last hypothesis is partially accepted.

This study is the first to demonstrate the potential role of calpains in the prolonged muscle weakness experienced after fatigue in dystrophic muscle. This adds evidence to support the hypothesis that improper Ca^{2+} handling contributes to the disease progression in DMD. However, DMD is a complex disease that should be approached from various perspectives. The multi-factorial aspect of the disease demands a combination of treatments targeting reductions in oxidative stress, increases antioxidant capacity, and improvements in Ca^{2+} handling in skeletal and cardiac muscle. Many studies using the *mdx* mouse have demonstrated the efficacy of drug treatments in decreasing muscle damage, reducing fibrosis, and improving muscle function in dystrophic muscle. Nevertheless, the *mdx* mouse does not manifest similar disease severity and progression as seen in DMD patients. Therefore, future studies will need to evaluate the effectiveness of treatments (alone and/or combined) in better animal models as well as patients with the disease.

Chapter 5: Review of Literature

Skeletal muscle plasticity

Skeletal muscle is a very plastic tissue with the ability to respond to many different stimuli (81; 107). Factors such as exercise training (i.e. endurance or resistance training), ageing, disuse (i.e. bed rest or immobilization), and various disease states (i.e. DMD or AIDS), induce changes in skeletal muscle. Yet, skeletal muscle adaptations are unique to each individual which shows the complexity of its control. For instance, this variability is fairly common in human exercise training studies, as it has been shown by Hubal and colleagues (83). They evaluated men and women undergoing unilateral resistance training (all subjects trained under the same conditions) and results showed that the muscle adaptations varied greatly between individuals (83). While some studies aim to better understand mechanism driving skeletal muscle adaptations in healthy muscles, other investigations evaluate molecular and cellular alterations leading to changes in muscles in diseased states. Hence, mechanisms inducing changes in diseased muscles are far less understood and more complex compared to normal muscle. Therefore, two major challenges are faced by scientists when studying diseased muscles: the first challenge is related to understanding mechanisms leading to disease, while the second pertains to proposing interventions to improve muscle function and lessen disease severity.

5.1 - Background on Duchenne muscular dystrophy

Duchenne muscular dystrophy (DMD) is one of the most frequent and devastating types of muscular dystrophy that affects the human race (154). Even though one in 3500 boys are born with the disease (2) and only a few cases affecting girls have been reported, DMD has received aggressive consideration due to its fast progression and early death of

patients (23; 144). The reduced lifespan, not extending beyond the age of 30, is a consequence of progressive muscle wasting which leads to cardiac and respiratory failure (23). Additionally, the loss of the ability to walk occurs in boys between the ages of six and 12 (16). However, the rate of progression of DMD may be different throughout the population diagnosed with the disease. Some subjects become wheelchair bound by the age of 8 while some others are able to sustain walking until the age of 15 (93). In addition to physical limitations observed in DMD, mental and biomechanical impairments have also been noted (23; 78; 161).

Duchenne muscular dystrophy is named after the French scientist Duchenne de Boulogne, who reported the first case of cognitive problems in a child during the second half of the 19^{th} century (23). Yet, the main cause of the disease, lack of the protein dystrophin, was not known until the 1980's (79). The gene responsible for DMD is one of the largest genes in the human genome (23), and is expressed in skeletal, cardiac, and smooth muscle and brain (103). The gene has at least seven promoters and is encoded by 79 exons spanning $\geq$2.4 million base pairs (103). Duchenne's is an X-linked disease, meaning that the defective gene can be passed on to either male or female offspring, but its occurrence is more common in the male population due to the single copy of the X chromosome (43). Duchenne muscular dystrophy has been reported in females, but the presence of one healthy X chromosome reduces the severity of muscle degeneration when compared to that seen in males (111). It is known that one in three new cases of DMD had no previous family history diagnosed, which demonstrates the complexity of a genetic disease (164).

Due to progressive muscle damage and atrophy, DMD patients require continued intense medical attention. The skeletal muscle of dystrophic patients has limited regenerating capacity and, as a result, is gradually replaced by fibrous and fat tissue (144). Moreover, lack of dystrophin can increase muscle tissue exposure to damage during contractions (25).

Patients with DMD undergo other medical difficulties. In late stages, there is a higher risk of developing osteoporosis, urinary problems, and gastrointestinal complications (155). Duchenne muscular dystrophy patients also increase their chances of developing scoliosis at an earlier age due to muscle weakness and being wheelchair bound (43; 155). The goal of medical treatment is to improve the quality of life and increase the patient's lifespan. The increase in the natural life span of those with DMD is due to multidisciplinary care coordinated by medical doctors, which include intense physical therapy, routine vaccinations, antibiotic prescriptions, and the use of corticosteroids to increase ambulation and slow the disease progression (155).

Children with DMD undergo kinetic and kinematic adaptations due to the progressive muscle weakness (65). Therefore, certain muscle groups are used more in order to compensate for the decrease in force and increase of stiffness of other muscles. As proposed by Gaudreault and colleagues (65), ambulation and posture support are maintained in patients with DMD by the hip and plantar flexors, and the hamstring group. The loss in range of motion, or joint contractures, follows muscle weakness and has relevant contribution to physical impairments in DMD (65). Thus, the outcome of joint contractures is an increased resistance to passive stretch in some joints (65). Bakker et al. (16) proposed that the decreased muscle strength in ankle dorsiflexion and extension of the hip may be key indicators of ambulation loss in DMD. Additionally, the same group suggested that information about ambulation restriction in patients with DMD is very limited (16).

The effect of exercise training in DMD has been controversial. It has been proposed that increasing muscle quality might be beneficial for children with DMD. Strength improvements have been reported in the literature, but restricted methodologies and subject selection still prevent conclusive findings (93). It is known that contractions that stretch the muscle, or eccentric contractions, contribute to the disease progression. However, potential

benefits from muscle shortening contractions, or concentric exercise, may be useful to preserve muscle strength in children with DMD (93; 136; 169) without damaging the muscle. Strengthening exercises prescribed for patients with DMD should aim to decrease the progression of muscle weakness rather than generate increase in strength (93). Decreasing disease progression may prolong the patient's life, and enhance their quality of life. However, exercise prescription for patients with DMD still needs further investigation in order to adequately assess its potential benefits.

5.2 - Mouse models for DMD

The most used mouse model for muscle degeneration studies until the early 1980's was the *dy* and dy^{2J} mutants. However, issues were raised about their similarity with DMD (28). It was not known if these animals were either myogenic or neurogenic in origin (28). Also, *dy* mutants demonstrate paralysis of their hind limbs between 3 and 4 weeks of age with an increased fragmentation in atrophied muscle fibres (28). In 1984, Bulfield and colleagues published an investigation that would greatly add to studies investigating the underlying mechanisms of DMD (28). The authors were the first to describe the *mdx* mouse, an animal with a natural mutation in the X chromosome from an original colony of C57BL/10 (28). The group reported that these animals had high levels of CK and pyruvate kinase, and demonstrated similar muscle histological lesions as DMD patients (28). After their discovery, hundreds of studies used the *mdx* mice to evaluate the underlying mechanisms in DMD. Studies have shown that the *mdx* mouse has decreased muscle specific force (1), increased damaged during lengthening contractions (112; 169), increased macrophage accumulation, and increased fibrosis with aging (88). However, the *mdx* mouse has a relatively normal lifespan and the only muscle group demonstrating similar disease

progression as seen in humans is the diaphragm (143). The *mdx* mice overexpresses utrophin, a protein with similar role as dystrophin, and that could be the reason for a normal lifespan (122).

It has been suggested that animals lacking both proteins, dystrophin and utrophin, would be a better model for DMD patients (37). To generate the double mutant mouse, Deconinck et al (50) first generated the $Utr^{-/-}$ mouse (49) and then crossed the $Utr^{-/-}$ into the *mdx* C57BL/10 background. Briefly, female C57Bl/10 *mdx* mice mated with male $Utr^{-/-}$ and resulted in the F1 generation containing utrophin heterozygous mice and either *mdx* heterozygous (females) or *mdx* male hemyzygous (50). Then, three other generations were crossed to generate the $Utr^{-/-}$/*mdx* male mouse (50). Contrarily from the *mdx* mouse, the $Utr^{-/-}$ /*mdx* have altered neuromuscular and myotendinous junctions, early onset of damage in the diaphragm, joint contractures, kyphosis, and premature death by the age of 20 weeks (50). Yet, the small number of studies comparing the two animal models limits the conclusion about which animal model is better for DMD studies.

The normal lifespan of the *mdx* mice has been related to continued satellite cell function. After an episode of muscle damage, satellite cells are activated, thus dividing and producing myoblasts that fuse at the site of muscle injury (30). Patients with DMD have great loss in functional muscle stem cells, while this is not as severe in the *mdx* mice (131). In a recent study, Sacco and colleagues reported that *mdx* mice also lacking the RNA component of telomerase (*mdx*/mTR), an enzyme related to maintaining telomere length, have similar disease progression as seen in DMD patients (131). The similar disease progression occurs due to the reduced size of telomeres, which are DNA repeats responsible for maintaining genomic stability (131). The study also demonstrated that satellite cell function in the *mdx*/mTR decreases with aging and it's parallel with muscle wasting (131).

Furthermore, *mdx*/mTR could be a better mouse model for future studies evaluating the underlying mechanisms affecting the muscle of dystrophic patients.

5.3 - Calcium handling in dystrophic muscle

Intracellular calcium (Ca^{2+}) participates in the process of force generation and controls the activity of signaling molecules. Abnormalities in Ca^{2+} control, especially increased Ca^{2+} levels at rest, have been implicated in making skeletal muscle cells more prone to necrosis (41) as well as activating Ca^{2+} dependent proteases (119). Several studies have investigated $[Ca^{2+}]_i$ in dystrophic muscle but results have been somewhat inconsistent. The purpose of this section is to discuss the current knowledge on $[Ca^{2+}]_i$ in muscles lacking dystrophin.

5.3.1 - Evidence of higher intracellular Ca^{2+} and SR Ca^{2+} dysfunction

Early studies have shown that muscle biopsies from DMD patients have increased Ca^{2+} content. Bodensteiner and Engel evaluated the localization of Ca^{2+} in muscle samples from DMD patients and individuals with other myopathies. Muscle samples were stained via von Kossa method, with alizarin red, and with glyoxalbis-(o-hydroxyanil) to measure Ca^{2+} positive fibres; results demonstrated that more than 40% of DMD muscle fibres were Ca^{2+} positive while this was rarely found in other myopathies (24). This was further confirmed by Cornelio and Dones (39). In addition to Ca^{2+} assessment, the authors also performed the staining for albumin (a marker of extracellular fluid inflow) in muscle lacking dystrophin (39). The amount of albumin was also higher in muscle samples from DMD patients compared to samples from individuals with other muscle diseases (39). Others have used fluorescent dyes to evaluate $[Ca^{2+}]_i$ in the dystrophic cells. Fluorescent dyes, such as Fura-2, measures intracellular free Ca^{2+} concentration in contrast to the methods used by

Bodensteiner and Engel (24) and Cornelio and Dones (39). Mongini et al. used the fluorescent dye quin 2 to measure resting and peak free Ca^{2+} in cultured dystrophic muscle samples. Results demonstrated that resting and peak free $[Ca^{2+}]_i$ were higher in dystrophic cells compared to controls (113).

Intracellular calcium levels were also evaluated in the *mdx* mouse. The increased resting $[Ca^{2+}]_i$ reported by Mongini et al. (113) was also confirmed by others, but in SMFs from dystrophic animals (14; 82). Yet, no differences in $[Ca^{2+}]_i$ levels between *mdx* muscle fibres and controls have also been reported (61; 102; 126). Most of the discrepancies in findings have been linked to a) differences in the methods applied for the use of Fura-2, b) age of the animals, and c) different muscles assessed.

The increase in resting $[Ca^{2+}]_i$ suggested a potential impairment in Ca^{2+} handling by the sarcoplasmic reticulum (SR). The SR is a major muscle organelle responsible for Ca^{2+} storage, release, and uptake. Moreover, the Ca^{2+} is released from the SR by the opening of the ryanodine receptors (RyR), and then eventually cleared from the cytoplasm by SR Ca^{2+} pumps (SERCA). Most of the Ca^{2+} located in the SR is bound to calsequestrin, and it has been reported that calsequestrin-like proteins in the SR of muscles lacking dystrophin are reduced (42). The SR is one of the key regulators of $[Ca^{2+}]_i$, and appropriate cycling of Ca^{2+} is required for muscle contraction and relaxation. It has been shown that SR function is altered in DMD. Isolated SR from dystrophic muscle has decreased velocity of Ca^{2+} uptake after electrical stimulation compared to controls (87). However, the Ca^{2+} sensitivity of SERCA is not changed between controls and *mdx* mice (87). Divet and Huchet-Cadiou (51) reported slower Ca^{2+} uptake by the SR in dystrophic muscle, but the authors suggested differences between fast and slow twitch muscles. Furthermore, it has been reported that the levels of Ca^{2+}-ATPase of fast-twitch skeletal muscle sarcoplasmic reticulum (SERCAla) is not the same across muscles that show different disease severity (40; 52; 53).

Different drugs can improve SERCA activity. Elevations in the levels of taurine have been shown to increase the uptake of Ca^{2+} by SERCA in normal muscle (84). This was later tested in *mdx* muscle fibres and results pointed to the beneficial effect of taurine supplementation on E-C coupling function, which was linked to improved SR Ca^{2+} uptake (48). Also, increasing the levels of CK in cultures of *mdx* myotubes has been shown to improve Ca^{2+} uptake, while not affecting Ca^{2+} entry from the extracellular space or Ca^{2+} efflux (127). Lately, studies have reported an improvement in dystrophic phenotype by overexpressing SERCA1 in dystrophic mice (69; 114), but replication of findings in animals models with similar disease progression as seen in humans is needed. Nevertheless, Morini and colleagues (114) studied the diaphragm of the *mdx* mouse, the muscle with greatest similarity in muscle pathology to human disease, and demonstrated increased SERCA1b levels (50% more compared to *mdx* mice) which correlated with improved force recovery after eccentric contraction. Another SR Ca^{2+} dysfunction present in dystrophic muscle is related to RyR. Takagi and colleagues (145) evaluated Ca^{2+} control by the SR and results showed an increased leakiness of Ca^{2+}. This has been linked with increases in resting Ca^{2+} levels, and further related to impaired Ca^{2+} release, which affects E-C coupling (48). Thus, the prolonged increase in resting Ca^{2+} levels can contribute to the saturation of SERCA (48). In 2009, Bellinger and colleagues demonstrated that RyR of *mdx* mice are hypernitrosylated. The hypernitrosylation of RyR increased SR Ca^{2+} leakage by depleting the channel complex of calstabin 1 (calcium channel stabilizing binding protein) (22). Furthermore, the hypernitrosylation of RyR with depletion of calstabin 1 and increased SR Ca^{2+} leakage is worsen as the dystrophic mice age (22).

5.3.2 - Stretch-activated channels and Ca^{2+} levels

The higher resting $[Ca^{2+}]_i$ levels in DMD have been associated with stretch-activated channels that allow greater influx of Ca^{2+} during eccentric contractions. For many years scientists have defended the idea that the lack of dystrophin increases chances of membrane tear during muscle contractions, thus increasing influx of Ca^{2+} from the extracellular space. The movement of large proteins, such as CK and albumin, through the cell membrane suggested that membrane defects might result from tears in the membrane (109). In 2000, Alderton and Steinhardt (3) reported an increased Ca^{2+} influx in dystrophic myotubes, which was shown to be inhibited with Ca^{2+} channel antagonists, suggesting that Ca^{2+} was probably not coming in the muscle through membrane tears. Also, although muscles are more liable to damage due to eccentric contractions and this damage is more pronounced in dystrophic muscle (169), it has been shown that Ca^{2+} entry in isolated SMFs of *mdx* mice occurs via channels rather than membrane tears (169). Stretch-activated Ca^{2+} channel blockers greatly reduced the influx of Ca^{2+} in the *mdx* mice following eccentric contractions (169). Thus, Ca^{2+} channel blockers such as streptomycin and the spider venom toxin GsMTx4 reduced the increase in resting $[Ca^{2+}]_i$, with eccentric contractions and partially suppressed the decline in tetanic $[Ca^{2+}]_i$ and force (169). The oral administration of streptomycin also demonstrated potential benefits to DMD, since muscles from treated animals had decreased central nucleation (a marker of muscle damage) compared to non-treated *mdx* mice (169).

The increased mechanosensitive channel activity has been suggested as a cause of increased Ca^{2+} influx in DMD. In 1994 Franco-Obregon and Lansman showed that the resting activity of mechanosensitive ion channels is elevated in dystrophin-deficient muscle compared to controls (59). Moreover, it was shown that these mechanosensitive channels are the store-operated channels belonging to the transient receptor potential canonical (TRPC) channel family, and such channels were responsible for the increased Ca^{2+} influx in DMD

(150). Antisense based inhibition of 3 types of TRPCs (TRPC 1, 3, and 6) decreased Ca^{2+} influx in dystrophic fibres by 90% (150). Blockers to stretch-activated channels have shown dramatic improvements in preventing an increase in $[Ca^{2+}]_i$ and minimizing the reduction in isometric force (66; 169). Thus, these blockers reduced the increase permeability occurring due to stretch contractions, which demonstrated that the increase permeability occurred as a secondary consequence to Ca^{2+} entry (160). It was further shown that the TRPC1 gene is one the candidates for being involved in the increased Ca^{2+} entry (66). Gervasio and colleagues (66) demonstrated that TRCP1 has a role in DMD by showing that TRCP1 binds to caveolin-3 (scaffolding protein related to binding and regulating other proteins) which increased Ca^{2+} entry through the plasma membrane. Moreover, the levels of TRPC1 and caleolin-3 are higher in *mdx* mice compared to controls (66). Another gene suggested to participate in the increased Ca^{2+} influx is the transient receptor potential vanilloid 2 (TRPV2). The downregulation TRPV2 was shown to decrease Ca^{2+} entry and ameliorate some features of DMD (85).

Interestingly, the stretch-activated channels are not directly activated by stretch and studies have demonstrated that reactive oxygen species (ROS) are a major activator (71; 125). The increased ROS production is one of the characteristics in DMD (128). Treating dystrophic muscle fibres with ROS greatly increases $[Ca^{2+}]_i$ levels (66) and is inhibited by streptomycin, which supported the idea that the activation of the stretch activated channels is dependent on ROS (66). In 2009 Millay and colleagues showed that overexpression of TRPC3 was sufficient to induce similar muscle phenotypic changes to those occurring in DMD (110). Although the control of Ca^{2+} channels is thought to be one of the potential targets for treating dystrophic muscles, it has been shown that such treatment has great limitations. The long-term blocking of Ca^{2+} channels streptomycin in the *mdx* mice was evaluated and results demonstrated delayed onset of disease, reduced fibrosis, and increased

sarcolemmal stability in skeletal muscle (86). However, no positive effects were reported in either diaphragm or heart muscle, in fact heart pathology was worse with prolonged inhibition of Ca^{2+} channels (86). Findings from the study demonstrate the importance of evaluating the long-term effect of drug treatments (86), and also testing muscles that have same disease progression as seen in DMD.

5.4 - Calpains

The maintenance of muscle size is dependent in the balance between protein synthesis and break-down. The decrease in muscle mass has been linked to increased protein turnover, which consequently decreases muscle function. It is known that catabolism of proteins and amino acids are increased during moderate exercise (129). On the other hand, the rates of protein synthesis surpass protein breakdown after exercise (129). This increased protein degradation and amino acid oxidation, during exercise, have been attributed to two types of proteases, the lysosomal proteases (i.e., the cathepsin family) and the non-lysosomal proteases (i.e., calpains) (21). Yet, some evidence suggests that the activity of such proteases is only increased post-exercise, and not during exercise (119; 89). Nonetheless, the specific role of proteases, specially the non-lysosomal calpains, has been the focus of many research groups. Thus, calpains have received great attention due to the implication of their activation in various disease states, such as sarcopenia, diabetes, cachexia, acquired immune deficiency syndrome (AIDS), and muscular dystrophy (20; 146; 167; 92; 11; 137). This section will focus in explaining the function, structure, and role of calpains in healthy and dystrophic muscle.

5.4.1 – Calpains: definition, isoforms, structure, and skeletal muscle location

The calcium-dependent cysteine proteinase, or calpain, was first discovered in the rat brain but later studies demonstrated its presence in various tissues and species (73; 90; 68). Over 14 types of calpains have been identified, but the ones most well characterized are calpain 1, calpain 2, and calpain 3 (also known as p94 or CAPE3) (137). Calpain-1 is commonly called μ-calpain while calpain-2 is known as m-calpain, names given based on the amount of Ca^{2+} necessary for their activation (116). Most calpains are ubiquitously expressed while calpain-3 has been thought to be exclusively expressed in muscle (116; 137). However, studies by Konig et al. (95) and Marcilhac et al. (106) have indentified calpain-3 in other tissues. The presence of calpain-3 in skeletal muscle might be greater than calpain-1 and calpain-2, since it has been shown that mRNA levels of calpain-3 are ten times greater compared to calpain-1 or calpain 2 (138).

Calpain-1, -2, and -3 share a similar structure. Calpain-1 and calpain-2 are heterodimers containing a large subunit, 80kDa, and a small subunit (approximately 28kDa) – the small subunit is removed to allow the proteolytic activity of calpain-1 and -2 (115; 116). Calpain-3, on the other hand, has a monomeric structure of 94kDa (45; 116). All three calpain isoforms are similar in structure by possessing four domains: i) the N-terminal domain containing the site for autolysis; ii) the proteolytic domain (45; 138); iii) a C2-like region involved in membrane phospholipid interaction; iv) the Ca^{2+}-binding site which contains five EF-hand domains (138). Calpain-3 also has three inserted sequences (NS, IS1, and IS2), which are not present in the other two calpains (116). The small subunit present in calpain-1 and calpain-2 has two different domains - domain V contains a site for autolysis and has also been linked to membrane interaction, while domain VI contains five EF-hand motifs (45).

Although calpain-1, -2, and -3 are present in skeletal muscle, their location within the muscle differs. The location of calpain-1 and calpain-2 within skeletal muscle has been investigated since the 1980's, but differences in location were identified due to the different techniques used for isolating, staining, and fixing of muscle samples, as well as lack of antibodies specific for each calpain. Barth and Elce (17) located calpain-2 in the sarcolemmal region while other investigators reported its location near the Z-line and sarcolemma (46; 68). According to Yoshimura et al. (170) the antisera used in these studies demonstrated cross-reactivity with calpain-1, which could have interfered with the findings. Therefore, Yoshimura and colleagues (170) performed a more thorough methodological approach using a double affinity purified monospecific antibody to calpain-1, which did not cross-react with calpain-2, to localize calpain-1 in skeletal muscle of rats. Results demonstrated that calpain-1 was localized in the I-band region, but was not exclusively associated with the Z-line (170). Calpain-2 has been mostly found in the cytoplasm, whereas calpain-3 has been described as being found in either the triad junction, SR membrane, or localized in the myofibrillar structure (attached to titin) (96; 91). Others have demonstrated that calpain-3 is bound to the M-line of titin, but no studies have replicated the findings (64). In a study by Murphy and Lamb (118) a novel technique was used to better determine the location of calpain-3 within skeletal muscle. Skinned fibres (fibres with the sarcolemma removed) were exposed to triton X-100 and then both wash solution and fibre were run on a western blot to analyze the proteins in each fraction (118). Results demonstrated that calpain-3 is not bound in the triad junction or SR, but rather tightly bound within the contractile protein in a location corresponding to the N2A line on titin (118). Therefore, calpain-3 might be related to the control of titin, consequently influencing muscle contractile function (force production).

5.4.2 - Activation of calpain-1 and -3 depends on increases in $[Ca^{2+}]_i$

Calpains do not perform their proteolytic role unless they are activated by increases in $[Ca^{2+}]_i$. Calpains become activated by the autolysis that occurs at the N-terminal part of both subunits (45). This leads to the formation of a 78 kDa and 76 kDa subunit for m- and µ-calpain, respectively (45). After the initial autolysis the $[Ca^{2+}]$ necessary for further proteolysis is reduced (132), but the concentration needs to be maintained above resting levels (120). There is evidence demonstrating that the interaction between calpains and phospholipids reduce the $[Ca^{2+}]$ necessary for the activation of calpains, suggesting that they can be activated at lower, more physiological Ca^{2+} concentrations (132; 38). The levels of both substrates in these studies, however, were much greater than in vivo concentrations, illustrating the limitations of most studies investigating the $[Ca^{2+}]$ requirement for calpain activation.

Other studies have used more physiological levels of Ca^{2+}. Verburg and colleagues (152) used skinned fibres to the test if calpain-3 activation played a role in disruption of E-C-coupling and results showed that calpain-3 was activated after brief exposure (1 to 3 minutes) of 2 to 8µM of Ca^{2+}. Increasing the $[Ca^{2+}]$ to ~1µM or more for 3 minutes caused an irreversible reduction in depolarization induced force production (152). This reduced force production was further suppressed with the calpain inhibitor leupeptin (152). Fibres exposed to Ca^{2+} and stretch showed proteolysis of titin, which was linked to the activation of calpain-3 (152). The autolysis of µ-calpain has also been evaluated. The exposure to low $[Ca^{2+}]$ ($\leq$ 200nM) for even 1 hour does not induce the autolysis of µ-calpain, but if the levels are raised to 5µM for only a few minutes a good fraction is autolyzed (120). It is thought that at rest or during normal activity the $[Ca^{2+}]_i$ does not reach the required level for the activation of µ-calpain in muscle, but in situations of eccentric damage and disease (i.e. DMD) the entry of extracellular Ca^{2+} can lead to excessive autolysis (120; 169; 105).

Studies investigating the activation of calpains linked eccentric damage and influx of Ca^{2+} to calpain autolysis. Although Belcastro (19) reported a very high Ca^{2+} sensitivity and activation of calpains (10% and 50% of maximal proteolytic activity at 100mM and 1µM Ca^{2+}) following an exercise bout in rats (running until exhaustion), the methods used for calpain isolation and/or the non-physiological solutions may have influenced the findings (120). If the activation of calpains occurred at low Ca^{2+} concentrations, then skeletal muscle would be constantly going through degradation of proteins is response to minimal stress (120). Furthermore, the $[Ca^{2+}]_i$ does not reach very high levels during concentric exercise, while $[Ca^{2+}]_i$ reach high levels in response to eccentric contractions. Thus, an "all-out" exercise bout (cycling) in humans did not activate either calpain-3 or calpain-1 (119), while humans undergoing a single bout of eccentric exercise showed the activation of calpain-3 (117). Therefore, it was thought that eccentric contractions, which elicit an increase in Ca^{2+} influx, could lead to the activation of calpains. In animals, eccentric damage was shown to disrupt contractile protein structure, reduce membrane stability, and decrease force in muscles (171). Yet, all these were mostly suppressed when the extracellular $[Ca^{2+}]$ was reduced to zero or when the muscle was treated with calpain inhibitor (leupeptin) (171). These findings suggested the role of eccentric damage and Ca^{2+} influx in calpain autolysis. Nevertheless, the damage due to eccentric contractions alone does not initiate the proteolytic activity of calpains. As shown by Murphy and Lamb, lengthening contractions followed by increased Ca^{2+} influx leads to an increase in resting $[Ca^{2+}]_i$, which consequently activates calpain-3 (118).

5.4.3 - Calpains and E-C coupling disruption

Studies linking increases in $[Ca^{2+}]_i$ with E-C-coupling disruption suggested the role of calpains in prolonged muscle weakness (159; 99; 123). This calcium-induced E-C-

uncoupling disruption has been suggested as a protective mechanism to avoid greater calcium dependent damage to muscle fibres (99). Small increases (slightly above average) in $[Ca^{2+}]_i$ near the triad junction has been shown to induce E-C coupling impairment (159). This Ca^{2+}-induced uncoupling also takes place after prolonged small increases in resting $[Ca^{2+}]_i$ (99). However, raising the $[Ca^{2+}]_i$ to relatively high levels (approximately 1mM) for short period of time (ten seconds) also disrupts E-C coupling (99).

Decreases in metabolite levels are not the cause of delayed muscle recovery from fatigue. Edwards and colleagues (55) reported a long lasting decrease in muscle force (more than one day) which was not caused by the depletion of high-energy phosphates or failure of electrical activity. Further studies showed that the level of metabolites used in muscle contraction (i.e. creatine phosphate and ATP) were not the cause of this long-lasting force deficit, since they are restored to normal values within 60 minutes (15; 55; 77). Also, this mechanism is not related to decreased Ca^{2+} sensitivity or Ca^{2+} induced force-generating capacity (159; 33). The decrease in low frequency force occurred as consequence of Ca^{2+} release failure, which happened due to interruption of coupling between voltage-sensor molecules (dihydropyridine receptors) and Ca^{2+} release channels (RyR) (33; 35; 99). The long-lasting decrease in Ca^{2+} release is even more pronounced when $[Ca^{2+}]_i$ are increased during fatigue stimulation (33). In addition, greater E-C coupling disruption takes place if the increases in $[Ca^{2+}]_i$ occur near the triad junction (151). The possible mechanism inciting E-C coupling disruption could be associated with activated Ca^{2+}-dependent proteases which could initiate degradation of proteins in the triad junction (151).

Sarcoplasmic reticulum Ca^{2+} uptake and release is linked to changes in E-C coupling. It has been shown that prolonged exercise decreases SR Ca^{2+} uptake in fast- and slow-twitch muscles by 20 to 40%, without affecting SR Ca^{2+} ATPase activity (57). This leads to an increase in resting $[Ca^{2+}]_i$. This was also observed by Westerblad and colleagues (159) after

subjecting muscle fibres to a long-lasting fatigue. Thus, the increase in $[Ca^{2+}]_i$ lasted for more than 30 minutes and averaged 40% more than normal (159). As suggested by Lamb and Cellini (97), the reduced Ca^{2+} uptake and increased resting Ca^{2+} can be explained by high increases in Ca^{2+} levels during tetanus, which might increase the Ca^{2+} leakage from the SR. Therefore, the increased resting Ca^{2+} and decreased Ca^{2+} uptake are factors which decrease SR Ca^{2+} release. This prolonged increase in resting $[Ca^{2+}]_i$ may induce the activation of calpains, which consequently induces E-C uncoupling even after the levels of metabolites and ions achieve baseline values.

5.4.4 - Calpains and Duchenne muscular dystrophy

Turner and colleagues (148) reported increased resting Ca^{2+} levels, reduced SR Ca^{2+} uptake, and elevated resting Ca^{2+} during SMF stimulation in dystrophic mice. They assessed whether proteolysis was involved by exposing SMF to different $[Ca^{2+}]$, and found that dystrophic animals had much greater net breakdown of proteins compared to controls (148). The dysfunctional Ca^{2+} handling (in muscle as well as myotubes) combined with the evidence of increased proteolytic activity in dystrophic muscle pointed to the potential role of calpains in DMD (113; 148; 58; 75). In 1995, Spencer and colleagues reported for the first time direct evidence linking calpains to the pathology of DMD (139). The levels of calpains were shown to be regulated differently during necrosis and regeneration of dystrophic muscle (139). At peak necrosis, the levels of calpain-2 protein were increased, yet, the levels of the autolyzed isoform (78 kDa) were not changed, indicating that while the amount of calpain-2 was higher, the activity was not increased (139). The levels of calpain-1 were not increased during necrosis, but the amount of the autolyzed isoform (76kDa) was higher (139). Lastly, the levels of autolyzed calpain-1 and calpain-2 went back to normal after the muscle was fully regenerated (139). Calpains change location as dystrophic muscle undergoes cycles of

degeneration and regeneration (142). Spencer & Tidball reported that the translocation of calpains to different areas of muscle fibres was associated with enzymatic cleavage, thus supporting the hypothesis of calpain activation during different stages of muscle regeneration and degeneration in DMD (142). The distribution of calpains is mostly similar between *mdx* and control mice in the prenecrotic stage, but *mdx* fibres demonstrated a higher amount of calpains associated with the plasma membrane (142). During the necrotic stage in dystrophic muscle, the majority of the calpains are found in the cytoplasm (142).

The effect of treating muscles lacking dystrophin with different calpain inhibitors has given some insight into the relationship between calpains and DMD. Intramuscular administration of leupeptin showed a decrease in muscle degeneration is *mdx* mice, which pointed to the potential effect of calpain inhibition in treating DMD (14). Yet, the animals were only treated for 30 days and the effects of multiple direct muscle injections were not accounted for. In a study investigating the hydrolysis of a calpain substrate in normal and dystrophic myotubes, Alderton and Steinhardt (3) showed that after the development of contractile activity, dystrophic myotubes had higher levels of calpain hydrolysis compared to normal myotubes. This high level of hydrolysis was dependent on external Ca^{2+}, and could be abolished by a calpain inhibitor (calpeptin) (3). The authors also demonstrated that the increased Ca^{2+} levels occurred due to abnormal activity of Ca^{2+}-specific leak channels, which could be reduced by using a Ca^{2+} channel antagonist (3). Although these studies evaluated the levels of calpains and their cleavage in dystrophic muscle, they did not assess if calpain activation precedes or occurs as consequence of cell death (140).

Spencer and Mellgren (140) generated *mdx* mice that overexpressed calpastatin, a potent endogenous inhibitor of calpains, to evaluate differences in the dystrophic phenotype due to calpain inhibition. The overexpression of calpastatin was sufficient to ameliorate the dystrophic pathology (140). The *mdx* mice overexpressing calpastatin (CS Tg/*mdx*) had

reduced muscle necrosis, regenerating areas, and membrane damage compared to *mdx* mice. Thus, the results demonstrate that calpains acted downstream of the primary muscle defect in DMD (140). Nevertheless, in 2008 another study using the CS Tg/*mdx* reported that increases in muscle calpain inhibitor did not ameliorate the dystrophic phenotype (27). Thus both groups, *mdx* and CS Tg/*mdx*, had similar percentage of muscle necrosis and regenerating areas. Yet, the authors showed a histological improvement by inhibiting the ubiquitin-proteasome pathway (27). In 2010, Selsby and colleagues used a technique to increase leupeptin concentration in *mdx* skeletal muscle by using carnitine to carry leupeptin in skeletal muscle but results did not show any improvement in *mdx* mice after 6 months of treatment (135). These results suggest that while calpains might have an acute effect in muscle function, that chronic suppression is not effective in preventing muscle damage or that other mechanisms play a role in the progression of the muscular dystrophy.

5.5 - Fatigue mechanisms in skeletal muscle

Muscle fatigue is characterized by the inability of the muscle to generate force (156). This event takes place when skeletal muscle undergoes constant stimulation, followed by decline in function. Many mechanisms have been proposed to influence fatigue (i.e. depletion of substrates such as glycogen, accumulation of metabolites, reduced Ca^{2+} release and reduced Ca^{2+} sensitivity of the myofilaments, etc.), but findings have been somewhat inconsistent (44). Results from some investigations are limited in their application due to unrealistic (non-physiological) concentrations of metabolites and ions (4). However, other studies have been carefully designed and results are more applicable; yet replication of findings is still necessary. It is not the purpose of this section to address differences between

studies and select well-designed investigations; rather, the aim of the present section is to discuss the recent progress in understanding the underlying mechanisms of fatigue.

Studies investigating the effects of fatigue on force production have taken place since the 1970's. When investigating muscle force recovery after fatiguing contractions, Edwards and colleagues (55) reported that the muscle's ability to generate force at high frequency after fatigue was reduced for approximately 20 minutes, while the force production at low frequency stimulation was greatly reduced for over 1 day. This was a very interesting finding regarding differences in the ability of the muscle to respond to low and high stimulation frequencies after fatigue. The authors also evaluated changes in muscle force between muscles subjected to low vs. high frequency stimulation during fatigue, and results demonstrated that the decrease in initial force was greater when the muscle was stimulated at low frequency compared to high frequency (55). Moreover, the deficit in low-frequency force was not attributed to decreases in the levels of high-energy phosphates or failure of electrical activity as assessed by electromyography (55).

To follow up in the previous study, Dawson and colleagues (47) used force measurements combined with phosphorus nuclear magnetic resonance as a technique to relate muscle functional changes to simultaneous biochemical and energetic alterations (47). Therefore, Dawson et al. (47) measured several different variables in the gastrocnemius muscle undergoing fatigue, which included: 1) isometric force development; 2) affinity for ATP hydrolysis; 3) rate of ATP hydrolysis; 4) changes in concentrations of creatine phosphate (CrP), ATP, free adenosine diphosphate (ADP), inorganic phosphorus (P_i), hydrogen ions (H^+), and creatine (Cr) (47). The mechanical changes during fatigue, as well as the decreases in force production and slower relaxation rate, were associated with the metabolic alterations in the fatigued muscle (47). The relaxation rate was related to all metabolite levels, but the authors could not explain which relationships were causal (47).

Yet, Dawson and colleagues (47) suggested that some metabolites, such as Cr, CrP, and ATP, could be ruled as contributors to altered relaxation rate. Further, decreases in affinity of ATP hydrolysis (a theoretical measure of the maximum amount of work accomplished per mole of ATP hydrolyzed) during prolonged stimulation were caused by increased product concentration and not by decreases in ATP concentration (47). Lastly, the authors concluded that the relationship between relaxation rate and ATP hydrolysis could be related to Ca^{2+} sequestration by the SR, since it is an ATP-dependent process, but the authors did not measure SR Ca^{2+} uptake (47). The link between biochemical and energetic alterations with fatigue gave new insight into factors contributing for the decrease in muscle force, but some questions were still unanswered.

Following the study by Dawson and coworkers (47), other groups investigated changes in muscle function during fatigue while applying different levels of various metabolites to skinned muscle fibre preparations where the sarcolemma is removed to allow direct access to the intracellular environment. However, this set-up required application of exogenous Ca^{2+} and did not allow scientists to measure force responses in relation to normal E-C coupling processes. In 1985, Grynkiewics, Poeni, and Tsien (72) published a study that changed muscle fatigue assessment. They developed fluorescent dyes (i.e. Fura-2) that could be used to measure real time Ca^{2+} levels in intact cells for monitoring changes in intracellular Ca^{2+} simultaneously with cell function (72). The development of new fluorescent dyes and the technique to dissect SMFs with the sarcolemmal membrane intact started a new era in the evaluation of fatigue, force, and intracellular Ca^{2+} levels. By the early 1990's more detailed analyses of the cellular mechanisms underlying muscle fatigue and its relationship to Ca^{2+} were possible.

One of the methods to evaluate the causes of fatigue in skeletal muscle used SMFs isolated from the flexor digitorum brevis of mice. This was a technique develop by

Lannergren & Westerblad (100), who measured changes in isometric force in SMFs exposed to different temperatures. In another study, Lannergreen and Westerblad (101) evaluated time to fatigue, force decline, acidification, and the effects of caffeine in force recovery in SMFs after fatigue exposure. The fatigue protocol involved electrically stimulating SMFs with repeated tetani at 70Hz once every 3.8s (for 2 minutes), and then continually reducing the resting time between tetani until the fibre reached fatigue, with fatigue being defined as 30% of initial force (101). Results demonstrated that endurance capacity of SMFs has great variability (between 2.5 to 24 minutes), but most fibres reach fatigue between 4 to 8 minutes (101). Results demonstrated that caffeine has no effect on force production in the rested state, but causes fast and dramatic increase in force when administered after fatigue (101). Lastly, the authors exposed SMFs to increased levels of acidosis, which decreased time to fatigue, but was somewhat recovered with the addition of caffeine (101). Furthermore, the two authors also identified three different phases of muscle fatigue: a) fast decline in tension to 90% of its initial recorded value (phase 1); b) plateau in tension production (phase 2); c) fast tension decline (phase 3) (101). It was proposed that the decrease in force in phases 1 and 3 of fatigue were due to different underlying intracellular mechanisms.

Following these findings, Westerblad and Allen (156) performed a study in which they used a Ca^{2+} indicator, known as Fura-2AM, to assess $[Ca^{2+}]_i$ in SMFs during fatigue. The study designed by Westerblad and Allen (156) was the first investigation combining the measurements of $[Ca^{2+}]_i$ using Fura-2AM and tension in mammalian SMFs. Results demonstrated an increase in resting (baseline) $[Ca^{2+}]_i$ as the fatiguing stimulation continued, a fact that could not be explained by the authors at the time (156). The investigators also pointed out that early tension decline could not be rescued by caffeine application, suggesting that metabolic changes were influencing force production in phase 1 of fatigue (156). Therefore, either an increase in P_i levels or intracellular acidosis (pH) was influencing the

fast decline in force to 90% of its original starting value (156). When discussing which possible factor could have influenced the fast tension decline in phase 3, the authors proposed that an impaired activation of cross-bridges by reduced intracellular Ca^{2+} could explain this mechanism (156). They supported their statement by demonstrating that application of caffeine, which elevated tetanic intracellular Ca^{2+} levels, was able to recover tension up to 80% of its initial value (156).

By the mid 1990's groups of investigators had focused in studying the mechanisms influencing Ca^{2+} release and Ca^{2+} sensitivity of the myofibrillar proteins, as well as the effects of pH during fatigue. Studies by Fryer et al. (60) and Owen et al. (121) suggested that reduction in Ca^{2+} release was influenced by both metabolic and non-metabolic factors. During the same time, it had been shown that pH influenced SR Ca^{2+} release (56), but other groups reported no effects (157). Differences in the methods used for assessing SR Ca^{2+} release were probably the cause for discrepancies in findings. While Favero et al. (56) used isolated SR from rabbit muscle, Westerblad and Allen measured SR Ca^{2+} release in intact SMF from mice. Studies using more physiological temperatures demonstrated that changes in pH had a reduced effect on SMF function (158). However, differences in the methodological approaches and thus discrepancies in findings limited the conclusions on the cellular mechanisms underlying muscle fatigue.

Chin and Allen (34) suggested that the role of pH changes in muscle fatigue was fiber-type specific as well as intensity dependent. The authors evaluated the differences in force, $[Ca^{2+}]_i$, and acidosis in SMFs exposed to different fatiguing protocols. While the two different fatiguing conditions involved stimulating SMFs at 100Hz, the time between repeated tetani varied between protocols (34). Their study compared the standard fatigue protocol, where fibres were stimulated once every 4s, then once every 3s, and so on, until force reached 30% of the initial value (each time block lasting 2 minutes) to a fatigue

protocol with only a very short (1s) rest period between tetani until force reached 30% (34). Fibres exposed to the higher frequency of tetani reached 30% of initial force faster than fibres exposed to the lower frequency of tetani (34). However, the decrease in $[Ca^{2+}]_i$ was more pronounced in SMFs exposed to low frequency fatigue (48%) compared to high frequency fatigue (35%) (34). The faster decrease in force at high rate of tetani was not due to Ca^{2+} release failure (34). In order to assess E-C-coupling failure, SMFs were treated with caffeine (5mM), a Ca^{2+} release channel agonist, as soon as the fibre reached 30% of its initial force (34). Caffeine was able to restore force in SMFs exposed to fatigue at low rate of tetani, but did not improve force recovery after high rate of tetani (34). This demonstrates that the reduced Ca^{2+} release during fatigue from rapidly occurring tetani, even with the addition of caffeine, is related to insufficient SR Ca^{2+} refilling (34). Changes in pH were also evaluated during low vs. high intensity fatigue (34). Results showed that high frequency tetani induced higher and faster increase in acidosis, which suggested that such mechanism plays a major role during the fatigue experienced when muscles are stimulated at high intensities with short recovery periods between tetani (34). These results also demonstrated that Ca^{2+} sensitivity is reduced to a greater extent when muscles are exposed to higher acidosis (34).

A broader attempt to characterize mechanisms affecting muscle fatigue was later undertaken by Danieli-Betto and colleagues (44). They aimed to investigate if fatigue also caused continual modifications of SR and myofibrillar proteins that contributed to the decrease of tension in mammalian fibres (44). Fast and slow-twitch fibres were evaluated for SR Ca^{2+} release and uptake, SR caffeine sensitivity, and myofibrillar proteins Ca^{2+} sensitivity using a skinned muscle fibre technique (44). Changes in myofibrillar protein properties, as well as SR function, are still present after the muscle fibre is skinned and has its myoplasm replaced with a new physiological medium (44). Maximal Ca^{2+} tension was the same in fatigued and rested skinned fibres from soleus muscle, which indicated that fatigue-induced

changes in Ca^{2+} sensitivity occurred due to modifications of myofibrillar proteins (44). The study also showed that the SR of slow-twitch fibres accumulated Ca^{2+} at a faster rate when skinned immediately after fatigue compared to fibres skinned prior to fatigue (44). Additionally, both slow- and fast-twitch chemically skinned fibres maintained SR Ca^{2+} release patterns after fatigue (44). On the other hand, Ca^{2+} removal in intact SMFs was slower which was explained by the increased metabolite levels in addition to posttranslational modifications of SR Ca^{2+} pump and/or phospholamban (transmembrane protein that regulates SR Ca^{2+} pump activity) (44). Posttranslational modifications of proteins responsible for SR and myofibrillar properties play an important role in force decline of mammalian slow-twitch fibres during fatigue, but do not appear to influence fast-twitch muscle fatigue (44).

High increases in $[Ca^{2+}]_i$ can also induce reductions in muscle force during fatigue. Muscle excitation results in the release of high amounts of $[Ca^{2+}]_i$ into the myoplasm, increasing intracellular Ca^{2+} concentrations from ~50nM to 1-2uM (156) . Previous studies suggested that elevated $[Ca^{2+}]_i$ itself plays a role in the development of long-lasting fatigue, but no previous study investigated if E-C coupling is disrupted by peak Ca^{2+} levels or the temporal accumulation of Ca^{2+} (33; 99; 151; 159). The study by Verburg and colleagues (151) used mechanically skinned fibres in order to manipulate Ca^{2+} levels and evaluate its effect on E-C uncoupling, defined as a reduction in Ca^{2+} release and force production in response to excitation. Results demonstrated that $[Ca^{2+}]_i$ needed to be elevated by 2μM for at least one minute to elicit E-C coupling disruption in fast-twitch fibres (151). Peak Ca^{2+}, and not the temporal accumulation of Ca^{2+}, was suggested to be the mechanism responsible for uncoupling (151). Uncoupling was only affected when peak Ca^{2+} levels were reached near the triad junction, and not near the center of the cytoplasm, thus, this E-C coupling disruption was caused by the failure of signal transmission at the triad junction (151). Furthermore, the authors suggested that coupling was only affected if the following were present: 1) Ca^{2+} was

elevated between one and three minutes and its level was similar to that achieved during maximal force production; and 2) peak Ca^{2+} in the vicinity of the triad junction is above its normal level (151).

Another study investigating potential mechanisms contributing to muscle fatigue was carried by Roots and colleagues (130). The authors aimed to evaluate fatigue that followed either (a) repeated short isometric contractions, or (b) repeated concentric contractions at three different temperatures (10°C, 20°C, and 30°C) (130). Repeated concentric contractions elicited greater force decrements in comparison to isometric contractions (130). Single muscle fibres exposed to isometric contractions during fatigue had a lesser decrease in force at 30°C (20%) than 10°C (30%) (130). Moreover, there was a relationship between absolute power and temperature, with absolute power increasing by more than ten-fold from 10°C to 30°C (20). Their results also suggested that the reduction of power following fatigue was greater at 10°C and lower at increased temperatures (130). Others have shown that pre-fatigue tetanic force as well as force and $[Ca^{2+}]_i$ reduction during fatigue, followed similar patterns at 37°C and 43°C (130). Although oxidative stress was higher at 43 °C, this increase did not contribute to premature fatigue (130).

Numerous investigators have studied the potential mechanisms contributing to muscle fatigue, but findings are still somewhat inconclusive due to methodological limitations and differences in techniques used to assess fatigue mechanisms. However, there is consensus across studies showing that factors such as intensity, duration, and type of contraction influence muscle fatigue (4). More recent studies are more carefully designed and tend to incorporate several variables, not just one, to understand the effect of combined mechanisms on muscle fatigue. This has been shown in the study by Place and colleagues (124) where the authors evaluated the combined effects of temperature and oxidative stress in muscle fibres. Another group had a different approach and implemented different

contraction patterns to evaluate how oxidative stress contributed to muscle fatigue at more physiological temperatures (130). Studies following this pattern represent the future approach of evaluating factors contributing to muscle fatigue.

5.6 - Summary

Duchenne muscular dystrophy is one of the most severe types of muscular dystrophy affecting humans. Although the main cause leading to DMD has been linked to the lack of protein dystrophin, many of the underlying mechanisms contributing to the increased muscle damage and progressive loss of muscle function are still unknown. Dystrophic animals, such as the *mdx* mouse, have been used in studies investigating potential disease treatments. However, the *mdx* mouse has a relatively normal lifespan, which is explained by the overexpression of utrophin and increased satellite cell function. Moreover, mice lacking both dystrophin and utrophin are thought to be a better model for DMD, but not many studies have evaluated differences between double mutants (animals lacking dystrophin and utrophin) vs. *mdx* mice.

Impaired intracellular Ca^{2+} handling is thought to be one the potential mechanisms contributing for DMD. Studies have shown that dystrophic muscle has higher resting $[Ca^{2+}]_i$, impaired SR Ca^{2+} control (increased SR Ca^{2+} leakage and slower SR Ca^{2+} uptake), and increased influx of Ca^{2+} from the extracellular space. Moreover, poor Ca^{2+} handling has been linked to activation of Ca^{2+}-activated proteases known as calpains. Skeletal muscle of dystrophic animals has reduced fatigue resistance due to greater disruption of E-C-coupling during fatigue. This greater E-C-uncoupling during fatigue is associated with poor Ca^{2+} handling and the possible activation of calpains. However, no study to date has evaluated if calpains play a role in the prolonged E-C-coupling disruption experienced by dystrophic muscles after fatiguing contractions. Also, no previous study has evaluated fatigue resistance

and the prolonged muscle weakness experienced after fatigue between the *mdx* and double mutant mouse models.

Appendix A

Fatigue data

Time to fatigue – comparison between all groups (both treatments – vehicle and ALLN) – one way Anova and Tukey HSD for post hoc analysis

ANOVA

VAR00004

	Sum of Squares	df	Mean Square	F	Sig.
Between Groups	356220.323	2	178110.161	1.376	.265
Within Groups	5048674.207	39	129453.185		
Total	5404894.530	41			

1= mdx 2= Utr-/-/mdx 3= con

Multiple Comparisons

VAR00048

Tukey HSD

(I) VAR00049	(J) VAR00049	Mean Difference (I-J)	Std. Error	Sig.	95% Confidence Interval	
					Lower Bound	Upper Bound
1.00	**2.00**	255.32468	156.13311	**.243**	-125.0636	635.7130
	3.00	95.06643	125.86569	**.732**	-211.5811	401.7140
2.00	**1.00**	-255.32468	156.13311	**.243**	-635.7130	125.0636
	3.00	-160.25824	168.67498	**.612**	-571.2024	250.6859
3.00	**1.00**	-95.06643	125.86569	**.732**	-401.7140	211.5811
	2.00	160.25824	168.67498	**.612**	-250.6859	571.2024

Fatigue data

Increase in resting during fatigue - between group comparison (both treatments – vehicle and ALLN) – one way Anova and Tukey HSD for post hoc analysis

ANOVA

VAR00048

	Sum of Squares	df	Mean Square	F	Sig.
Between Groups	.004	2	.002	.278	.759
Within Groups	.267	39	.007		
Total	.271	41			

1= mdx 2= Utr-/-/mdx 3= con

Multiple Comparisons

VAR00048

Tukey HSD

(I) VAR00049	(J) VAR00049	Mean Difference (I-J)	Std. Error	**Sig.**	95% Confidence Interval	
					Lower Bound	Upper Bound
1.00	**2.00**	.023208	.035899	**.795**	-.06425	.11067
	3.00	-.004671	.028940	**.986**	-.07518	.06583
2.00	**1.00**	-.023208	.035899	**.795**	-.11067	.06425
	3.00	-.027879	.038783	**.754**	-.12237	.06661
3.00	**1.00**	.004671	.028940	**.986**	-.06583	.07518
	2.00	.027879	.038783	**.754**	-.06661	.12237

Fatigue data

Time to fatigue - between group comparison (ALLN only) – one way Anova and Tukey HSD for post hoc analysis

ANOVA

VAR00009

	Sum of Squares	df	Mean Square	F	Sig.
Between Groups	517910.714	2	258955.357	1.115	.348
Within Groups	4411421.433	19	232180.075		
Total	4929332.148	21			

1= mdx 2= Utr-/-/mdx 3= con

Multiple Comparisons

VAR00059

Tukey HSD

(I) VAR00060	(J) VAR00060	Mean Difference (I-J)	Std. Error	Sig.	95% Confidence Interval	
					Lower Bound	Upper Bound
1.00	**2.00**	334.23333	288.91538	**.491**	-393.9982	1062.4649
	3.00	229.23333	220.66276	**.561**	-326.9627	785.4294
2.00	**1.00**	-334.23333	288.91538	**.491**	-1062.4649	393.9982
	3.00	-105.00000	323.01721	**.944**	-919.1876	709.1876
3.00	**1.00**	-229.23333	220.66276	**.561**	-785.4294	326.9627
	2.00	105.00000	323.01721	**.944**	-709.1876	919.1876

Fatigue data

Time to fatigue - between group comparison (Vehicle only) – one way Anova and Tukey HSD for post hoc analysis

ANOVA

VAR00059

	Sum of Squares	df	Mean Square	F	Sig.
Between Groups	91811.025	2	45905.513	1.762	.208
Within Groups	364782.857	14	26055.918		
Total	456593.882	16			

1= mdx 2= Utr-/-/mdx 3= con

Multiple Comparisons

VAR00059

Tukey HSD

(I) VAR00060	(J) VAR00060	Mean Difference (I-J)	Std. Error	Sig.	95% Confidence Interval	
					Lower Bound	Upper Bound
1.00	**2.00**	78.00000	111.38932	**.767**	-213.5371	369.5371
	3.00	-115.14286	86.28179	**.400**	-340.9665	110.6808
2.00	**1.00**	-78.00000	111.38932	**.767**	-369.5371	213.5371
	3.00	-193.14286	111.38932	**.228**	-484.6799	98.3942
3.00	**1.00**	115.14286	86.28179	**.400**	-110.6808	340.9665
	2.00	193.14286	111.38932	**.228**	-98.3942	484.6799

Fatigue data

Increase in resting during fatigue - between group comparison (ALLN only) – one way Anova and Tukey HSD for post hoc analysis

ANOVA

VAR00015

	Sum of Squares	df	Mean Square	F	Sig.
Between Groups	.010	2	.005	.603	.556
Within Groups	.170	21	.008		
Total	.180	23			

1= mdx 2= Utr-/-/mdx 3= con

Multiple Comparisons

VAR00061

Tukey HSD

(I) VAR00062	(J) VAR00062	Mean Difference (I-J)	Std. Error	**Sig.**	95% Confidence Interval	
					Lower Bound	Upper Bound
1.00	**2.00**	.04113	.05689	**.753**	-.1022	.1845
	3.00	-.02820	.04345	**.795**	-.1377	.0813
2.00	**1.00**	-.04113	.05689	**.753**	-.1845	.1022
	3.00	-.06933	.06360	**.530**	-.2296	.0910
3.00	**1.00**	.02820	.04345	**.795**	-.0813	.1377
	2.00	.06933	.06360	**.530**	-.0910	.2296

Fatigue data

Increase in resting during fatigue - between group comparison (Vehicle only) – one way Anova and Tukey HSD for post hoc analysis

ANOVA

VAR00015

	Sum of Squares	df	Mean Square	F	Sig.
Between Groups	.001	2	.000	.058	.944
Within Groups	.089	15	.006		
Total	.089	17			

1= mdx 2= Utr-/-/mdx 3= con

Multiple Comparisons

VAR00061

Tukey HSD

(I) VAR00062	(J) VAR00062	Mean Difference (I-J)	Std. Error	**Sig.**	95% Confidence Interval	
					Lower Bound	Upper Bound
1.00	**2.00**	.008143	.048195	**.984**	-.11704	.13333
	3.00	.014000	.041101	**.938**	-.09276	.12076
2.00	**1.00**	-.008143	.048195	**.984**	-.13333	.11704
	3.00	.005857	.048195	**.992**	-.11933	.13104
3.00	**1.00**	-.014000	.041101	**.938**	-.12076	.09276
	2.00	-.005857	.048195	**.992**	-.13104	.11933

Fatigue data

Time to fatigue – within group comparison (CON) (Vehicle vs. ALLN) – One-way Anova

ANOVA

VAR00017

	Sum of Squares	df	Mean Square	F	**Sig.**
Between Groups	40268.720	1	40268.720	3.515	**.088**
Within Groups	126004.357	11	11454.942		
Total	166273.077	12			

Increase in resting during fatigue – within group comparison (CON) (Vehicle vs. ALLN) – One-way Anova

ANOVA

VAR00017

	Sum of Squares	df	Mean Square	F	**Sig.**
Between Groups	.007	1	.007	.817	**.385**
Within Groups	.092	11	.008		
Total	.098	12			

Time to fatigue – within group comparison (mdx) (Vehicle vs. ALLN) – One-way Anova

ANOVA

VAR00019

	Sum of Squares	df	Mean Square	F	**Sig.**
Between Groups	258513.839	1	258513.839	1.146	**.297**
Within Groups	4512484.933	20	225624.247		
Total	4770998.773	21			

Increase in resting during fatigue – within group comparison (mdx) (Vehicle vs. ALLN) – One-way Anova

ANOVA

VAR00021

	Sum of Squares	df	Mean Square	F	**Sig.**
Between Groups	.000	1	.000	.010	**.920**
Within Groups	.122	20	.006		
Total	.122	21			

Time to fatigue – within group comparison (UTR-/-/MDX) (Vehicle vs. ALLN) – One-way Anova

ANOVA

VAR00023

	Sum of Squares	df	Mean Square	F	**Sig.**
Between Groups	123.857	1	123.857	.006	**.943**
Within Groups	111278.500	5	22255.700		
Total	111402.357	6			

Increase in resting during fatigue – within group (UTR-/-/MDX) (Vehicle vs. ALLN) – One-way Anova

ANOVA

VAR00023

	Sum of Squares	df	Mean Square	F	**Sig.**
Between Groups	.001	1	.001	.164	**.702**
Within Groups	.045	5	.009		
Total	.046	6			

Fura-2 ratio resting values

Resting Fura-2 ratio - between groups comparison – One-way ANOVA with Tukey HSD for post hoc analysis

ANOVA

DedepentV

	Sum of Squares	df	Mean Square	F	**Sig.**
Between Groups	.009	2	.005	4.399	**.016**
Within Groups	.073	70	.001		
Total	.082	72			

1 = CON 2= mdx 3= Utr-/-/mdx

Multiple Comparisons

DedepentV

Tukey HSD

(I) Groups	(J) Groups	Mean Difference (I-J)	Std. Error	**Sig.**	95% Confidence Interval	
					Lower Bound	Upper Bound
1.00	**2.00**	-.030392*	.010462	**.013**	-.05544	-.00534
	3.00	-.018440	.012726	**.322**	-.04891	.01203
2.00	**1.00**	.030392*	.010462	**.013**	.00534	.05544
	3.00	.011951	.009849	**.449**	-.01163	.03554
3.00	**1.00**	.018440	.012726	**.322**	-.01203	.04891
	2.00	-.011951	.009849	**.449**	-.03554	.01163

*. The mean difference is significant at the 0.05 level.

Time to 75% of Fura-2 peak clearance

Mdx - 50Hz vs 120Hz - paired T-test

Paired Samples Test

		Paired Differences					t	df	Sig. (2-tailed)
		Mean	Std. Deviation	Std. Error Mean	95% Confidence Interval of the Difference Lower	Upper			
Pair 1	VAR00042 - VAR00043	-.00588	.03331	.00589	-.01789	.00613	-.999	31	**.326**

Utr-/-/mdx - 50Hz vs 120Hz - paired T-test

Paired Samples Test

		Paired Differences					t	df	Sig. (2-tailed)
		Mean	Std. Deviation	Std. Error Mean	95% Confidence Interval of the Difference Lower	Upper			
Pair 1	VAR00044 - VAR00045	.00962	.01915	.00677	-.00639	.02564	1.421	7	**.198**

CON - 50Hz vs 120Hz - paired T-test

Paired Samples Test

		Paired Differences					t	df	Sig. (2-tailed)
		Mean	Std. Deviation	Std. Error Mean	95% Confidence Interval of the Difference Lower	Upper			
Pair 1	VAR00044 - VAR00045	-.00315	.01254	.00348	-.01073	.00442	-.907	12	**.382**

Time to 75% of Fura-2 peak clearance

Between groups - 50Hz - One-way ANOVA with Tukey HSD for post hoc analysis
1 = mdx 2 = Utr-/-/mdx 3 = con

ANOVA

VAR00044

	Sum of Squares	df	Mean Square	F	**Sig.**
Between Groups	.018	2	.009	4.461	**.016**
Within Groups	.102	50	.002		
Total	.120	52			

1 = mdx 2 = Utr-/-/mdx 3 = con

Multiple Comparisons

VAR00044

Tukey HSD

(I) VAR00046	(J) VAR00046	Mean Difference (I-J)	Std. Error	**Sig.**	95% Confidence Interval	
					Lower Bound	Upper Bound
1.00	**2.00**	-.04129	.01785	**.063**	-.0844	.0018
	3.00	.01898	.01485	**.414**	-.0169	.0549
2.00	**1.00**	.04129	.01785	**.063**	-.0018	.0844
	3.00	.06027*	.02029	**.012**	.0113	.1093
3.00	**1.00**	-.01898	.01485	**.414**	-.0549	.0169
	2.00	-.06027*	.02029	**.012**	-.1093	-.0113

*. The mean difference is significant at the 0.05 level.

Time to 75% of Fura-2 peak clearance

Between group comparison - 120Hz - One-way ANOVA with Tukey HSD for post hoc analysis

ANOVA

VAR00044

	Sum of Squares	df	Mean Square	F	**Sig.**
Between Groups	.011	2	.006	3.460	**.039**
Within Groups	.082	50	.002		
Total	.093	52			

1 = mdx 2 = Utr-/-/mdx 3 = con

Multiple Comparisons

VAR00044

Tukey HSD

(I) VAR00046	(J) VAR00046	Mean Difference (I-J)	Std. Error	**Sig.**	95% Confidence Interval	
					Lower Bound	Upper Bound
1.00	**2.00**	-.02578	.01600	**.250**	-.0644	.0129
	3.00	.02171	.01331	**.242**	-.0104	.0539
2.00	**1.00**	.02578	.01600	**.250**	-.0129	.0644
	3.00	.04749*	.01819	**.031**	.0036	.0914
3.00	**1.00**	-.02171	.01331	**.242**	-.0539	.0104
	2.00	-.04749*	.01819	**.031**	-.0914	-.0036

*. The mean difference is significant at the 0.05 level.

Fibre size

Fibre diameter

ANOVA

VAR00001

	Sum of Squares	df	Mean Square	F	**Sig.**
Between Groups	749.163	2	374.582	7.823	**.001**
Within Groups	3207.922	67	47.879		
Total	3957.086	69			

1-way ANOVA with Tukey HSD for post hoc analysis
1 = mdx 2 = Utr-/-/mdx 3 = con

Multiple Comparisons

VAR00001

Tukey HSD

(I) VAR00002	(J) VAR00002	Mean Difference (I-J)	Std. Error	**Sig.**	95% Confidence Interval	
					Lower Bound	Upper Bound
1.00	**2.00**	8.17276*	2.12919	**.001**	3.0693	13.2762
	3.00	-.02504	2.19009	**1.000**	-5.2744	5.2243
2.00	**1.00**	-8.17276*	2.12919	**.001**	-13.2762	-3.0693
	3.00	-8.19780*	2.66514	**.008**	-14.5858	-1.8098
3.00	**1.00**	.02504	2.19009	**1.000**	-5.2243	5.2744
	2.00	8.19780*	2.66514	**.008**	1.8098	14.5858

*. The mean difference is significant at the 0.05 level.

Fibre size

Fibre length

ANOVA

VAR00001

	Sum of Squares	df	Mean Square	F	**Sig.**
Between Groups	10733.997	2	5366.998	1.007	**.371**
Within Groups	357245.489	67	5332.022		
Total	367979.486	69			

1-way ANOVA with Tukey HSD for post hoc analysis
1 = mdx 2 = Utr-/-/mdx 3 = con

Multiple Comparisons

VAR00001

Tukey HSD

(I) VAR00002	(J) VAR00002	Mean Difference (I-J)	Std. Error	**Sig.**	95% Confidence Interval	
					Lower Bound	Upper Bound
1.00	**2.00**	29.67774	22.46907	**.389**	-24.1780	83.5334
	3.00	18.91950	23.11182	**.693**	-36.4768	74.3158
2.00	**1.00**	-29.67774	22.46907	**.389**	-83.5334	24.1780
	3.00	-10.75824	28.12498	**.923**	-78.1705	56.6540
3.00	**1.00**	-18.91950	23.11182	**.693**	-74.3158	36.4768
	2.00	10.75824	28.12498	**.923**	-56.6540	78.1705

Peak Fura-2 fluorescence

10Hz - Between group comparison - One-way ANOVA with Tukey HSD for post hoc analysis

ANOVA

VAR00001

	Sum of Squares	df	Mean Square	F	**Sig.**
Between Groups	.076	2	.038	1.791	**.174**
Within Groups	1.476	70	.021		
Total	1.551	72			

1 = mdx 2 = Utr-/-/mdx 3 = con

Multiple Comparisons

VAR00001

Tukey HSD

(I) VAR00002	(J) VAR00002	Mean Difference (I-J)	Std. Error	**Sig.**	95% Confidence Interval	
					Lower Bound	Upper Bound
1.00	**2.00**	.04120	.04432	**.624**	-.0649	.1473
	3.00	.08285	.04561	**.172**	-.0264	.1921
2.00	**1.00**	-.04120	.04432	**.624**	-.1473	.0649
	3.00	.04165	.05593	**.738**	-.0923	.1756
3.00	**1.00**	-.08285	.04561	**.172**	-.1921	.0264
	2.00	-.04165	.05593	**.738**	-.1756	.0923

Peak Fura-2 fluorescence

30Hz - Between group comparison - One-way ANOVA with Tukey HSD for post hoc analysis

ANOVA

VAR00001

	Sum of Squares	df	Mean Square	F	**Sig.**
Between Groups	.112	2	.056	.751	**.476**
Within Groups	5.216	70	.075		
Total	5.328	72			

1 = mdx 2 = Utr-/-/mdx 3 = con

Multiple Comparisons

VAR00001 Tukey HSD

(I) VAR00002	(J) VAR00002	Mean Difference (I-J)	Std. Error	**Sig.**	95% Confidence Interval	
					Lower Bound	Upper Bound
1.00	**2.00**	.05767	.08332	**.769**	-.1419	.2572
	3.00	.09793	.08574	**.492**	-.1074	.3033
2.00	**1.00**	-.05767	.08332	**.769**	-.2572	.1419
	3.00	.04026	.10514	**.922**	-.2115	.2920
3.00	**1.00**	-.09793	.08574	**.492**	-.3033	.1074
	2.00	-.04026	.10514	**.922**	-.2920	.2115

Peak Fura-2 fluorescence

50Hz - Between group comparison - One-way ANOVA with Tukey HSD for post hoc analysis

ANOVA

VAR00001

	Sum of Squares	df	Mean Square	F	**Sig.**
Between Groups	.167	2	.084	.687	**.507**
Within Groups	8.516	70	.122		
Total	8.683	72			

1 = mdx 2 = Utr-/-/mdx 3 = con

Multiple Comparisons

VAR00001Tukey HSD

(I) VAR00002	(J) VAR00002	Mean Difference (I-J)	Std. Error	**Sig.**	95% Confidence Interval	
					Lower Bound	Upper Bound
1.00	**2.00**	.09297	.10646	**.659**	-.1620	.3479
	3.00	.10511	.10956	**.605**	-.1572	.3674
2.00	**1.00**	-.09297	.10646	**.659**	-.3479	.1620
	3.00	.01214	.13434	**.996**	-.3095	.3338
3.00	**1.00**	-.10511	.10956	**.605**	-.3674	.1572
	2.00	-.01214	.13434	**.996**	-.3338	.3095

Peak Fura-2 fluorescence

70Hz - Between group comparison - One-way ANOVA with Tukey HSD for post hoc analysis

ANOVA

VAR00001

	Sum of Squares	df	Mean Square	F	**Sig.**
Between Groups	.207	2	.104	.676	**.512**
Within Groups	10.572	69	.153		
Total	10.779	71			

1 = mdx 2 = Utr-/-/mdx 3 = con

Multiple Comparisons

VAR00001 Tukey HSD

(I) VAR00002	(J) VAR00002	Mean Difference (I-J)	Std. Error	**Sig.**	95% Confidence Interval	
					Lower Bound	Upper Bound
1.00	**2.00**	.12758	.11979	**.539**	-.1594	.4145
	3.00	.08627	.12325	**.764**	-.2090	.3815
2.00	**1.00**	-.12758	.11979	**.539**	-.4145	.1594
	3.00	-.04131	.15077	**.959**	-.4024	.3198
3.00	**1.00**	-.08627	.12325	**.764**	-.3815	.2090
	2.00	.04131	.15077	**.959**	-.3198	.4024

Peak Fura-2 fluorescence

100Hz - Between group comparison - One-way ANOVA with Tukey HSD for post hoc analysis

ANOVA

VAR00001

	Sum of Squares	df	Mean Square	F	**Sig.**
Between Groups	.176	2	.088	.423	**.657**
Within Groups	13.925	67	.208		
Total	14.101	69			

1 = mdx 2 = Utr-/-/mdx 3 = con

Multiple Comparisons

VAR00001 Tukey HSD

(I) VAR00002	(J) VAR00002	Mean Difference (I-J)	Std. Error	**Sig.**	95% Confidence Interval	
					Lower Bound	Upper Bound
1.00	**2.00**	.12902	.14028	**.630**	-.2072	.4653
	3.00	.03332	.14429	**.971**	-.3125	.3792
2.00	**1.00**	-.12902	.14028	**.630**	-.4653	.2072
	3.00	-.09570	.17559	**.849**	-.5166	.3252
3.00	**1.00**	-.03332	.14429	**.971**	-.3792	.3125
	2.00	.09570	.17559	**.849**	-.3252	.5166

Peak Fura-2 fluorescence

120Hz - Between group comparison - One-way ANOVA with Tukey HSD for post hoc analysis

ANOVA

VAR00001

	Sum of Squares	df	Mean Square	F	**Sig.**
Between Groups	.144	2	.072	.325	**.724**
Within Groups	14.654	66	.222		
Total	14.798	68			

1 = mdx 2 = Utr-/-/mdx 3 = con

Multiple Comparisons

VAR00001Tukey HSD

(I) VAR00002	(J) VAR00002	Mean Difference (I-J)	Std. Error	**Sig.**	95% Confidence Interval	
					Lower Bound	Upper Bound
1.00	**2.00**	.11571	.14542	**.707**	-.2329	.4644
	3.00	.01023	.14955	**.997**	-.3483	.3688
2.00	**1.00**	-.11571	.14542	**.707**	-.4644	.2329
	3.00	-.10548	.18149	**.831**	-.5406	.3297
3.00	**1.00**	-.01023	.14955	**.997**	-.3688	.3483
	2.00	.10548	.18149	**.831**	-.3297	.5406

Peak Fura-2 fluorescence

150Hz - Between group comparison - One-way ANOVA with Tukey HSD for post hoc analysis

ANOVA

VAR00001

	Sum of Squares	df	Mean Square	F	**Sig.**
Between Groups	.191	2	.096	.415	**.662**
Within Groups	14.980	65	.230		
Total	15.171	67			

1 = mdx 2 = Utr-/-/mdx 3 = con

Multiple Comparisons

VAR00001

Tukey HSD

(I) VAR00002	(J) VAR00002	Mean Difference (I-J)	Std. Error	**Sig.**	95% Confidence Interval	
					Lower Bound	Upper Bound
1.00	**2.00**	.11177	.14860	**.733**	-.2447	.4682
	3.00	-.04767	.15280	**.948**	-.4142	.3188
2.00	**1.00**	-.11177	.14860	**.733**	-.4682	.2447
	3.00	-.15944	.18490	**.666**	-.6029	.2841
3.00	**1.00**	.04767	.15280	**.948**	-.3188	.4142
	2.00	.15944	.18490	**.666**	-.2841	.6029

Pre vs. Post peak values

mdx (ALLN) – pre vs. post-fatigue comparison – paired t-test

Paired Samples Statistics

		Mean	N	Std. Deviation	Std. Error Mean
Pair 1	Pre-10hz	.6889	15	.12962	.03347
	post-10Hz	.6359	15	.16461	.04250
Pair 2	Pre-30Hz	1.0115	15	.25397	.06558
	post-30Hz	.9019	15	.32089	.08285
Pair 3	Pre-50Hz	1.1955	15	.33623	.08681
	post-50Hz	1.0413	15	.41894	.10817
Pair 4	Pre-70Hz	1.3106	15	.38545	.09952
	post-70Hz	1.1564	15	.45052	.11632
Pair 5	Pre-100Hz	1.3849	15	.43515	.11236
	post-100Hz	1.2008	15	.52459	.13545
Pair 6	Pre-120Hz	1.4275	15	.45089	.11642
	post-120Hz	1.2622	15	.53501	.13814
Pair 7	Pre-150Hz	1.4341	15	.45323	.11702
	post-150Hz	1.2878	15	.54214	.13998

Paired Samples Test

		Paired Differences					t	df	**Sig. (2-tailed)**
		Mean	Std. Deviation	Std. Error Mean	95% Confidence Interval of the Difference Lower	Upper			
Pair 1	Pre-10hz – post-10Hz	.05307	.12468	.03219	-.01598	.12211	1.648	14	**.122**
Pair 2	Pre-30Hz – post-30Hz	.10967	.25647	.06622	-.03236	.25170	1.656	14	**.120**
Pair 3	Pre-50Hz – post-50Hz	.15420	.36152	.09334	-.04600	.35440	1.652	14	**.121**
Pair 4	Pre-70Hz – post-70Hz	.15420	.42980	.11097	-.08382	.39222	1.390	14	**.186**
Pair 5	Pre-100Hz – post-100Hz	.18407	.46998	.12135	-.07620	.44433	1.517	14	**.152**
Pair 6	Pre-120Hz – post-120Hz	.16533	.45808	.11828	-.08834	.41901	1.398	14	**.184**
Pair 7	Pre-150Hz – post-150Hz	.14633	.43888	.11332	-.09671	.38938	1.291	14	**.217**

Pre vs. Post peak values
mdx (Vehicle) – pre vs. post-fatigue comparison – paired t-test

Paired Samples Statistics

		Mean	N	Std. Deviation	Std. Error Mean
Pair 1	Pre-10hz	.7215	15	.16015	.04135
	post-10Hz	.6130	15	.14876	.03841
Pair 2	Pre-30Hz	1.0641	15	.32138	.08298
	post-30Hz	.8985	15	.34039	.08789
Pair 3	Pre-50Hz	1.2664	15	.42505	.10975
	post-50Hz	1.0641	15	.46232	.11937
Pair 4	Pre-70Hz	1.3887	15	.48520	.12528
	post-70Hz	1.1495	15	.53178	.13730
Pair 5	Pre-100Hz	1.4993	15	.54517	.14076
	post-100Hz	1.2161	15	.61062	.15766
Pair 6	Pre-120Hz	1.5206	15	.55415	.14308
	post-120Hz	1.2116	15	.59881	.15461
Pair 7	Pre-150Hz	1.5125	15	.53551	.13827
	post-150Hz	1.2151	15	.61154	.15790

Paired Samples Test

		Paired Differences					t	df	Sig. (2-tailed)
		Mean	Std. Deviation	Std. Error Mean	95% Confidence Interval of the Difference Lower	Upper			
Pair 1	Pre-10hz – post-10Hz	.10847	.15539	.04012	.02241	.19452	2.703	14	**.017**
Pair 2	Pre-30Hz – post-30Hz	.16567	.30669	.07919	-.00417	.33550	2.092	14	**.055**
Pair 3	Pre-50Hz – post-50Hz	.20233	.39567	.10216	-.01678	.42145	1.981	14	**.068**
Pair 4	Pre-70Hz – post-70Hz	.23913	.45915	.11855	-.01514	.49340	2.017	14	**.063**
Pair 5	Pre-100Hz – post-100Hz	.28320	.52730	.13615	-.00881	.57521	2.080	14	**.056**
Pair 6	Pre-120Hz – post-120Hz	.30900	.51238	.13229	.02526	.59274	2.336	14	**.035**
Pair 7	Pre-150Hz – post-150Hz	.29740	.48581	.12544	.02837	.56643	2.371	14	**.033**

Pre vs. Post peak values
con (Vehicle) – pre vs. post-fatigue comparison – paired t-test

Paired Samples Statistics

		Mean	N	Std. Deviation	Std. Error Mean
Pair 1	Pre-10hz	.5864	5	.14814	.06625
	post-10Hz	.6324	5	.16871	.07545
Pair 2	Pre-30Hz	.8268	5	.25881	.11574
	post-30Hz	.9462	5	.35236	.15758
Pair 3	Pre-50Hz	.9750	5	.33691	.15067
	post-50Hz	1.1382	5	.45356	.20284
Pair 4	Pre-70Hz	1.0764	5	.37798	.16904
	post-70Hz	1.2890	5	.56192	.25130
Pair 5	Pre-100Hz	1.2114	5	.47874	.21410
	post-100Hz	1.4220	5	.63618	.28451
Pair 6	Pre-120Hz	1.2718	5	.51146	.22873
	post-120Hz	1.4742	5	.66290	.29646
Pair 7	Pre-150Hz	1.3864	5	.57331	.25639
	post-150Hz	1.5402	5	.69970	.31291

Paired Samples Test

		Paired Differences					t	df	Sig. (2-tailed)
		Mean	Std. Deviation	Std. Error Mean	95% Confidence Interval of the Difference Lower	Upper			
Pair 1	Pre-10hz – post-10Hz	-.04600	.09805	.04385	-.16775	.07575	-1.049	4	**.353**
Pair 2	Pre-30Hz – post-30Hz	-.11940	.19239	.08604	-.35828	.11948	-1.388	4	**.238**
Pair 3	Pre-50Hz – post-50Hz	-.16320	.26715	.11947	-.49491	.16851	-1.366	4	**.244**
Pair 4	Pre-70Hz – post-70Hz	-.21260	.31600	.14132	-.60497	.17977	-1.504	4	**.207**
Pair 5	Pre-100Hz – post-100Hz	-.21060	.35263	.15770	-.64845	.22725	-1.335	4	**.253**
Pair 6	Pre-120Hz – post-120Hz	-.20240	.34789	.15558	-.63436	.22956	-1.301	4	**.263**
Pair 7	Pre-150Hz – post-150Hz	-.15380	.32483	.14527	-.55713	.24953	-1.059	4	**.349**

Pre vs. Post peak values
con (ALLN) – pre vs. post-fatigue comparison – paired t-test

Paired Samples Statistics

		Mean	N	Std. Deviation	Std. Error Mean
Pair 1	Pre-10hz	.7014	5	.11674	.05221
	post-10Hz	.7322	5	.09319	.04168
Pair 2	Pre-30Hz	1.2878	5	.30151	.13484
	post-30Hz	1.2580	5	.22051	.09861
Pair 3	Pre-50Hz	1.2686	5	.35983	.16092
	post-50Hz	1.2600	5	.28664	.12819
Pair 4	Pre-70Hz	1.5224	5	.43858	.19614
	post-70Hz	1.4966	5	.37642	.16834
Pair 5	Pre-100Hz	1.7310	5	.54063	.24178
	post-100Hz	1.6766	5	.47786	.21371
Pair 6	Pre-120Hz	1.8158	5	.60779	.27181
	post-120Hz	1.7752	5	.57654	.25784
Pair 7	Pre-150Hz	1.9724	5	.61917	.27690
	post-150Hz	1.5648	5	.77900	.34838

Paired Samples Test

		Paired Differences					t	df	Sig. (2-tailed)
		Mean	Std. Deviation	Std. Error Mean	95% Confidence Interval of the Difference Lower	Upper			
Pair 1	Pre-10hz – post-10Hz	-.03080	.16746	.07489	-.23872	.17712	-.411	4	**.702**
Pair 2	Pre-30Hz – post-30Hz	.02980	.09138	.04087	-.08367	.14327	.729	4	**.506**
Pair 3	Pre-50Hz – post-50Hz	.00860	.10951	.04898	-.12738	.14458	.176	4	**.869**
Pair 4	Pre-70Hz – post-70Hz	.02580	.10353	.04630	-.10275	.15435	.557	4	**.607**
Pair 5	Pre-100Hz – post-100Hz	.05440	.16150	.07223	-.14613	.25493	.753	4	**.493**
Pair 6	Pre-120Hz – post-120Hz	.04060	.17334	.07752	-.17462	.25582	.524	4	**.628**
Pair 7	Pre-150Hz – post-150Hz	.40760	.77025	.34447	-.54880	1.36400	1.183	4	**.302**

Pre vs. Post peak values
Utr-/-/mdx (Vehicle) – pre vs. post-fatigue comparison – paired t-test

Paired Samples Statistics

		Mean	N	Std. Deviation	Std. Error Mean
Pair 1	Pre-10hz	.8225	2	.09263	.06550
	post-10Hz	.5540	2	.27153	.19200
Pair 2	Pre-30Hz	1.2265	2	.09263	.06550
	post-30Hz	.7055	2	.46598	.32950
Pair 3	Pre-50Hz	1.4550	2	.09051	.06400
	post-50Hz	.7770	2	.54589	.38600
Pair 4	Pre-70Hz	1.5915	2	.09970	.07050
	post-70Hz	.7970	2	.56710	.40100
Pair 5	Pre-100Hz	1.7240	2	.11031	.07800
	post-100Hz	.7600	2	.49497	.35000
Pair 6	Pre-120Hz	1.6775	2	.00212	.00150
	post-120Hz	.7665	2	.49992	.35350
Pair 7	Pre-150Hz	1.5495	2	.02758	.01950
	post-150Hz	.7880	2	.53033	.37500

Paired Samples Test

		Paired Differences					t	df	Sig. (2-tailed)
		Mean	Std. Deviation	Std. Error Mean	95% Confidence Interval of the Difference Lower	Upper			
Pair 1	Pre-10hz – post-10Hz	.26850	.17890	.12650	-1.33883	1.87583	2.123	1	**.280**
Pair 2	Pre-30Hz – post-30Hz	.52100	.37335	.26400	-2.83344	3.87544	1.973	1	**.299**
Pair 3	Pre-50Hz – post-50Hz	.67800	.45538	.32200	-3.41340	4.76940	2.106	1	**.282**
Pair 4	Pre-70Hz – post-70Hz	.79450	.46740	.33050	-3.40490	4.99390	2.404	1	**.251**
Pair 5	Pre-100Hz – post-100Hz	.96400	.38467	.27200	-2.49209	4.42009	3.544	1	**.175**
Pair 6	Pre-120Hz – post-120Hz	.91100	.49780	.35200	-3.56158	5.38358	2.588	1	**.235**
Pair 7	Pre-150Hz – post-150Hz	.76150	.50275	.35550	-3.75556	5.27856	2.142	1	**.278**

Pre vs. Post peak values
Utr-/-/mdx (ALLN) – pre vs. post-fatigue comparison – paired t-test

Paired Samples Statistics

		Mean	N	Std. Deviation	Std. Error Mean
Pair 1	Pre-10hz	.7710	2	.01980	.01400
	post-10Hz	.6235	2	.36982	.26150
Pair 2	Pre-30Hz	1.1475	2	.01909	.01350
	post-30Hz	.9030	2	.74529	.52700
Pair 3	Pre-50Hz	1.3560	2	.04950	.03500
	post-50Hz	1.0570	2	.94187	.66600
Pair 4	Pre-70Hz	1.4830	2	.05374	.03800
	post-70Hz	1.1480	2	1.06349	.75200
Pair 5	Pre-100Hz	1.6255	2	.02899	.02050
	post-100Hz	1.1705	2	1.07551	.76050
Pair 6	Pre-120Hz	1.6765	2	.00071	.00050
	post-120Hz	1.0645	2	.92136	.65150
Pair 7	Pre-150Hz	1.6280	2	.13859	.09800
	post-150Hz	.6525	2	.33870	.23950

Paired Samples Test

		Paired Differences					t	df	**Sig. (2-tailed)**
		Mean	Std. Deviation	Std. Error Mean	95% Confidence Interval of the Difference Lower	Upper			
Pair 1	Pre-10hz – post-10Hz	.14750	.35002	.24750	-2.99729	3.29229	.596	1	**.658**
Pair 2	Pre-30Hz – post-30Hz	.24450	.76438	.54050	-6.62320	7.11220	.452	1	**.730**
Pair 3	Pre-50Hz – post-50Hz	.29900	.99136	.70100	-8.60805	9.20605	.427	1	**.743**
Pair 4	Pre-70Hz – post-70Hz	.33500	1.11723	.79000	-9.70290	10.37290	.424	1	**.745**
Pair 5	Pre-100Hz – post-100Hz	.45500	1.10450	.78100	-9.46855	10.37855	.583	1	**.664**
Pair 6	Pre-120Hz – post-120Hz	.61200	.92065	.65100	-7.65974	8.88374	.940	1	**.520**
Pair 7	Pre-150Hz – post-150Hz	.97550	.20011	.14150	-.82243	2.77343	6.894	1	**.092**

Bibliography

1. **Abresch RT, Fowler WM JR, and Larson DB.** Contractile abnormalities in Dystrophinless (*mdx*) mice. *Med Sci Sports Med* 25: S15, 1993.

2. **Ahn AH and Kunkel LM.** The structural and functional diversity of dystrophin. *Nat Genet* 3:283-291, 1993.

3. **Alderton JM and Steinhardt RA.** Calcium influx through calcium leak channels is responsible for the elevated levels of calcium-dependent proteolysis in dystrophic myotubes. *J Biol Chem* 275: 9452–9460, 2000.

4. **Allen DG.** Fatigue in working muscles. *J Appl Physiol* 106: 358-359, 2009.

5. **Allen DG, Duty S, and Westerblad H.** Metabolic changes in muscle during exercise: their effects on muscle function. *Proc Aust Physiol Pharmacol Soc* 1993

6. **Allen DG, Gervasio OL, Young EW, and Whitehead NP.** Calcium and the damage pathways in muscular dystrophy. *Can J Physiol Pharmocol* 88: 83-91, 2010.

7. **Allen DG, Lamb GD, and Westerblad H.** Skeletal muscle fatigue: cellular mechanisms. *Physiol Rev* 88: 287-332, 2008.

8. **Allen DG, Lee JA, and Westerblad H**. Intracellular calcium and tension during fatigue in isolated single muscle fibres from *Xenopus laevis*. *J Physiol* 415: 433-458, 1989.

9. **Anderson JE, Bressler BH, and Ovalle WK.** Functional regeneration in the hind limb skeletal muscle of the *mdx* mouse. *J Muscle Res Cell Motil* 9: 499-515, 1998.

10. **Andrade FH, Reid MB, Allen DG, and Westerblad H.** Effect of hydrogen peroxide and dithiothreitol on contractile function of single skeletal muscle fibres from the mouse. *J Physiol* (London) 509:565-575, 1998.

11. **Arahata K and Sugita H. Dystrophin and the membrane hypothesis of muscular** dystrophy. *Trends Pharm Sci* 10: 437–439, 1989.

12. **Ashley CC, Mulligan IP, and Lea TJ.** Ca^{2+} and activation mechanisms in skeletal muscle. *Q Rev Biophys* 24: 1-73, 1991.

13. **Augusto V, Padovani CR, and Rocha Campos GE.** Skeletal muscle fiber types in C57BL6J mice. *Braz J Morphol Sci* 21:89-94, 2004.

14. **Badalamente M and Stracher A.** Delay of muscle degeneration and necrosis in *mdx* mice by calpain inhibition. *Muscle Nerve* 23: 106–111, 2000.

15. **Baker AJ, Kostov KG, Miller RG, and Weiner MW.** Slow force recovery after long-duration exercise: metabolic and activation factors in muscle fatigue. *J Appl Physiol* 74:2294-3000, 1993.

16. **Bakker JP, De Groot IJ, Beelen A, and Lankhorst GJ.** Predictive factors of cessation of ambulation in patients with Duchenne muscular dystrophy. *Am J Phys Med Rehabil* 81: 906-912, 2002.

17. **Barth R and Elce JS.** Immunofluorescent localisation of a Ca^{2+}-dependent neutral protease in hamster muscle. *Am J Physiol* 240: E493-E498, 1981.

18. **Batchelor CL and Winder SJ.** Sparks, signals and shock absorbers: how dystrophin loss causes muscular dystrophy. *Trends Cell Biol* 16: 198–205, 2006.

19. **Belcastro AN.** Skeletal muscle calcium-activated neutral protease (calpain) with exercise. *J Appl Physiol* 74: 1381–1386, 1993.

20. **Belcastro AN, Machan C, and Gilchrist JS.** Diabetes enhances calpain degradation of cardiac myofibrils and easily releasable myofilaments. In: Nagmo M, Dhalla NS (eds). The diabetic heart. Raven Press, New York, 301-310, 1991.

21. **Belcastro AN, Shewchuk LD, and Raj DA.** Exercise-induced muscle injury: a calpain hypothesis. *Mol Cell Biochem* 179: 135-145, 1998.

22. **Bellinger AM, Reiken S, Carlson C, Mongillo M, Liu X, Rothman L, Matecki S, Lacampagne A, and Marks AR.** Hypernitrosylated ryanodine receptor calcium release channels are leaky in dystrophic muscle. *Nat Med* 15:325–330, 2009.

23. **Blake DJ and Kroger S.** The neurobiology of Duchenne muscular dystrophy: learning lessons from muscle? *Trends Neurosci* 23: 92-99, 2000.

24. **Bodensteiner JB and Engel AG.** Intracellular calcium accumulation in Duchenne dystrophy and other myopathies: a study of 567,000 muscle fibers in 114 biopsies. *Neurology* 28: 439-446, 1978.

25. **Bouchentouf M, Benadballah BF, Mills P, and Tremblay JP.** Exercise improves the success of myoblast transplantation in mdx mice. *Neuromuscul Disord* 16:518-29, 2006.

26. **Branca D, Gugliucci A**, **Bano D, Brini M, and Carafoli E.** Expression, partial purification and functional properties of the muscle-specific calpain isoform p94. *Eur J Biochem* 265: 839-846, 1999.

27. **Briguet A, Erb M, Courdier-Fruh I, Barzaghi P, Santos G, Herzner H, Lescop C, Siendt H, Henneboehle M, Weyermann P, Magyar JP, Dubach-Powell J, Metz G, and Meier T.** Effect of calpain and proteasome inhibition on Ca^{2+}-dependent proteolysis and muscle histopathology in the *mdx* mouse. *FASEB J* 22: 4190–4200, 2008.

28. **Bulfield G, Siller WG, Wight PA, and Moore KJ.** X chromosome-linked muscular dystrophy (*mdx*) in the mouse. *Proc Natl Acad Sci* USA 81:1189-1192, 1984.

29. **Capote J, DiFranco M, and Vergara JL.** Excitation-contraction coupling alterations in *mdx* and utrophin/dystrophin double knockout mice: a comparative study. *Am J Physiol Cell Physiol*: In Print, 2010.

30. **Charge´ SB and Rudnicki MA.** Cellular and molecular regulation of muscle regeneration. *Physiol Rev* 84: 209-238, 2004.

31. **Chin ER.** Role of Ca^{2+}/calmodulin-dependent kinases in skeletal muscle plasticity. *J Appl Physiol* 99:414-423, 2005.

32. **Chin ER and Allen DG.** Raised intracellular calcium can cause subsequent failure of calcium-release in mammalian skeletal-muscle. *J Physiol - London* 487: 19-20, 1995.

33. **Chin ER and Allen DG.** The role of elevations in intracellular [Ca^{2+}] in the development of low frequency fatigue in mouse single muscle fibres. *J Physiol* 491: 813-824, 1996.

34. **Chin ER and Allen DG.** The contribution of pH-dependent mechanisms to fatigue at different intensities in mammalian single muscle fibres. *J Physiol* 512: 831-840, 1998.

35. **Chin ER, Balnave CD, and Allen DG.** Role of intracellular calcium and metabolites in low-frequency fatigue of mouse skeletal muscle. *Am J Physiol Physiol* 272: C550-C559, 1997.

36. **Collet C, Allard B, Tourneur Y, and Jacquemond V.** Intracellular calcium signals measured with indo-1 in isolated skeletal muscle fibres from control and *mdx* mice. *J Physiol* 520: 417-429, 1999.

37. **Collins CA and Morgan JE.** Duchenne's muscular dystrophy: animal models used to investigate pathogenesis and develop therapeutic strategies. *Int J Exp Pathol* 84: 165-172, 2003.

38. **Coolican SA and Hathaway DR.** Effect of L-a-phosphatidylinositol on a vascular smooth muscle Ca^{2+}-dependent protease. *J Biol Chem* 259: 11627-11630, 1984.

39. **Cornelio F and Dones I.** Muscle fiber degeneration and necrosis in muscular dystrophy and other muscle diseases: cytochemical and immunocyto-chemical data. *Ann Neurol* 16: 694-701, 1984.

40. **Culligan K, Banville N, Dowling P, and Ohlendieck K.** Drastic reduction of calsequestrin-like proteins and impaired calcium binding in dystrophic *mdx* muscle. *J Appl Physiol* 92: 435-445, 2002.

41. **Culligan K and Ohlendieck K.** Abnormal calcium handling in muscular dystrophy. *Bas Appl Myol* 12, 147-157, 2002. (a)

42. **Culligan K and Ohlendieck K.** Diversity of the brain Dystrophin-Glycoprotein Complex. *J Biomed Bio-tech* 2: 31-36, 2002. (b)

43. **D'Angelo MG, Berti M, Piccinini L, Romei M, Guglieri M, Bonato S, Degrate A, Turconi AC, and Bresolin N.** Gait pattern in Duchenne muscular dystrophy. *Gait & Posture* 29:36-41, 2009.

44. **Danieli-Beto D, Germinario E, Esposito A, Biral D, and Betto R.** Effects of fatigue on sarcoplasmic reticulum and myofibrillar proprieties of rat single muscle fibers. *J Appl Physiol* 89: 891-898, 2000.

45. **Dargelos E, Poussard S, Brule C, Daury L, and Cottin P.** Calcium-dependent proteolytic system and muscle dysfunctions: A possible role of calpains in sarcopenia. *Bioch* 90 (2): 359-368, 2008.

46. **Dayton WR and Schollmeyer JV.** Immunocytochemical localisation of a calcium activated protease in skeletal muscle cells. *Exp Cell Res* 136:423-433, 1981.

47. **Dawson MJ, Gadian DG, and Wilkie DR.** Mechanical relaxation rate and metabolism studied in fatiguing muscle by phosphorus nuclear magnetic resonance. *J Physiol* 299: 465-484, 1980.

48. **De Luca A, Pierno S, Liantonio A, Cetrone M, Camerino C, Simonetti S, Papadia F, and Camerino DC**. Alteration of excitation-contraction coupling mechanism in extensor digitorum longus muscle fibres of dystrophic *mdx* mouse and potential efficacy of taurine. Br J Pharmacol 132: 1047–1054, 2001.

49. **Deconinck AE, Potter AC, Tinsley JM, Wood SJ, Vater R, Young C, Metzinger L, Vincent A, Slater CR, and Davies KE.** Postsynaptic abnormalities at the neuromuscular junctions of utrophin-deficient mice. *J Cell Biol* 136: 883-894, 1997. (a)

50. **Deconinck AE, Rafael JA, Skinner JA, Brown SC, Potter AC, Metzinger L, Watt DJ, Dickson JG, Tinsley JM, and Davies KE.** Utrophin-dystrophin-deficient mice as a model for Duchenne muscular dystrophy. Cell 90: 717-727, 1997. (b)

51. **Divet A and Huchet-Cadiou C.** Sarcoplasmic reticulum function in slow- and fast-twitch skeletal muscles from *mdx* mice. *Pflügers Arch* 444: 634-643, 2002.

52. **Dowling P, Culligan K, and Ohlendieck K.** Distal *mdx* muscle groups exhibiting up-regulation of utrophin and rescue of dystrophin-associated glycoproteins exemplify a protected phenotype in muscular dystrophy. Naturwissenschaften 89: 75-78, 2002.

53. **Dowling P, Lohan J, and Ohlendieck K.** Comparative analysis of Dp427-deficient *mdx* tissues shows that the milder dystrophic phenotype of extraocular and toe muscle fibres is associated with a persistent expression of beta-dystroglycan. *Eur J Cell Biol* 82: 222-230, 2003.

54. **Dupont-Versteegden EE, McCarter RJ, and Katz MS.** Voluntary exercise decreases the progression of muscular dystrophy in diaphragm of *mdx* mice. *J Appl Physiol* 77:1736-1741, 1994.

55. **Edwards RHT, Hill DK, Jones DA, Merton PA.** Fatigue of long duration in human skeletal muscle after fatigue. *J Physiol* 272: 769-778, 1977.

56. **Favero TG, Zable AC, Bowman MB, Thompson A, and Abramson JJ.** Metabolic end products inhibit sarcoplasmic reticulum Ca^{2+} release and [^{3}H]ryonadine binding. *J Appl Physiol* 78: 1665-1672, 1995.

57. **Fitts RH, Courtright JB, Kim DH, and Witzmann FA.** Muscle fatigue with prolonged exercise: contractile and biochemical alterations. *Am J Physiol Cell Physiol* 242: 65-73, 1982.

58. **Fong P, Turner PR, Denetclaw WF, and Steinhardt RA.** Increased activity of calcium leak channels in myotubes of Duchenne human and mdx mouse origin. *Science* 250: 673-676, 1990.

59. **Franco-Obregon Jr. A and Lansman JB.** Mechanosensitive ion channels in skeletal muscle from normal and dystrophic mice. *J Physiol* 481:299-309, 1994.

60. **Fryer MW, Owen VJ, Lamb GD, and Stephenson DG.** Effects of creatine phosphate and Pi on Ca^{2+} movements and tension development in rat skinned skeletal muscle fibres. *J Physiol* 482: 123-140, 1995.

61. **Gailly P, Boland B, Himpens B, Casteels R, and Gillis JM.** Critical evaluation of cytosolic calcium determination in resting muscle fibres from normal and dystrophic (*mdx*) mice. *Cell Calcium* 14: 473-483, 1993.

62. **Gailly P, De Becker F, Van Schoor M, and Gillis JM.** In situ measurements of calpain activity in isolated muscle fibres from normal and dystrophic-lacking *mdx* mice. *J Physiol* 582: 1261-1275, 2007.

63. **Garcia Diaz BE, Gauthier S, and Davies PL.** Ca^{2+} dependency of calpain-3 (p94) activation. *Biochemistry* 45: 3714-3722, 2006.

64. **Garcia Diaz BE, Moldoveanu T, Kuiper MJ, Campbell RL, and Davies PL.** Insertion sequence 1 of muscle-specific calpain, p94, acts as an internal propeptide. *J Biol Chem* 279: 27656–66, 2004.

65. **Gaudreault N, Gravel D, and Nadeau S.** Evaluation of plantar flexion contracture contribution during the gait of children with Duchenne muscular dystrophy. *J Electromyogr Kinesiol* 19: 180-186, 2007.

66. **Gervásio OL, Whitehead NP, Yeung EW, Phillips WD, and Allen DG.** TRPC1 binds to caveolin-3 and is regulated by Src kinase-role in Duchenne muscular dystrophy. *J Cell Sci* 12: 2246-2255, 2008.

67. **Goll DE, Thompson VF, Li H, Wei W, and Cong J.** The calpain system. *Physiol Rev* 83: 731-801, 2003.

68. **Goll DE, Shannon JD, Edmunds T, Sathe SK, Kleese WC, and Nagainis PA.** Properties and regulation of the Ca^{2+}-dependent proteinase. In: de Bernard B, Sottocassa GL, Sandri G, Carafoli E, Taylor AN, Vanaman TC, Williams RJP, (eds) Elsevier Science Publishers. BV, Amsterdam New York, pp 19-35, 1983.

69. **Goonasekera, Lam CK, Millay DP, Sargent MA, Hajjar RJ, Kranias EG, and Molkentin JD.** Mitigation of muscular dystrophy in mice by SERCA overexpression in skeletal muscle. *J Clin Invest* 121:1044-1052, 2011.

70. **Grady RM, Teng H, Nichol MC, Cunningham JC, Wilkinson RS, and Sanes JR.** Skeletal and cardiac myopathies in mice lacking utrophin and dystrophin: a model for Duchenne muscular dystrophy. *Cell* 90: 729-738, 1997.

71. **Groschner K, Rosker C, and Lukas M.** Role of TRP channels in oxidative stress. *Novartis Found Symp* 258: 222–230, discussion 231–235, 263–266, 2004.

72. **Grynkiewics G, Poeni M, and Tsien RY.** A new generation of Ca^{2+} indicators with greatly improved fluorescence properties. *J Biol Chem* 260: 3440-3450, 1985.

73. **Guroff G.** A neutral, calcium activated proteinase from the soluble fraction of rat brain. *J Biol Chem* 239:149-155, 1964

74. **Hayes A, Lynch GS, and Williams DA.** The effects of endurance exercise on dystrophic *mdx* mice: I. Contractile and histochemical properties of intact muscles. *Proc R Soc Lond B Biol Sci* 253: 19-25, 1993.

75. **Head SI.** Membrane potential, resting calcium and calcium transients in isolated muscle fibres from normal and dystrophic mice. *J Physiol* 469: 11-19, 1993.

76. **Head SI.** Branched fibres in old dystrophic *mdx* muscle are associated with mechanical weakening of the sarcolemma abnormal Ca^{2+} transients and a breakdown of Ca^{2+}homeostasis during fatigue. *Exp Physiol*, In Print 2010.

77. **Hill CA, Thompson MW, Ruell PA, Thom JM, and White MJ.** Sarcoplasmic reticulum function and muscle contractile character following fatiguing exercise in humans. *J Physiol* 531: 871–878, 2001.

78. **Hinton VJ, De Vivo DC, Nereo NE, Goldstein E, and Stern Y.** Poor verbal working memory across intellectual level in boys with Duchenne dystrophy. *Neurology* 54: 2127-2132, 2000.

79. **Hoffman EP, Brown Jr. RH, and Kundel LM.** Dystrophin: the protein product of the Duchenne muscular dystrophy locus. *Cell* 51(6): 919-928, 1987.

80. **Hollingworth S, Zeiger U, and Baylor SM.** Comparison of the myoplasmic calcium transient elicited by an action potential in intact fibres of *mdx* and normal mice. *J Physiol* 586: 5063–5075, 2008.

81. **Holloszy JO.** Biochemical adaptations in muscle. Effects of exercise on mitochondrial oxygen uptake and respiratory enzyme activity in skeletal muscle. *J Biol Chem* 242: 2278-2282, 1967.

82. **Hopf FW, Turner PR, Denetclaw WF Jr, Reddy P, and Steinhardt RA.** A critical evaluation of resting intracellular free calcium regulation in dystrophic *mdx* muscle. *Am J Physiol* 271: C1325-C1339, 1996.

83. **Hubal MJ, Gordish-Dressman H, Thompson PD, Price TB, Hoffman EP, Angelopoulos TJ, Gordon PM, Moyna NM, Pescatello LS, Visich PS, Zoeller RF, Seip**

RL, and Clarkson PM. Variability in muscle size and strength gain after unilateral resistance training. *Med Sci Sports Exerc* 37: 964-972, 2005.

84. **Huxtable R and Bressler R.** Effect of taurine on a muscle intracellular membrane. *Biochim Biophys Acta* 323: 573-578, 1973.

85. **Iwata Y, Katanosaka Y, Arai Y, Shigekawa M, and Wakabayashi S.** Dominant-negative inhibition of Ca^{2+} influx via TRPV2 ameliorates muscular dystrophy in animal models. *Hum Mol Genet* 18(5): 824-834, 2009.

86. **Jorgensen LH, Blain A, Greally E, Laval SH, Blamire AM, Davison BJ, Brinkmeier H, MacGowan GA, Schoder HD, Bushby K, Straub V, and Lochmuller H.** Long-term blocking of calcium channels in *mdx* mice results in differential effects on heart and skeletal muscle. *Am J Pathol* 178: 273-283, 2011.

87. **Kargacin ME and Kargacin GJ.** The sarcoplasmic reticulum calcium pump is functionally altered in dystrophic muscle. *Biochim Biophys Acta* 1290: 4-8, 1996.

88. **Karpati G, Carpenter S, and Prescott S.** Small-caliber skeletal fibers do not suffer necrosis in *mdx* mouse dystrophy. *Muscle Nerve* 11:795-803, 1988.

89. **Kasperek GJ and Snider RD.** Total and myofibrillar degradation in isolated soleus muscles after exercise. *Am J Physiol* 257: E1-E5, 1989.

90. **Kay J.** Ca^{2+}-activated proteinases, protein degradation and muscular dystrophy. In: Heidland A, Horl WH (eds) Proteinases, potential role in health and disease. Plenum Press, New York, pp. 519-532, 1983.

91. **Keira Y, Noguchi S, Minami N, Hayashi YK, and Nishino I.** Localization of calpain 3 in human skeletal muscle and its alteration in limb-girdle muscular dystrophy 2A muscle. *J Biochem* 133: 659–664, 2003.

92. **Kettelhut IC, Wing SS, and Goldberg AL.** Endocrine regulation of protein breakdown in skeletal muscle. *Diabetes Metab Rev* 4: 751–772, 1988.

93. **Kilmer DD.** Response to resistive strengthening exercise training in humans with neuromuscular disease. *Am J Phys Med Rehabil* 81:121–126, 2002.

94. **Kometani K, Tsugeno H, and Yamada K.** Mechanical and energetic properties of dystrophic (*mdx*) mouse muscle. *Jap J Physiol* 40: 541-549, 1990.

95. **Konig N, Raynaud F, Feane H, Durand M, Mestre-Frances N, Rossel M, Ouali A, and Benyamin Y.** Calpain 3 is expressed in specific glial cells of the rodent and primate brain. *J Chem Neuroanat* 25: 129-136, 2003.

96. **Kramerova I, Kudryashova E, Wu B, Ottenheijm C, Granzier H, and Spencer MJ.** Novel role of calpain-3 in the triad-associated protein complex regulating calcium release in skeletal muscle. *Hum Mol Genet* 17: 3271–80, 2008.

97. **Lamb GD and Cellini MA.** High intracellular [Ca^{2+}] alters sarcoplasmic reticulum function in skinned skeletal muscle fibres of the rat. *J Physiol* 519: 815-827, 1999.

98. **Lamb GD, Junukar PR, Stephenson DG.** Abolition of excitation-contraction coupling in skeletal muscle by raised intracellular [Ca^{2+}]. *Proceedings of the Australian Physiological and Pharmacological Society* 25: 76, 1994.

99. **Lamb GD, Junankar PR, and Stephenson DG.** Raised intracellular [Ca^{2+}] abolishes excitation-contraction coupling in skeletal muscle fibres of rat and toad. *J Physiol* 489: 349-362, 1995.

100. **Lannergren J and Westerblad H.** The temperature dependence of isometric contractions of single, intact fibres dissected from a mouse foot muscle. *J Physiol* 390: 285-293, 1987.

101. **Lannergren J, and Westerblad H.** Force decline due to fatigue and intracellular acidification in isolated fibres from isolated skeletal muscle. *J Physiol* 434: 307-322, 1991.

102. **Leijendekker WJ, Passaquin AC, Metzinger L, and Ruegg UT.** Regulation of cytosolic calcium in skeletal muscle cells of the *mdx* mouse under conditions of stress. *Br J Pharmacol* 118: 611-616, 1996.

103. **Love DR, Byth BC, Tinsley JM, Blake DJ, and Davies KE.** Dystrophin and dystrophin-related proteins: a review of protein and RNA studies. *Neuromuscul Disord* 3: 5-21, 1993.

104. **Lovering ML, Michaelson L, Ward CW.** Malformed *mdx* myofibres have normal cytoskeletal architecture yet altered E-C coupling and stress-induced Ca^{2+} signaling. *Am J Cell Physiol* 297: 571-580, 2009.

105. **Mallouk N, Jacquemond V, and Allard B.** Elevated subsarcolemmal Ca^{2+} in mdx mouse skeletal muscle fibers detected with Ca^{2+}-activated K^{+} channels. *Proc Natl Acad Sci USA* 97: 4950–4955, 2000.

106. **Marcilhac A, Raynaud F, Clerc I, and Benyamin Y.** Detection and localization of calpain 3-like protease in a neuronal cell line: possible regulation of apoptotic cell death through degradation of nuclear IkappaBalpha. *Int J Biochem Cell Biol* 38: 2128-2140, 2006.

107. **Marimuthu K, Murton AJ, and Greenhaff PL.** Mechanisms regulating muscle mass during disuse atrophy and rehabilitation in humans. *J Appl Physiol* 110: 555-560, 2011.

108. **Mázala DAG and Chin ER.** Effects of ex vivo denervation on intracellular Ca^{2+} ratios in intact mammalian single muscle fibres. *Med Sci Sports Exerc* (Abstract), 2010.

109. **McNeil PL and Khakee R.** Disruptions of muscle fiber plasma membranes. Role in exercise-induced damage. *Am J Pathol* 140: 1097-1109, 1992.

110. **Millay DP, Goonasekera SA, Sargent MA, Maillet M, Aronow BJ, and Molkentin JD.** Calcium influx is sufficient to induce muscular dystrophy through a TRPC-dependent mechanism. *Proc Natl Acad Sci USA* 106: 19023-19028, 2009.

111. **Mizuno Y, Nonaka I, Hirai S, and Ozawa E.** Reciprocal expression of dystrophin and utrophin in muscles of Duchenne muscular dystrophy patients, female DMD-carriers and control subjects. *J Neurol Sci* 119: 43-52, 1993.

112. **Moens P, Baatsen PH, and Marechal G.** Increased susceptibility of EDL muscles from *mdx* mice to damage induced by contractions with stretch. *J Muscle Res Cell Motil* 14:446-451, 1993.

113. **Mongini T, Chigo D, Doriguzzi C, Bussolino F, Escarmona G, Pollo B, Schiffler D, and Bosia A.** Free cytoplasmic Ca^{2+} at rest and after cholinergic stimulus is increased in cultured muscle cells from Duchenne muscular dystrophy patients. *Neurol* 38: 476-480, 1988.

114. **Morini K, Sleeper MM, Barton ER, and Sweeney L.** Overexpression of SERCA1a in the *mdx* diaphragm reduces susceptibility to contraction induced damage. *Hum Gene Ther* 21: 1735-1739, 2010.

115. **Murachi T.** Calpain and calpastatin. *Trends Biochem Sci* 8: 167-169, 1983.

116. **Murphy RM.** Calpains, skeletal muscle function and exercise. *Clin and Exper Pharma and Physiol* 40: 95-102, 2010.

117. **Murphy RM, Goodman CA, McKenna MJ, Bennie J, Leikis M, and Lamb GD.** Calpain-3 is autolyzed and hence activated in human skeletal muscle 24h following a singe bout of eccentric exercise. *J Appl Physiol* 103: 926-931, 2007.

118. **Murphy RM and Lamb GD.** Endogenous calpain-3 activation is primarily governed by small increases in resting cytoplasmic Ca^{2+} and is not dependent on stretch. *J Biol Chem* 284: 7811-7819, 2009.

119. **Murphy RM, Snow RJ, and Lamb GD.** μ-Calpain and calpain-3 are not autolyzed with exhaustive exercise in humans. *Am J Physiol Cell Physiol* 290: C116–122, 2006.

120. **Murphy RM, Verburg E, and Lamb GD.** Ca^{2+} activation of diffusible and bound pools of μ-calpain in rat skeletal muscle. *J Physiol* 576:595-612, 2006.

121. **Owen VJ, Lamb GD, and Stephenson DG.** Effect of low [ATP] on depolarization-induced Ca^{2+} release in skeletal muscle fibres of the toad. *J Physiol* 493: 309-315, 1996.

122. **Ohlendieck K, Ervasti JM, Matsumura K, Kahl SD, Leveille CJ, and Campbell KP.** Dystrophin-related protein is localized to neuromuscular junctions of adult skeletal muscle. *Neuron* 7:499-508, 1991.

123. **Pape PC, Jong DS, Chandler WK, and Baylor SM.** Effect of fura-2 on action potential-stimulated calcium release in cut twitch fibers from frog muscle. *J Gen Physiol* 102:295-332, 1993.

124. **Place N, Yamada T, Zhang S, Westerblad H, and Bruton JD.** High temperature does not alter fatigability in intact mouse skeletal muscle fibers. *J Physiol* 587: 4717-4724, 2009.

125. **Poteser M, Graziani A, Rosker C, Eder P, Derler I, Kahr H, Zhu MX, Romanin C, and Groschner K.** TRPC3 and TRPC4 associate to form a redox-sensitive cation channel. Evidence for expression of native TRPC3-TRPC4 heteromeric channels in endothelial cells. *J Biol Chem* 281: 13588-13595, 2006.

126. **Pressmar J, Brinkmeier H, Seewald MJ, Naumann T, and Rudel R.** Intracellular Ca^{2+} concentrations are not elevated in resting cultured muscle from Duchenne (DMD) patients and in *mdx* mouse muscle fibres. *Pflügers Arch* 426: 499-505, 1994.

127. **Pulido SM, Passaquin AC, Leijendekker WJ, Challet C, Wallimann T, and Rue Egg UT.** Creatine supplementation improves intracellular Ca^{2+} handling and survival in *mdx* skeletal muscle cells. *FEBS Lett* 439: 357-362, 1998.

128. **Rando TA.** Oxidative stress and the pathogenesis of muscular dystrophies. *Am J Phys Med Rehabil* 81(11 Suppl): S175-S186, 2002.

129. **Rennie MJ, Edwards HT, Krywawych S, Davies CTM, Halliday D, Waterlow JC, and Millward DJ.** Effect of exercise in protein turnover in man. *Clin Sci* 6: 627-639, 1981.

130. **Roots H, Ball G, Talbot-Ponsonby J, King M, McBeath K, and Ranatunga KW**. Muscle fatigue examined at different temperatures in experiments on intact mammalian (rat) muscle fibers. *J Appl Physiol* 106: 378-384, 2009.

131. **Sacco A, Mourkioti F, Tran R, Choi J, Llewellyn M, Kraft P, Shkreli M, Delp S, Pomerantz JH, Artandi SE, and Blau HM.** Short telomeres and stem cell exhaustion model Duchenne muscular dystrophy in *mdx*/mTR mice. *Cell* 143:1059-1071, 2010.

132. **Saido TC, Shibata M, Takenawa WA, Murofushi H, and Suzuki K.** Positive regulation of mu-calpain action by phosphoinositides. *J Biol Chem* 267: 24585-24590, 1992.

133. **Sano M, Yokota T, Endo T, and Tsukagoshi H.** A developmental change in the content of parvalbumin in normal and dystrophic mouse (*mdx*) muscle. *J Neurol Sci* 97: 261–272, 1990.

134. **Schertzer JD, van der Poel C, Shavlakadze T, Grounds MD, and Lynch GS.** Muscle-specific overexpression of IGF-I improves E-C coupling in skeletal muscle fibres from dystrophic *mdx* mice. *Am J Physiol Cell Physiol* 294: 161-168, 2008.

135. **Selsby JT, Pendrak K, Zadel M, Tian Z, Pham J, Carver T, Acosta P, Barton ER, and Sweeney HL.** eupeptin based inhibitors do not improve the mdx phenotype. *Am J Physiol Regul Integr Comp Physiol* 299: 1192-1201, 2010.

136. **Skura CL, Padden TM, and Fowler EG.** The effect of concentric exercise for two children with Duchenne Muscular Dystrophy. *Pediatr Phys Ther* 17:84 2005.

137. **Smith IJ, Lecker, SH, and Hasselgren P.** Calpain activity and muscle wasting in sepsis. *Am J Physiol Endocrinol Metab* 295: 762-771, 2008.

138. **Sorimachi H, Imajoh-Ohmi S, Emori Y, Kawasaki H, Ohno S, Minami Y, and Suzuki K.** Molecular Cloning of a novel mammalian calcium-dependent protease distinct from m- and μ-types. Specific expression of the mRNA in skeletal muscle. *J Biol Chem* 264: 20106–11, 1989.

139. **Spencer MJ, Croall DE, and Tidball JG.** Calpains are activated in necrotic fibers from *mdx* dystrophic mice. *J Biol Chem* 270: 10909–10914, 1995.

140. **Spencer MJ and Mellgren RL.** Overexpression of a calpastatin transgene in *mdx* muscle reduces dystrophic pathology. *Hum Mol Genet* 11:2645-2655, 2002.

141. **Spencer MJ and Tidball JG.** Calpain concentration is elevated although net calcium-dependent proteolysis is suppressed in dystrophin-deficient muscle. *Exp Cell Res* 203: 107-114, 1992.

142. **Spencer MJ and Tidball JG.** Calpain translocation during muscle fiber necrosis and regeneration in dystrophin-deficient mice. *Exp Cell Res* 226: 264–272, 1996.

143. **Stedman HH, Sweeney HL, Shrager JB, Maguire HC, Panettieri RA, Petrof B, Marusawa M, Leferocich JM, Sladky JT, and Kelly AM.** The *mdx* mouse diaphragm reproduces the degenerative changes of Duchenne muscular dystrophy. *Nature* 352: 536-539, 1991.

144. **Stillwell E, Vitale J, Zhao Q, Beck A, Schneider J, Khadim F, Elson G, Altaf A, Yehia G, Dong J-H, Liu J, Mark W, Bhaumik M, Grange R, and Fraidenraich D.** Blastocyst injection of wild type embryonic stem cells induces global corrections in *mdx* mice. *PLos ONE* 4: 1-15, 2009.

145. **Takagi A, Kojima S, Ida M, and Araki M.** Increased leakage of calcium ion from the sarcoplasmic reticulum of the *mdx* mouse. *J Neurol Sci* 1992; 110: 160-164, 1992.

146. **Temparis S, Asensi M, Taillandier D, Aurousseau E, Larbaud D, Obled A, Bechet D, Ferrara M, Estrela JM, and Attaix D.** Increased ATP-ubiquitin-dependent proteolysis in skeletal muscles of tumor-bearing rats. *Cancer Res* 54: 5568–5573, 1994.

147. **Turner PR, Fong PY, Denetclaw WF, and Steinhardt RA.** Increased calcium influx in dystrophic muscle. *J Cell Biol* 115: 1701-1712, 1991.

148. **Turner PR, Westwood T, Regen CM, and Steinhardt RA.** Increased protein degradation results from elevated free calcium levels found in muscle from mdx mice. *Nature* 335, 735-738, 1988.

149. **van Deutekom JC and van Ommen GJ.** Advances in Duchenne muscular dystrophy gene therapy. *Nat Rev Genet* 4: 774-783, 2003.

150. **Vandebrouck C, Martin D, Colson-Van Schoor M, Debaix H, and Gailly P.** Involvement of TRPC in the abnormal calcium influx observed in dystrophic (*mdx*) mouse skeletal muscle fibers. *J Cell Biol* 158: 1089–1096, 2002.

151. **Verburg E, Dutka TL, and Lamb GD.** Long-lasting muscle fatigue: partial disruption of excitation-contraction coupling by elevated cytosolic Ca^{2+} concentration during contractions. *Am J Physiol Cell Physiol* 290: C1199-C1208, 2006.

152. **Verburg E, Murphy RM, Stephenson DG, and Lamb GD.** Disruption of excitation-contraction coupling and titin by endogenous Ca^{2+} -activated proteases in toad muscle fibres. *J Physiol* 564: 775-990, 2005.

153. **Vorndran C, Minta A, Poenie M.** New fluorescent calcium indicators designed for cytosolic retention or measuring calcium near membranes. *Biophys J* 66: 926-928, 1995.

154. **Wagner KR.** Approaching a new age in Duchenne muscular dystrophy treatment. *Neurotherapeutics* 5:583-591, 2008.

155. **Wagner KR, Lechtzin N, and Judge DP.** Current treatment of adult Duchenne muscular dystrophy. *Biochim Biophys Acta* 1772:229-237, 2007.

156. **Westerblad H and Allen DG.** Changes of myoplasmic calcium concentration during fatigue in single mouse muscle fibers. *J Gen Physiol* 98: 615-635, 1991.

157. **Westerblad H and Allen DG.** Changes in intracellular pH due to repetitive stimulation of single fibres from mouse skeletal muscle. *J Physiol* 449: 49-71, 1992.

158. **Westerblad H, Bruton JD, and Lannergren J.** The effects of intracellular pH on contractile function of intact, single fibres of mouse muscle declines with increasing temperatures. *J Physiol* 500: 193-204, 1997.

159. **Westerblad H, Duty S, and Allen DG.** Intracellular calcium concentration during low-frequency fatigue in isolated single fibres of mouse skeletal muscle. *J Appl Physiol* 75: 382-388, 1993.

160. **Whitehead NP, Streamer M, Lusambili LI, Sachs F, and Allen DG.** Streptomycin reduces stretch-induced membrane permeability in muscles from *mdx* mice. *Neuromuscul Disord* 16(12): 845-854, 2006.

161. **Wicksell RK, Kihlgren M, Melin L, and Eeg-Olofsson O.** Specific cognitive deficits are common in children with Duchenne muscular dystrophy. *Dev Med Child Neurol* 46: 154-159, 2004.

162. **Wineinger MA, Walsh SA, and Abresch RT.** The effect of age and temperature on *mdx* muscle fatigue. *Muscle Nerve* 21: 1075-1077, 1998.

163. **Williams DA and Fay FS.** Intracellular calibration of the fluorescent calcium indicator fura-2. *Cell Calcium* 11:75-83, 1990

164. **Wilton SD and Fletcher S.** Novel compounds for the treatment of Duchenne muscular dystrophy: emerging therapeutic agents. *Appl Clin Gen* 4: 29-44, 2011.

165. **Woods CE, Novo D, DiFranco M, Capote J, and Vergara JL.** Propagation in the transverse tubular system and voltage dependence of calcium release in normal and *mdx* muscle fibres. *J Physiol* 568: 867-880, 2005.

166. **Woods CE, Novo D, DiFranco M, and Vergara JL.** The action potential-evoked sarcoplasmic reticulum calcium release is impaired in *mdx* mouse muscle fibres. *J Physiol* 557: 59-75, 2004.

167. **Wrzolek MA, Sher JH, Kozlowski PB, and Rao C.** Skeletal muscle pathology in AIDS: an autopsy study. *Muscle Nerve* 13: 508–515, 1990.

168. **Yeung EW, Head SI, and Allen DG.** Gadolinium reduces short-term stretch-induced muscle damage in isolated mdx mouse muscle fibres. *J Physiol* 552: 449, 2003.

169. **Yeung EW, Whitehead NP, Suchyna TM, Gottlieb PA, Sachs F, and Allen DG.** Effects of stretch-activated channel blockers on $[Ca^{2+}]_i$ and muscle damage in the *mdx* mouse. *J Physiol* 562: 367-380, 2005.

170. **Yoshimura N, Murachi T, Heath R, Kay J, Jasani B, and Newman GR.** Immunogold electron microscopic localization of calpain I in skeletal muscle of rats. *Cell Tissue Res* 244: 265-270, 1986.

171. **Zhang B, Yeung SS, Allen DG, Qin L, and Yeung EW.** Role of the calcium-calpain pathway in cytoskeletal damage after eccentric contractions. *J Appl Physiol* 105:352-357, 2008.